

Experimental evaluation of remaining prestress force and center negative bending-moment in  
railroad ties removed from track after 25 years of service

by

James Daniel Scott

B.S., Kansas State University, 2014

AN ABSTRACT OF A DISSERTATION

submitted in partial fulfillment of the requirements for the degree

DOCTOR OF PHILOSOPHY

Department of Civil Engineering  
College of Engineering

KANSAS STATE UNIVERSITY  
Manhattan, Kansas

2019

## **Abstract**

To better understand the appropriate level of prestress force necessary in a prestressed concrete railroad tie that will both mitigate the propensity for longitudinal splitting and also result in a long-term service life, a study was conducted on 12 different designs of existing ties removed from track to evaluate the remaining prestress force in the ties. The existing ties selected for the study had performed well in track for over 25 years and remained in good condition upon removal from track, with no signs of longitudinal splitting. Four different experimental test methods were conducted to evaluate the remaining prestress force in the existing ties. The experimental methods used included the flexural crack reopening method, the newly developed direct tension method, the strain gage method, and the measurement of the length change of wires extracted from the ties. New ties were manufactured with internal vibrating-wire strain gages to provide ties with known prestress forces at the time of testing, and used for comparison to the experimental results. Test results indicate that the direct tension test was the most accurate of the four methods, and that existing ties tended to have prestressing forces in the range of 82-93 kips.

Additional testing was conducted to evaluate the center negative cracking moments of the existing ties and compare the results to the current requirements of the AREMA Chapter 30 center negative bending-moment test. Results indicate that of the 12 tie designs investigated, 8 would meet the requirements of the AREMA 30 test in their current state. Knowing current condition and track performance of the existing ties, their level of remaining prestress force, and their center negative bending capacity, new ties could be designed with similar parameters to ensure a durable long-term performance in track while reducing the longitudinal splitting propensity of the tie.

Experimental evaluation of remaining prestress force and center negative bending-moment in  
railroad ties removed from track after 25 years of service

by

James Daniel Scott

B.S., Kansas State University, 2014

A DISSERTATION

submitted in partial fulfillment of the requirements for the degree

DOCTOR OF PHILOSOPHY

Department of Civil Engineering  
College of Engineering

KANSAS STATE UNIVERSITY  
Manhattan, Kansas

2019

Approved by:

Major Professor  
Dr. Robert J. Peterman

# Copyright

© James Scott 2019.

## **Abstract**

To better understand the appropriate level of prestress force necessary in a prestressed concrete railroad tie that will both mitigate the propensity for longitudinal splitting and also result in a long-term service life, a study was conducted on 12 different designs of existing ties removed from track to evaluate the remaining prestress force in the ties. The existing ties selected for the study had performed well in track for over 25 years and remained in good condition upon removal from track, with no signs of longitudinal splitting. Four different experimental test methods were conducted to evaluate the remaining prestress force in the existing ties. The experimental methods used included the flexural crack reopening method, the newly developed direct tension method, the strain gage method, and the measurement of the length change of wires extracted from the ties. New ties were manufactured with internal vibrating-wire strain gages to provide ties with known prestress forces at the time of testing and used for comparison to the experimental results. Test results indicate that the direct tension test was the most accurate of the four methods, and that existing ties tended to have prestressing forces in the range of 82-93 kips.

Additional testing was conducted to evaluate the center negative cracking moments of the existing ties and compare the results to the current requirements of the AREMA Chapter 30 center negative bending-moment test. Results indicate that of the 12 tie designs investigated, 8 would meet the requirements of the AREMA 30 test in their current state. Knowing current condition and track performance of the existing ties, their level of remaining prestress force, and their center negative bending capacity, new ties could be designed with similar parameters to ensure a durable long-term performance in track while reducing the longitudinal splitting propensity of the tie.

# Table of Contents

List of Figures .....	viii
List of Tables .....	xii
Acknowledgements .....	xiii
Chapter 1 - Introduction.....	1
Background.....	1
Objectives .....	2
Organization of Dissertation.....	3
Chapter 2 - Literature Review.....	5
Estimated Prestress Loss.....	5
Instrumentation .....	6
Structural Dynamic Response.....	8
Dynamic Relaxation .....	10
Flexural Cracking .....	11
Chapter 3 - Tie Description.....	14
Existing Ties Removed from Track.....	14
New Tie Designs.....	16
Chapter 4 - Flexural Crack Reopening .....	20
Flexural Test Setup .....	20
Flexural Test Results .....	24
Determination of Crack Reopening Load.....	31
Discussion.....	36
Chapter 5 - Direct Tension Test.....	38
Concrete Mix Details .....	39
Prism Testing .....	40
Experimental Setup.....	41
Results.....	46
Preliminary Tie Test .....	51
Experimental Setup.....	52
Results.....	58

Discussion .....	60
Full-Scale Tie Testing.....	62
Experimental Setup.....	62
Results for new ties .....	66
Results for existing ties.....	70
Chapter 6 - Strain Gage Method .....	76
Experimental Program .....	76
Results.....	82
Test for Bowing of Wire.....	90
Chapter 7 - Length Change of Extracted Wire .....	95
Method 1: Full Length Measurement .....	95
Method 1 Results .....	103
Method 2: 60 Inch Gage Length.....	105
Method 2 Results .....	107
Chapter 8 - Center negative Cracking Moment .....	110
Theoretical Cracking Moments .....	110
Experimental Cracking Moments .....	111
AREMA Center negative Test Comparison .....	115
Chapter 9 - Conclusions.....	119
References.....	123
Appendix A - Pictures of Existing Ties and Mid-span Cross-sections.....	127
Appendix B - Summary of Testing Conducted on Ties.....	139
Appendix C - Net Effect of Elastic Shortening and the Weight of the Top Block on tie D-4....	141

## List of Figures

Figure 3.1 Typical 3-D model of a tie obtained from scanning.....	14
Figure 3.2 Crosstie graveyard at TTCI in Pueblo, Colorado .....	15
Figure 3.3 VWSG installed at center of a Rocla tie.....	18
Figure 3.4 VWSG installed at center of a Nortrak tie.....	18
Figure 4.1 Schematic of four-point flexural test.....	21
Figure 4.2 Typical flexural configuration.....	22
Figure 4.3 Clip gage instrumented over crack .....	23
Figure 4.4 Comparison of Load vs COD results for each design group.....	25
Figure 4.5 Load vs COD for tie design group A.....	25
Figure 4.6 Load vs COD for tie design group B.....	26
Figure 4.7 Load vs COD for tie design group C.....	26
Figure 4.8 Load vs COD for tie design group D.....	27
Figure 4.9 Load vs COD for tie design group E.....	27
Figure 4.10 Load vs COD for tie design group F .....	28
Figure 4.11 Load vs COD for tie design group G.....	28
Figure 4.12 Load vs COD for tie design group H.....	29
Figure 4.13 Load vs COD for tie design group J .....	29
Figure 4.14 Load vs COD for tie design group K.....	30
Figure 4.15 Load vs COD for tie design group L .....	30
Figure 4.16 Load vs COD for tie design group M.....	31
Figure 4.17 Load vs COD for Rocla Tie 1.....	32
Figure 4.18 Load vs COD for Rocla Tie 2.....	33
Figure 4.19 Load vs COD for Rocla Tie 3.....	33
Figure 4.20 Percent offset required for Rocla Tie 1 .....	34
Figure 4.21 Percent offset required for Rocla Tie 2 .....	35
Figure 4.22 Percent offset required for Rocla Tie 3 .....	35
Figure 4.23 Change of cross section as crack propagates.....	37
Figure 5.1 Effective cross section of a tie in tension before and after crack opening .....	39
Figure 5.2 Typical prism cross section .....	41

Figure 5.3 Typical notch in prism.....	42
Figure 5.4 Typical groove in prism.....	42
Figure 5.5 Prisms with rebar cages prior to casting blocks .....	43
Figure 5.6 Prisms after casting blocks .....	44
Figure 5.7 Typical LVDT setup.....	45
Figure 5.8 Test configuration for prism testing .....	45
Figure 5.9 Prism 1 test results.....	47
Figure 5.10 Prism 2 test results.....	48
Figure 5.11 Prism 3 test results.....	49
Figure 5.12 Prism 4 test results.....	50
Figure 5.13 Tie D4 used for the preliminary tie test.....	52
Figure 5.14 Typical mid-span cross section of ties in design group D.....	52
Figure 5.15 Notch cut at mid-span of tie D4 .....	53
Figure 5.16 Reduced cross section at notch location.....	53
Figure 5.17 Grooves added at ends of tie .....	54
Figure 5.18 Rebar caging used for preliminary tie testing.....	55
Figure 5.19 Clip gage instrumented over the notch.....	56
Figure 5.20 Test configuration for preliminary tie test.....	57
Figure 5.21 Preliminary tie test results .....	59
Figure 5.22 Comparison of actual and theoretical load-displacement curves for steel at various gauge lengths ( $E = 28,500,000$ psi) .....	61
Figure 5.23 Reduced cross section at notch location.....	63
Figure 5.24 Typical rebar cage .....	64
Figure 5.25 Test configuration for tension test of all ties except D-4 .....	65
Figure 5.26 Typical instrumentation configuration for tension test .....	65
Figure 5.27 Tension test results for tie R-4.....	66
Figure 5.28 Tension test results for tie NT-1 .....	67
Figure 5.29 Tension test results for tie CXT-1 .....	67
Figure 5.30 Tension test results for tie A-6 .....	70
Figure 5.31 Tension test results for tie B-7.....	71
Figure 5.32 Tension test results for tie D-2 .....	71

Figure 5.33 Tension test results for tie D-7 .....	72
Figure 5.34 Tension test results for tie D-8 .....	72
Figure 5.35 Tension test results for tie F-6.....	73
Figure 5.36 Tension test results for tie H-3 .....	73
Figure 5.37 Tension test results for tie K-5 .....	74
Figure 5.38 Tension test results for tie L-6.....	74
Figure 6.1 Typical dimensions of removed cover on tie R-5 .....	77
Figure 6.2 Typical dimensions of removed cover on tie NT-1.....	78
Figure 6.3 Typical dimensions of removed cover on tie CXT-1 .....	79
Figure 6.4 Gage placement on tie R-5 .....	81
Figure 6.5 Gage placement on tie NT-1.....	81
Figure 6.6 Gage placement on tie CXT-1 .....	82
Figure 6.7 Strain measurements of wires cut on tie R-5.....	84
Figure 6.8 Strain measurements of wires cut on tie NT-1 .....	85
Figure 6.9 Final strain measurement for gage 1 of tie NT-1 .....	85
Figure 6.10 Final strain measurement for gage 2 of tie NT-1 .....	86
Figure 6.11 Close up of gages 1 and 2 on tie NT-1 .....	86
Figure 6.12 Wire in bent position after cutting.....	87
Figure 6.13 Wire straightened out after cutting .....	87
Figure 6.14 Final strain measurement for gage 3 of tie NT-1 .....	88
Figure 6.15 Strain measurements from CXT 505S tie test .....	89
Figure 6.16 Bow in unstressed wire.....	91
Figure 6.17 Curvature of a wire .....	91
Figure 6.18 Wire bow test setup .....	92
Figure 6.19 Strain gages instrumented on opposite faces of wire .....	93
Figure 6.20 Strain measurements from wire bow test .....	94
Figure 7.1 Initial gage length, $L_0$ , for Method 1 measurement.....	96
Figure 7.2 Wire measuring apparatus .....	97
Figure 7.3 Length of rebar used as gage block .....	97
Figure 7.4 Smoothened wire surfaces for length measurement (bottom row).....	98
Figure 7.5 Measurement of wires in tie .....	98

Figure 7.6 Conical end piece at end of tie .....	99
Figure 7.7 Conical piece centered on the end of a wire.....	99
Figure 7.8 Micrometer measuring wire length .....	100
Figure 7.9 Extraction of wires from tie.....	101
Figure 7.10 Wires extracted from tie R-5 .....	101
Figure 7.11 Wires extracted from tie CXT-2.....	101
Figure 7.12 Clamping used to keep wires straight.....	102
Figure 7.13 Conical end piece centered on wire.....	102
Figure 7.14 Micrometer centered on wire.....	103
Figure 7.15 Wires exposed on bottom surface of tie .....	105
Figure 7.16 Wire scriber with a set 60" gage length.....	106
Figure 7.17 Wires exposed on tie for marking 60 inch gage length.....	106
Figure 7.18 Typical mark from wire scriber .....	107
Figure 8.1 Center negative bending test schematic .....	112
Figure 8.2 Flexural test setup.....	112
Figure 8.3 AREMA center negative test setup (ARMEA, 2017) .....	117

## List of Tables

Table 3.1 Description of tie design groups .....	16
Table 3.2 Typical cross-section values for existing tie designs .....	16
Table 3.3 Description of new tie designs .....	17
Table 3.4 Typical cross-section values for new tie designs .....	17
Table 3.5 Initial VWSG readings and prestress forces after detensioning .....	19
Table 4.1 Prestress force in Rocla ties prior to testing .....	32
Table 5.1 Mix A proportions for prism and preliminary tie test.....	39
Table 5.2 Mix B proportions for full-scale tie test.....	40
Table 5.3 Summary of prism test results .....	51
Table 5.4 VWSG readings before and after notching tie.....	68
Table 5.5 Adjusted prestress force estimates .....	69
Table 5.6 Comparison of prestress force results for new tie designs.....	69
Table 5.7 Summary of prestress force estimates for existing ties.....	75
Table 6.1 VWSG readings at each stages of testing .....	83
Table 6.2 Prestress force estimates from the strain gage method .....	90
Table 6.3 Comparison of prestress force, in kips, from strain gage method and VWSG readings .....	90
Table 7.1 Method 1 results for tie R-5.....	103
Table 7.2 Force per wire results from Method 1 for CXT 505S tie.....	104
Table 7.3 Summary of results from Method 1 .....	104
Table 7.4 Force per wire results from Method 2 for Rocla tie .....	107
Table 7.5 Force per wire results from Method 2 for CXT 505S tie.....	108
Table 7.6 Summary of results from Method 2.....	109
Table 8.1 Section properties and theoretical cracking moments .....	111
Table 8.2 Average center negative cracking moments .....	114
Table 8.3 Factored center negative bending-moments .....	116
Table 8.4 AREMA center negative test results.....	118

## **Acknowledgements**

I would like to thank the Federal Railroad Administration (FRA) for providing the majority of funding that made this research possible. I would also like to thank Dr. Hailing Yu at the John A. Volpe National Transportation Systems Center for her valuable suggestions and parallel analysis work. Additionally, I wish to thank the Precast/Prestressed Concrete Institute (PCI) for establishing an industry advisory panel to the project.

I would like to thank Dr. Robert J. Peterman for his help and guidance with this project. I would like to express gratitude to the other three members of my committee: Dr. Terry Beck, Dr. Hayder Rasheed, and Dr. Christopher Jones.

I would also like to recognize my fellow graduate students that helped with the research throughout this project: Robert Schweiger, Aref Shafiei, Adrijana Savic, and Aaron Robertson. Thanks to Ryan Benteman, Cody Delaney, and Benjamin Thurlow for their assistance with laboratory work throughout this project.

# Chapter 1 - Introduction

## Background

The use of prestressed concrete railroad ties in the United States has expanded as an alternative to wood ties as the railroad industry continues to become more efficient. Concrete ties are often preferred over wooden ties for longer service life, lower maintenance costs, environmental impact, durability, and ability to support high loads from large rail cars (Hanna, 1979). To achieve the high load-carrying capacity of concrete railroad ties, the ties are first prestressed.

To fabricate pretensioned concrete railroad ties, the prestressing tendons, typically indented wire or strands, are tensioned. The ties are then cast around the already-tensioned tendons and, once the concrete has cured, the tension is released. As the tension is released, the force in the tendons is gradually transferred into the tie. The length over which this transferring of the force occurs is known as the “Transfer Length” (Kaar, La Fraugh, & Maas, 1963; Gross & Burns, 1995; Peterman, Ramirez, & Olek, 2000).

For a prestressed concrete railroad tie to operate at its maximum capacity throughout its service life, the prestress force must be fully introduced into the tie prior to the location of the application of load (Murphy, 2012). As load is applied at the rail seat of a railroad tie, transfer lengths should be shorter than the distance from the end of the tie to the rail seat. With the typical distance of the rail seat from the end of the tie being 21 inches, it is imperative that transfer lengths be less than 21 inches.

Since ensuring that the prestress force is transferred prior to the rail-seat location is vital to the long-term performance of the, the research team at Kansas State University has conducted extensive research to determine the effects of concrete properties (Bodapati, et al., 2014) and

prestressing wire properties (Arnold, et al., 2013; Holste, et al. 2013) on bond and transfer lengths. Throughout this research a significant amount of data has indicated that high bonding stress between the steel and concrete can lead to longitudinal splitting cracks along the tie (Holste, et al. 2014). When longitudinal cracks are present, the full prestress force is not introduced to the tie prior to the rail seat, and the load-carrying capacity of the tie is drastically reduced. When splitting cracks occur, they often occur during the first few weeks after fabrication (Savic, 2019). However, longitudinal splitting can also lead to failure of ties installed in track (Yu, 2017).

While previous research has investigated the effects of prestressing steel and concrete properties on bond as it relates to transfer lengths, current research is now focused on how these properties relate to a tie's propensity for longitudinal splitting. In an investigation to better understand the interaction between prestressing steel and concrete that results in a durable long-term track performance, existing railroad ties that had been removed from track after 25 plus years of service were studied. These existing railroad ties remained in good condition throughout the entirety of their service life. By investigating the concrete materials, prestressing steel properties, and the level of prestress force in the existing ties, the properties that correlate to a long-term performance can be determined.

## **Objectives**

The purpose of this research program was to experimentally determine the prestress force remaining in the existing ties removed from track, and to quantify the prestress force necessary to provide a durable long-term performance in track while mitigating a tie's splitting propensity.

Four different test methods for evaluating the prestress force in a prestressed beam were investigated. Two of the methods, the flexural crack reopening and the strain gage method, have been used often throughout the literature with varying results. Two additional methods, the direct tension test and the wire extraction method, were developed as a part of this work. To determine the method that provides the best estimation of the internal prestress force, new ties instrumented with vibrating-wire strain gages were tested using each of the four methods.

Since the level of prestress force directly correlates to the level of bond stress between the prestressing steel and concrete in the end region of the ties, a reduction in prestress force would reduce the bond stress and in turn decrease the splitting propensity of a tie. However, a reduction of prestress force also results in a reduction of the tie's resistance to flexural cracking. Knowing the existing ties had sufficient capacity to handle the load demands in track, determining their prestress forces helps quantify the level of prestress force that mitigates splitting while providing optimal capacity. In this investigation, the existing ties were evaluated for their center negative cracking capacity, and these capacities were compared to current American Railway Engineering and Maintenance-of-Way Association (AREMA) design requirements.

## **Organization of Dissertation**

Chapter 2 details the existing methods that have been utilized to estimate the prestress force in prestressed concrete members. These methods include experimental and analytical approaches for estimating the prestress force in a variety of prestressed applications such as bridge girders, Euler beams, and nuclear containment facilities.

Chapter 3 describes the existing ties removed from track that were investigated in this study. Additionally, the new ties used periodically throughout the study are described.

Chapter 4 details the application of the flexural crack reopening method to the existing ties to estimate the remaining prestress force.

Chapter 5 introduces the newly-developed direct-tension test for determining the prestress force in concrete railroad. This chapter goes through the validation of the method, and the application of the test on the existing ties in the study.

Chapter 6 describes the use of the strain gage method for evaluating the prestress force in a tie.

Chapter 7 describes the method for evaluating the prestress force by measuring the change in length of wires extracted from a tie.

Chapter 8 evaluates the center negative cracking moments of the existing ties. The experimental values are compared to the current design standards outlined in Chapter 30 of the AREMA manual.

Chapter 9 discusses the conclusions made from the testing conducted throughout this investigation.

## **Chapter 2 - Literature Review**

Over time, prestressed concrete members experience a loss of prestress force. While the loss of prestress force has minimal effect on the ultimate capacity of a member, underestimating prestress losses in design can lead to pre-mature cracking and larger service-load deflections. Additionally, over estimating prestress losses results in an inefficient design and higher camber in members with eccentric prestress force. Losses in prestressed members over time are caused by concrete creep, an increase in strain under a sustained load, shrinkage, the volumetric change of concrete as moisture is lost from the concrete, and relaxation of prestressing steel, where the stress in the steel decreases over time while held at constant strain. To ensure proper design and performance conditions in service, several previous investigations have focused on estimating the prestress force either experimentally or through modeling. Below are descriptions of some of the more common methods used to determine the prestress losses and the remaining prestress force.

### **Estimated Prestress Loss**

Several models have been proposed for estimating the prestress losses due to creep, shrinkage, and relaxation. More common approaches for estimating the prestress loss are described in the PCI Design Handbook (2010), and in the AASHTO LRFD Specification (2012). Additionally, several more advanced time-step analyses have been proposed for estimating prestress loss including ones from Tadros, Ghali, & Bilger (1977), and Swartz (2010). The method outlined in the PCI Design Handbook is a simple method where losses due to the effect of elastic shortening, creep, shrinkage, and relaxation are calculated and added together for a total loss. Factors included in the PCI method include the initial (at time of prestressing) and 28-day

modulus of elasticity for concrete, the size of the member, average relative humidity, and initial losses due to anchorage seating and friction. The PCI method is based on a method proposed by Zia et al. (1979), and is used primarily for building applications. For specialized cases, PCI recommends a more in depth method for estimation of prestress losses.

The AASHTO LRFD Bridge Design Specification presents a refined method for estimating prestress losses based on the research of Tadros et al. (2003). This method is predominantly used for the application of bridge girders but can be applied to other prestress members. The AASHTO method separates loss calculations into two different time intervals, with the first between the transfer of prestressing steel and placement of the bridge deck, and the second interval is for a time beyond the pouring of the bridge deck. The AASHTO method also accounts for losses due to elastic shortening, friction, anchorage set, and both short and long term effects of creep, shrinkage, and relaxation. This method is applicable only for normal weight concrete and considers factors such as the size and shape of the member, humidity, and the age and maturity of the concrete.

## **Instrumentation**

One of the more accurate ways to monitor the prestress force and prestress losses in a prestressed beam is by instrumenting them with either vibrating-wire strain gages (VWSGs) or fiber optic cables. Using this instrumentation is advantageous in that the nature of determining the prestress force is non-destructive, and that they are not single use equipment, so the losses can be tracked over time. The biggest drawback of this method is that the instrumentation must be installed prior to actually casting the beam.

To determine the prestress force from VWSG readings, gages are typically installed at the prestressing steel centroid once the steel has been tensioned, and an initial gage reading is taken. Readings after the steel is detensioned can be used along with the initial reading to determine the change in strain between the two states. Next, the change in steel stress is determined by multiplying the change in strain by the Modulus of Elasticity of the prestressing tendons. This method assumes there is perfect bond between the concrete and steel prestressing tendons.

VWSGs are able to measure the strain accurately through the vibration of small tensioned steel wire inside the gage. Coils close to the wire are subjected to a pulse with a varying frequency, causing the wire to vibrate at its resonant frequency (Geokon). As the gage is subjected to strains, the tension in the steel wire changes, as does the resonant frequency of the wire. This change in resonant frequency can be used to determine the strain the gage was subjected to. Geokon, a VWSG manufacturer, provides Equation (1) for calculating the change in strain,  $\Delta\mu\epsilon$ . The change in strain is taken as the difference between the current and initial readings,  $R_1$  and  $R_0$ , respectively, where  $B$  is the batch factor, which is an adjustment for small changes to the length of the steel wire during manufacturing, and is provided by the supplier of the gage. Due to the difference in the coefficient of expansion between steel,  $C_1$ , and concrete,  $C_2$ , the gage experiences temperature induced strains. For this reason, most VWSGs are equipped with a thermistor, and the change in strain calculated in Equation (1) is corrected by multiplying the difference of the coefficient of expansion for steel and concrete by the difference between the current and initial temperature readings,  $T_1$  and  $T_0$ , respectively (Geokon). In an experiment that compared various experimental methods for evaluating prestress loss in concrete bridge girders, Baran et al. (2005) concluded that the use of VWSGs was the most effective method, while

noting there is a small stress change in the tendons between the initial tensioning, and the time the gage is installed and zeroed, that should be accounted for.

$$\Delta\mu\varepsilon = (R_1 - R_o)B + (T_1 - T_o)(C_1 - C_2) \quad (1)$$

Several cases exist where fiber optic cables have been placed in concrete structures for the purpose of structural health monitoring. De Vries et al. (1997) used optical fiber sensors for the non-destructive evaluation of column to beam connections in a concrete structure, and to monitor the strain of composite prestressing tendons. Xuan et al. (2009) have implemented fiber optic cabling in a large scale sewage treating tank to monitor the prestress loss over time. To monitor the prestress force, Xuan attached a reflector to the prestressing strands in the sewage tank. One optical fiber is used to send light from a laser to the reflector, which is reflected back to a photoelectronic checker, and another optical fiber is used to send a reference of the initial laser light. As the strain of steel tendon changes, the intensity of the reflected light changes with a linear response. The change in the intensity of the reflected light is then converted into a corresponding change in stress in the tendons.

### **Structural Dynamic Response**

The relation between the prestress force in a beam and the beam's response to dynamic excitation have been investigated as a way to directly measure the prestress force in a beam in a non-destructive manner. Abraham et al. (1995) attempted to measure prestress loss using a damage index based on the derivatives of mode shapes, but found that as prestress force is lost, the mode shapes remain almost identical. Saiidi et al. (1994) observed that changes in the

prestress force effect the modal frequencies for lower modes, but higher vibration modes are less sensitive to the prestress force. Kim et al. (2004), Law and Lu (2005), and Lu et al. (2008) used changes in the natural frequency to identify prestress loss using an inverse problem formulation. In the formulation, modal superposition was used to formulate the equation of dynamic equilibrium for a given prestress force under the assumption of a constant prestress force throughout the beam. The equation was then inverted such that the prestress force could be solved for using measured displacements.

Law and Lu (2005) formulated the dynamic response using the Euler-Bernoulli beam model, and ran numerical simulations to estimate the prestress force. Beams were subjected to simulated sinusoidal, and impact loading. Displacements were measured over a duration of time at several locations along the beam. The measurements were then used to calculate the prestress force at each time step in the simulation. While the calculated value of the prestress force was constantly changing, it was observed to oscillate around the actual value, and a least-squares method was used to determine the prestress force. The numerical simulations predicted the force in the beam with a minimum error of 21.6%.

Lu et al. (2008) conducted a similar formulation and numerical simulation, but instead modeled the beam as a Timoshenko beam. Using the formulation derived for a Timoshenko beam, the minimum error from the numerical solutions reduced to 17%. Lu et al. also conducted an experiment on a beam concentrically prestressed with a seven-wire strand in an ungrouted duct. Modal tests were run, both prior to, and after tensioning the strand to establish the natural frequencies. Strain gages were instrumented along the bottom of the beam, and the beam was excited with an impulse load. Strain measurements were recorded for the first one second of response for use in the formulation. A load cell attached to the strand indicated a prestress force

of 162.7 kN, and the estimated force from the modeling was 148.3 kN, resulting in an error of 8.9%. This verified the feasibility of measuring the prestress force in a beam based from its dynamic response.

## **Dynamic Relaxation**

Otter et al. (1966) defines dynamic relaxation as system of stress analysis that is applicable to continuous structures in either one, two, or three dimensions. The governing equations for dynamic relaxation are derived using the equations for elastic isotropic materials. The stress-strain relations of an element while in motion are considered separately from the dynamic equilibrium equations of the element. A viscous damping term is included in the equilibrium equation and a finite difference solution is used for the two equations. Otter et al. (1966) derives the one dimensional formulation in an example of a rod subjected to dynamic tension. The rod is divided into multiple elements with the initial boundary conditions of displacements and velocities are zero at a time of zero. Stresses are calculated for small increments of time, and used to calculate new displacements and velocities. After enough iterations, the solution converges to have the resulting stresses and displacements. This simple example yields results equivalent to the application of Hooke's law, but the same formulation can be applied to more complex problems.

The basic example provided above is the basis of using dynamic relaxation to determine the prestress force in a tendon. Prestressing tendons of a beam are exposed at some distance past the transfer length, and instrumented such that the strain is recorded as the tendons are cut. The application of strain gages to the exposed tendons in bridge beams has been used by Halsey and Miller (1996), Labia et al. (1997), and Baran et al. (2005), with mixed results. Halsey and Miller

(1996) observed that this method resulted in higher estimations of prestress loss when compared to other methods. In an experimental study conducted by Baran et al., prestress losses measured using the strand cutting method were 1.5 times larger than losses measured using vibrating-wire strain gages. Czaderski and Motavalli, (2006) used a mechanical strain gage called a deformer to measure strain changes and evaluate the scatter in strain of prestressing tendons in bridge girders. They observed that when a tendon was cut, there was minimal strain redistribution between uncut tendons. They concluded that the prestress forces measured using this method were in good agreement with calculated prestress force after losses. Additionally, Remennikov and Kaewunruen (2014) used strain gages on exposed tendons to estimate the prestress force in concrete crossties. Their results indicated that the prestressing force in the tie was lower than expected, containing only 40% of design prestress after losses.

### **Flexural Cracking**

A common method used for experimentally determining the remaining prestress force in bridge girders removed from service, is through monitoring cracking during flexural tests. Using either the flexural crack initiation load or the crack reopening load, the prestress force can be back calculated using statics.

In the case of the flexural crack initiation method, the stress in the bottom fiber is equal to the modulus of rupture of concrete. The flexural crack initiation load may be determined using several methods. Labia et al. (1997) compared the crack initiation load of 20 year old box girders from visual inspection, the use of crack detection gages, accelerogram, and by calculating the cracking moment using measured material properties. Visual inspection was seen to over-estimate the cracking load, as the cracks are difficult to see until they have opened wide enough.

Crack detection gages were found to be not suitable for detecting crack initiation, but rather they could only capture crack propagation. The accelerogram provided the best crack initiation detection, with spikes in the readings occurring at applied moments that were reasonably close to the calculated cracking moments.

Baran et al. (2005) also used visual inspection and crack detection gages for determining the crack initiation load of prestressed bridge girders, as well as strain gages on the bottom surface. Similarly, visual inspection tended to over-estimate the cracking load. The crack detection gages gave inconsistent results from test to test, occasionally predicting crack initiation loads higher than those determined from visual inspection. The strain gages on the bottom surface were used to monitor the tensile strain on the bottom surface during loading. The crack initiation load was able to be consistently determined through the variation in strains between the gages.

As the previous method depends on experimentally the crack initiation load, it is necessary that the beams are initially un-cracked. Since much of literature focuses on testing of girders removed from service and an un-cracked beam may not be the case, the crack reopening method was used in the current study. This method consists of loading beams until flexural cracking is observed, then reloading the beams and monitoring the cracks to determine the load at which the crack re-opens, or the decompression load. Unlike the crack initiation method, the crack reopening method does not depend on the tensile strength of the concrete as the moment the crack re-opens corresponds to zero stress at the bottom fiber.

To determine the decompression load, instrumentation is placed on the bottom of the beam to measure crack opening displacements (COD). Curves of load-versus-COD tend to exhibit a bilinear profile, which is used to estimate the decompression load. Rabbat (1984),

Halsey and Miller (1996), and Labia et al. (1997) have taken the decompression load to be the load corresponding to the intersection point of the tangents of the two linear portions of the curve. Finite element modeling conducted by Lundqvist (2012) showed that the intersection method can significantly over predict the decompression load. Pessiki et al. (1996), Baran et al. (2005), and Larson et al. (2005) used the load at the end of the initial linear portion as the decompression load.

The ability to determine the decompression load from these curves is greatly influenced by the instrumentation used to monitor the cracks. Pessiki et al. (1996) and Baran et al. (1996) use strain gages mounted on either side of the crack. In both cases, decompression loads were able to be determined from some, but not all of the tests conducted. Pessiki reported that in some cases, the load vs strain curves were not distinct enough to determine the load, and Baran thought the presence of multiple cracks and the order in which cracks opened would change the strain readings captured by the gages. Pessikki et al. (1996), Labia et al. (1997), Baran et al. (2005), and Larson et al. (2005) have measured the COD through the use of LVDTs instrumented over the cracks, and Halsey and Miller (1996) instrumented a clip gage over the crack. The measurement of the opening of an individual crack creates a more distinct bilinear curve than compared to the use of strain gages.

In a comparison of the flexural crack initiation and crack reopening methods, Baran et al. (2005) conducted testing on girders instrumented with vibrating-wire strain gages. When compared to prestress losses determined from the vibrating-wire strain gages, the results of both methods drastically over-predicted the loss of prestress, or under-predicted the remaining prestress force, with the crack initiation method having the larger error.

## Chapter 3 - Tie Description

The ties investigated as a part of this study included 25+ year old ties that were removed from track and where the initial prestress force is unknown, and newer ties with a known initial prestress force. The new ties were never in track and were stored at Kansas State University (KSU) since they were manufactured. Prior to any destructive testing, each tie was evaluated for any existing damage such as cracking and abrasion. Each tie was scanned using a Creaform HandySCAN 700 non-contact scanner to obtain a 3-D model similar to that in Figure 3.1. The models were “sliced” at 0.5 inch intervals to generate cross-sections. For each cross-sectional slice, the area, neutral axis location, eccentricity of the wire centroid, and the area moment of inertia were calculated.

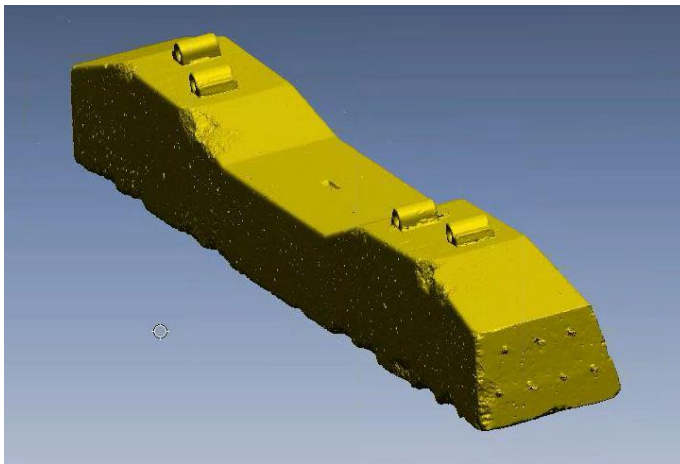


**Figure 3.1 Typical 3-D model of a tie obtained from scanning**

### Existing Ties Removed from Track

The existing ties used in this portion of the study were obtained from the crosstie graveyard at the Transportation Technology Center, Inc. (TTCI) in Pueblo Colorado (shown in Figure 3.2), and also from Amtrak after removal from service. Ties at the graveyard had been

subjected to in-track heavy-haul loading for over 25 years and contained varying degrees of damage. Ties selected for this portion of the study were still in good condition (i.e. minimal cracking and abrasion) after being removed from track.



**Figure 3.2 Crosstie graveyard at TTCI in Pueblo, Colorado**

Twelve different tie designs varying in geometry, type of tendon, and number of prestressing tendons, were selected. At least six ties of each tie design were obtained. For identification, each tie was assigned a letter and a number (e.g. A-1), where the letter indicates which of the 12 different design groups the tie belongs to, and the number distinguishes between the different ties of that design group. Pictures of each tie design and typical mid-span cross-sections are presented in Appendix A. Table 3.1 details the type and number of prestressing tendons for each design group and lists the manufacturer of the tie. Typical values of the area,  $A$ , neutral axis location from the bottom surface of the tie,  $y_b$ , moment of inertia,  $I$ , and eccentricity of the wire centroid,  $e$ , at the rail seat and center of tie are listed in Table 3.2 for each design group.

**Table 3.1 Description of tie design groups**

Tie Design	Manufacturer	Tendon Type	Indentations	No. of Tendons	Diameter
A	ITISA	Wire	Non-indentated	4	0.415 in.
B	Abetong	Strand	Non-indentated	7	0.375 in.
C	Florida East Coast (F.E.C.)	Strand	Indented	6	0.375 in.
D	Santa Fe/San Vel	Strand	Indented	8	0.375 in.
E	CXT 497S	Wire	Indented	18	5.30 mm
F	Con-Force Costain	Wire	Indented	26	4.86 mm
G	Koppers	Strand	Indented	8	0.385 in.
H	Rocla	Wire	Indented	24	4.97 mm
J	Rocla	Wire	Indented	24	4.94 mm
K	Costain	Wire	Indented	24	4.95 mm
L	CXT	Wire	Indented	28	4.97 mm
M	Rocla	Wire	Indented	28	5.02 mm

**Table 3.2 Typical cross-section values for existing tie designs**

Tie Design	Rail Seat (average of both sides)					Center				
	A (in <sup>2</sup> )	y <sub>b</sub> (in)	I (in <sup>4</sup> )	e (in)	H (in)	A (in <sup>2</sup> )	y <sub>b</sub> (in)	I (in <sup>4</sup> )	e (in)	H (in)
A	93.3	4.50	628	0.97	9.13	58.9	3.48	235	-0.05	7.05
B	91.9	4.77	690	1.01	9.88	70.6	3.59	293	-0.17	7.36
C	79.2	4.05	382	0.64	7.95	59.6	3.13	163	-0.28	6.06
D	96.2	4.87	703	0.77	9.69	73.0	3.67	298	-0.43	7.20
E	79.5	4.33	474	0.88	8.66	61.5	3.49	224	0.04	6.85
F	73.2	4.09	367	1.50	8.27	52.0	2.99	126	0.40	5.67
G	79.4	4.09	401	0.60	8.03	71.4	3.64	288	0.15	7.24
H	84.0	4.55	516	0.71	8.94	68.3	3.63	273	-0.21	7.05
J	73.2	4.25	390	1.06	8.23	59.6	3.48	204	0.30	6.57
K	88.9	4.48	552	0.89	8.98	71.0	3.61	274	0.03	7.20
L	74.3	4.12	379	0.91	8.19	57.4	3.35	169	0.14	6.38
M	74.3	4.04	389	0.72	8.07	60.7	3.25	203	-0.07	6.34

### New Tie Designs

The new ties included in the study were recently manufactured using current designs, and had never been placed in track. The new ties consisted of six heavy haul Vossloh 101L ties manufactured by Rocla, two heavy haul turnout ties by Nortrak, and two CXT 505S ties. The new ties were labeled R-1 through R-6 for the Rocla ties, NT-1 and NT-2 for the Nortrak ties,

and CXT-1 and CXT-2 for the CXT ties. The number of prestressing tendons, initial prestress force, and the manufacturing year for each tie is listed in Table 3.3. The new ties underwent the same 3-D scanning process as the existing ties prior to any destructive testing. Typical cross-sectional parameters at the rail-seat and center locations for each design are listed in Table 3.4.

**Table 3.3 Description of new tie designs**

Manufacturer	Year Manufactured	Tendon Type	No. of Tendons	Indentations	Diameter	Initial Prestress* (kips)
Rocla	2016	Wire	18	Indented	5.25 mm	123.7
Nortrak	2014	Wire	24	Indented	5.32 mm	168.0
CXT	2011	Wire	20	Indented	5.32 mm	140.0

\*After jacking and seating losses

**Table 3.4 Typical cross-section values for new tie designs**

Tie Design	Rail Seat (average of both sides)				Center			
	A (in <sup>2</sup> )	y <sub>b</sub> (in)	I (in <sup>4</sup> )	e (in)	A (in <sup>2</sup> )	y <sub>b</sub> (in)	I (in <sup>4</sup> )	e (in)
Rocla	82.5	4.34	516	0.46	65.8	3.37	253	-0.52
NT	109.1	5.16	963	-0.52	109.6	5.17	975	-0.51
CXT	88.3	4.69	646	0.67	60.0	3.88	289	-0.15

At the time of manufacturing, the Rocla and Nortrak ties were instrumented with VWSGs at the wire centroid at the center of the tie, as shown in Figure 3.3 and Figure 3.4, respectively. Initial VWSG readings taken prior to detensioning, along with the known initial prestress force, can be used with subsequent readings to determine the prestress force in the tie at any time. For determining prestress force from VWSG readings, the prestressing tendon modulus of elasticity was assumed to be 28,500 ksi. Initial readings and prestress forces (after detensioning) for ties instrumented with VWSGs are listed in Table 3.5.

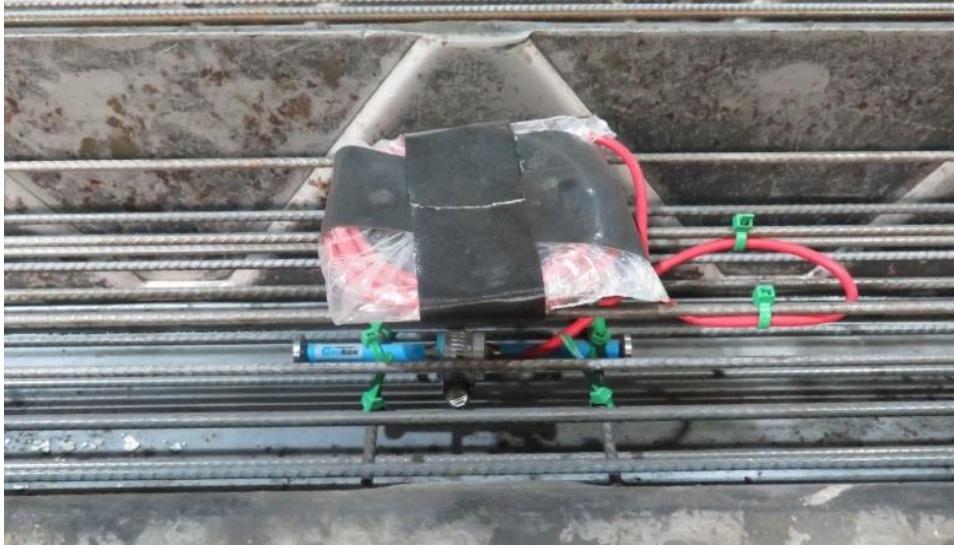


**Figure 3.3 VWSG installed at center of a Rocla tie**

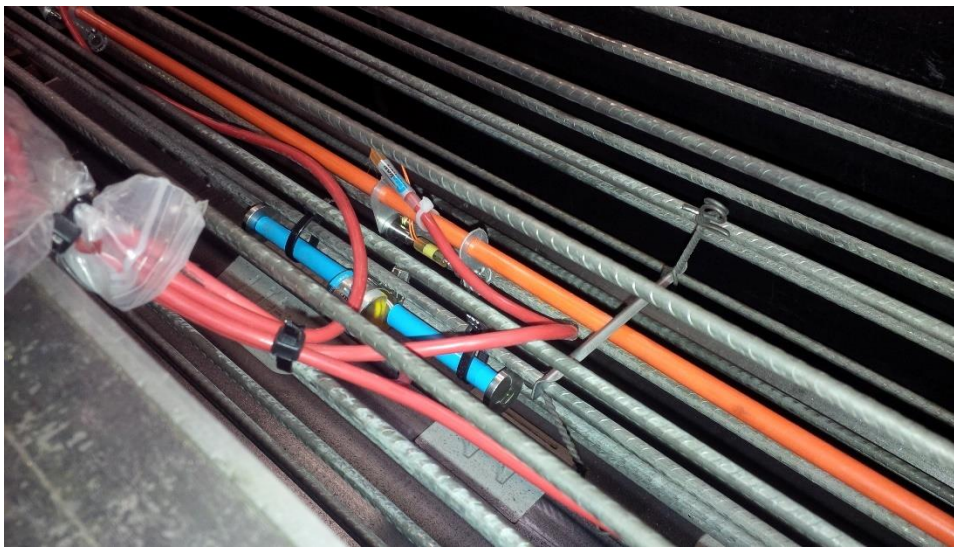


**Figure 3.4 VWSG installed at center of a Nortrak tie**

**Table 3.5 Initial VWGS readings and prestress forces after detensioning**

Tie	Jacking Stress* (ksi)	Before Detensioning		After Detensioning		$\Delta$ Strain ( $\mu\epsilon$ )	$\Delta$ Stress (ksi)	After Detensioning	
		R <sub>0</sub> ( $\mu\epsilon$ )	T <sub>0</sub> (°C)	R <sub>1</sub> ( $\mu\epsilon$ )	T <sub>1</sub> (°C)			Stress (ksi)	Prestressing Force (kips)
R-1	204.7	3549.0	50.9	3021.2	49.9	-519.4	-14.8	189.9	114.7
R-2	204.7	3554.3	53.7	3085.1	52.7	-462.0	-13.2	191.6	115.7
R-3	204.7	3489.2	54.5	3048.5	53.4	-434.3	-12.4	192.4	116.2
R-4	204.7	3622.6	54.2	3165.8	53.1	-450.1	-12.8	191.9	115.9
R-5	204.7	3646.9	29	31469	28.7	-490.7	-14.0	190.8	115.2
NT-1	203.2	3414.9	41.8	2989.3	35.7	-426.3	-12.1	191.0	158.0
NT-2	203.2	3391.9	42.5	2656.0	19.6	-764.2	-21.8	181.4	150.0

\*After seating losses

A summary of all the ties investigated in this study and the different test methods they were subjected to throughout this project is provided in Appendix B.

## Chapter 4 - Flexural Crack Reopening

This chapter discusses the application of the flexural crack reopening method, described in Chapter 2, to evaluate the remaining prestress force in a railroad tie. A minimum of three ties from each tie design group were investigated. Considering equilibrium at the extreme tension fiber when a tie is subjected to flexure, the prestress force,  $P_e$ , can be calculated using Equation (2), where  $A$  is the cross-sectional area,  $I$  is the area moment of inertia,  $e$  is the eccentricity of the wire group centroid,  $y_t$  is the distance from the neutral axis to the extreme fiber in tension,  $M$  is the applied moment, and  $\sigma_t$  is the tensile stress in the concrete. As stated in Chapter 2, if the tie is first pre-cracked and then reloaded,  $\sigma_t$  is equal to zero when the crack reopens. In this method, the ties are first pre-cracked, then reloaded to determine the load at which the crack reopens. Using this load along with the geometrical parameters for each tie listed in Chapter 3, the prestress force becomes the only unknown value in Equation (2) and, rearranging for  $P_e$ , can be calculated from Equation (3).

$$-\frac{P_e}{A} + \frac{P_e e y_t}{I} + \frac{M y_t}{I} = \sigma_t \quad (2)$$

$$P_e = -\frac{M y_t A}{A e y_t - I} \quad (3)$$

### Flexural Test Setup

Ties were tested up-side down and simply supported at the rail seats, inducing center negative bending when loaded. This was done to initiate flexural cracking on the top (form-cast side) of the ties where the surface is smooth, and cracks are easier to observe during testing than

on the bottom surface. A 15 inch spreader beam was used to load the ties in four-point bending, shown schematically in Figure 4.1, creating a constant-moment region at the center of the tie where flexural cracking initiated. Two Linear Variable Differential Transformers (LVDTs) were used (one on each side of the tie) at mid-span for deflection measurement. The typical flexural test configuration is shown in Figure 4.2.

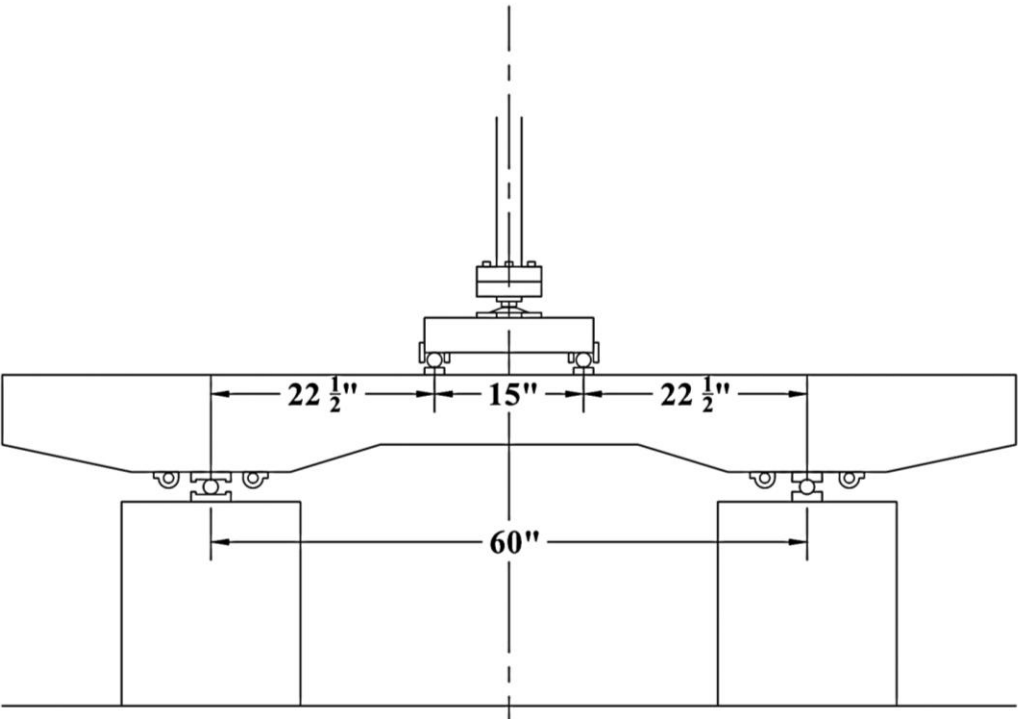


**Figure 4.1 Schematic of four-point flexural test**



**Figure 4.2 Typical flexural configuration**

The ties were loaded at a rate of 1,000 pounds per minute using a 50-kip-capacity hydraulic actuator and MTS servo-hydraulic controller. Load was applied until flexural cracking within the constant moment region was visually observed under flood lighting. Once cracking was observed, the load was held constant, and the crack was marked on the top (as-tested bottom surface) of the tie.

After flexural cracking had initiated, the ties were subjected to cyclic loading for 200 cycles at 0.5 Hz. The load was cycled between a peak load equal the observed cracking load, and a minimum load of 200 pounds. The 200-pound lower limit was set such that the load was low enough to allow cracks to fully close, but high enough so that the actuator remained in contact with the spreader beam during cycling.

Cyclic load has been shown to reduce the effects of aggregate interlock during crack reopening by smoothing out the surfaces at the crack interface (Larson, 2005). This results in the curves of load-versus-COD to have a more pronounced knee bend at the crack reopening load.

To evaluate the effects of the number of cycles on the crack opening, a test was conducted on a tie where the crack opening displacement was measured after cycle counts of 200, 400, 600, 800, 1,000, and 2,000. It was observed from testing that after 200 cycles there was minimal effect on the shape of the curve.

Next, an MTS Model 632.02F-20 clip gage was mounted over the previously marked crack to measure the crack opening displacement. The clip gage was mounted on thin knives that were superglued to the tie with a 0.2 inch gage length centered about the crack, shown in Figure 4.3. The knives are 0.068 inches thick, allowing the clip gage to be mounted close the surface of the tie while measuring the crack opening displacement. The ties were then loaded once more at a rate of 1,000 pounds per minute and the crack opening displacement was measured.

Measurements of the crack opening displacement and mid-span deflection were captured at five pound intervals using an MTS FlexTest Controller and the MultiPurpose TestWare 793 software.



**Figure 4.3 Clip gage instrumented over crack**

## Flexural Test Results

For each tie tested, the load was plotted against the crack opening displacement. Figure 4.4 shows the load vs COD results for one tie from each design group. Results for the individual design groups A-M are presented in Figure 4.5 through Figure 4.16, respectively. Variations in the cracking behavior between ties of the same design group can be observed from the test results. In each case, prior to crack opening, there is a linear relation between load and the COD. As the crack begins to open, the relation between the load and the displacement diverges from the initial linearity. The crack reopening load,  $P_{cr}$ , was estimated from these curves, and the corresponding bending moment,  $M$ , was calculated from Equation (4). The actual bending moment would also include moment due to self-weight, but the contribution of self-weight was found to be small and was neglected for in this study. Then, the bending moment from Equation (4) was plugged into Equation (2) to calculate the remaining effective prestress force.

$$M = \frac{P_{cr}}{2} (22.5") \quad (4)$$

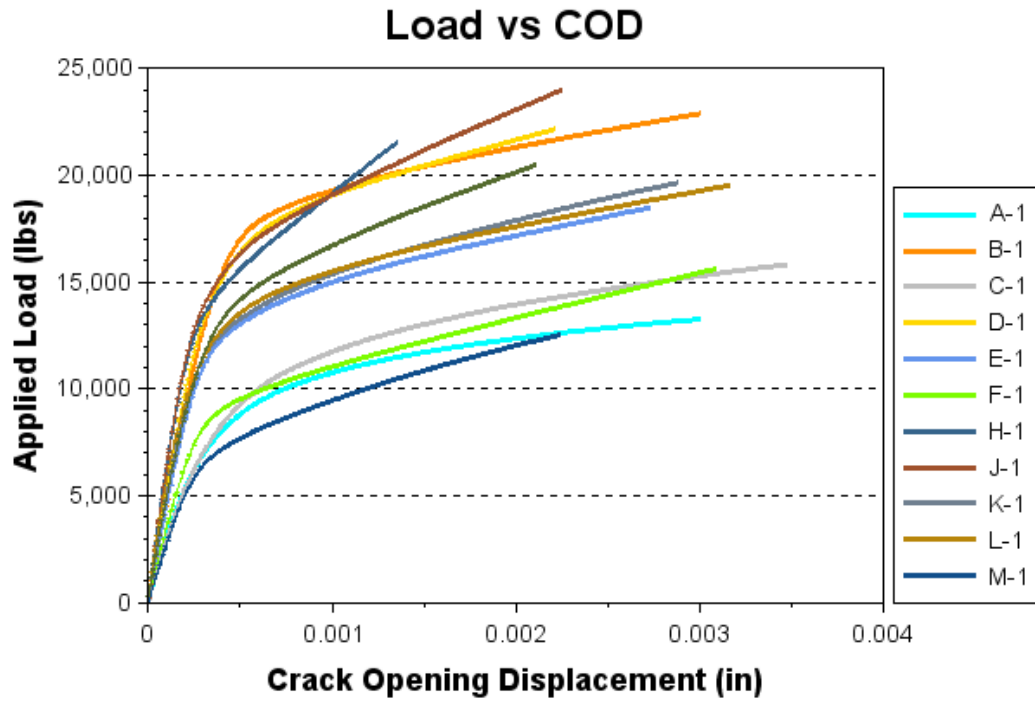


Figure 4.4 Comparison of Load vs COD results for each design group

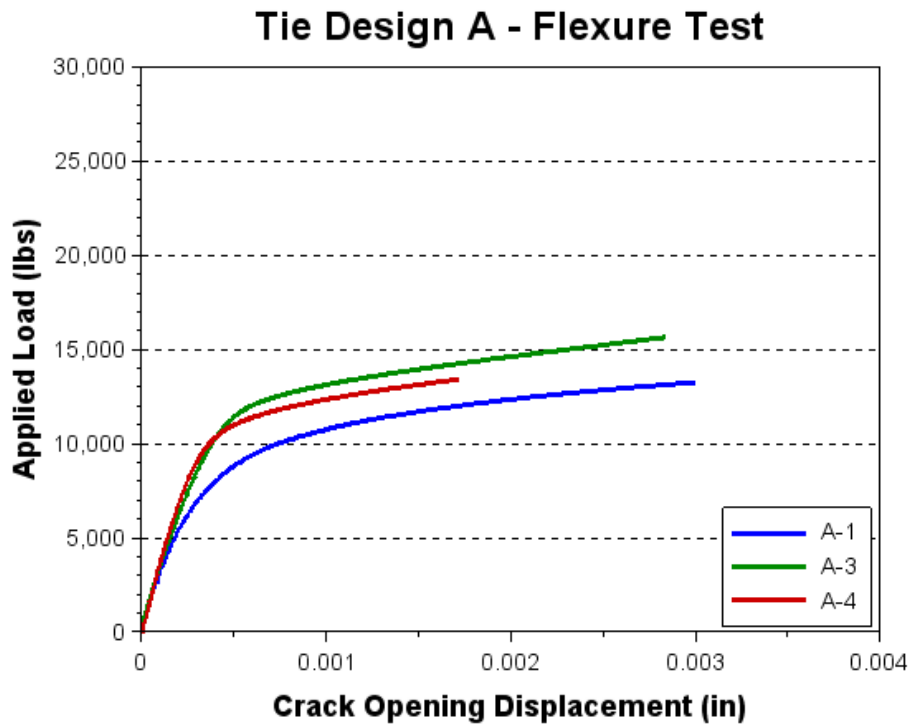


Figure 4.5 Load vs COD for tie design group A

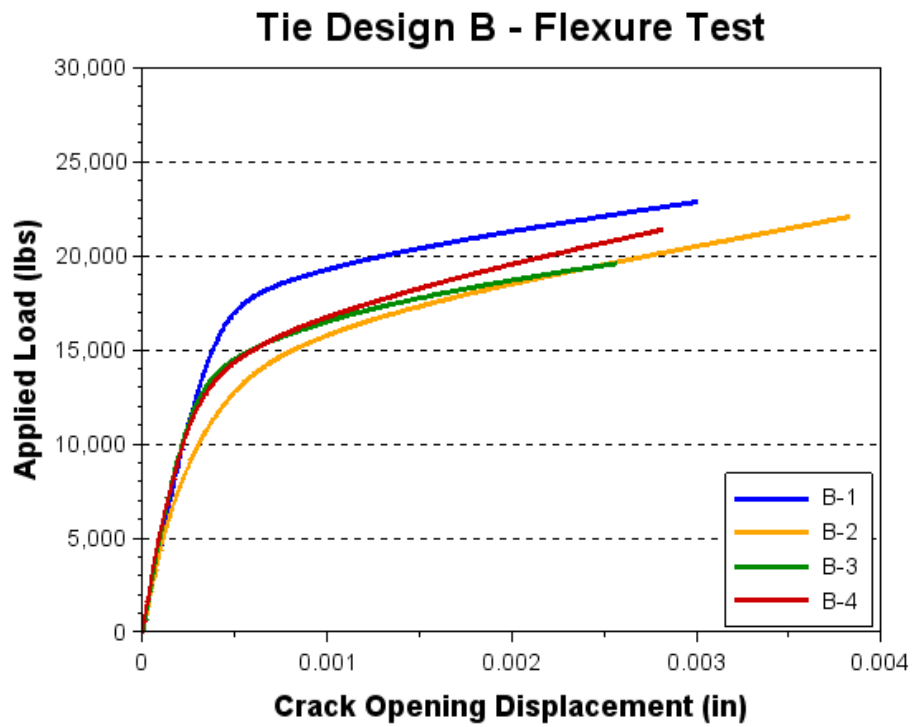


Figure 4.6 Load vs COD for tie design group B

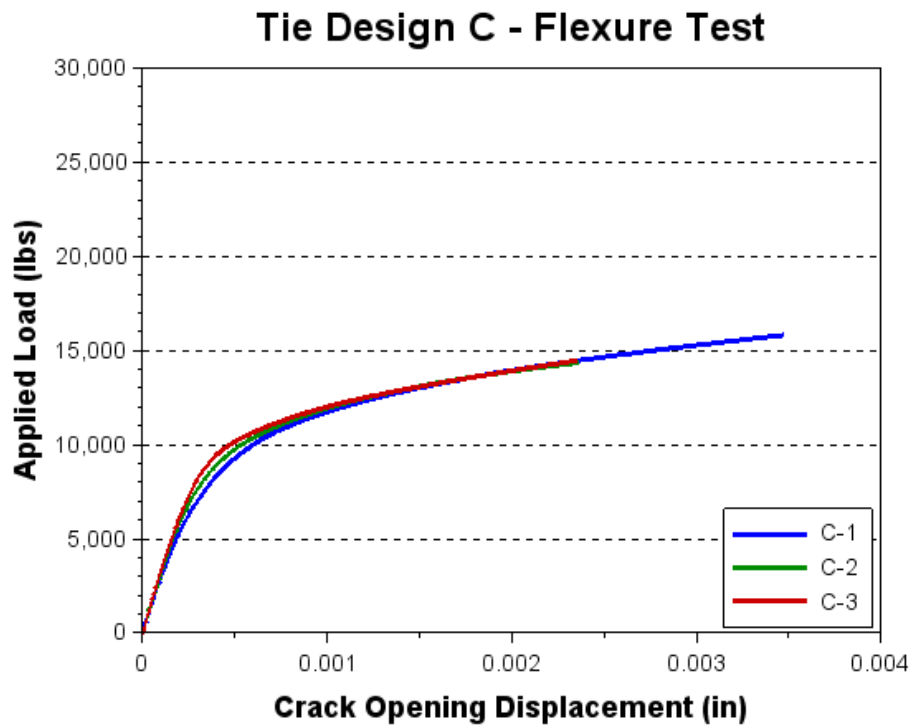


Figure 4.7 Load vs COD for tie design group C

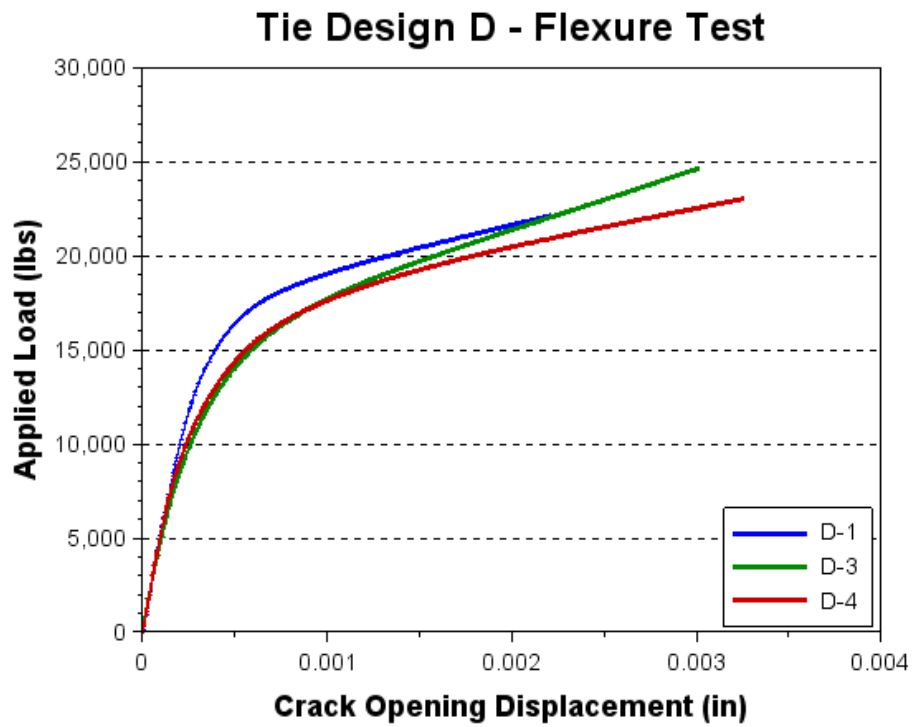


Figure 4.8 Load vs COD for tie design group D

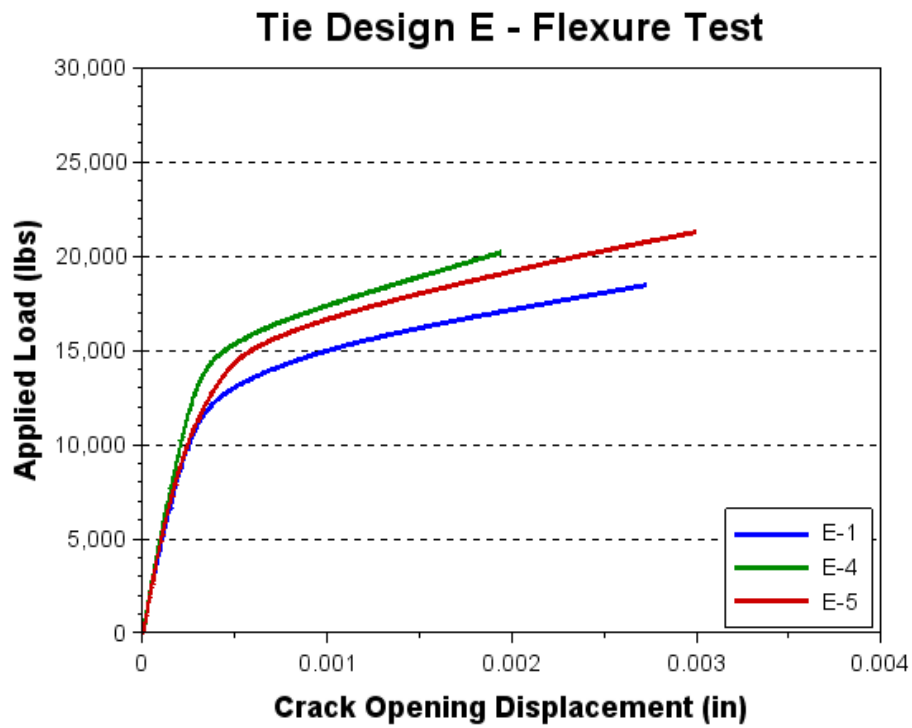


Figure 4.9 Load vs COD for tie design group E

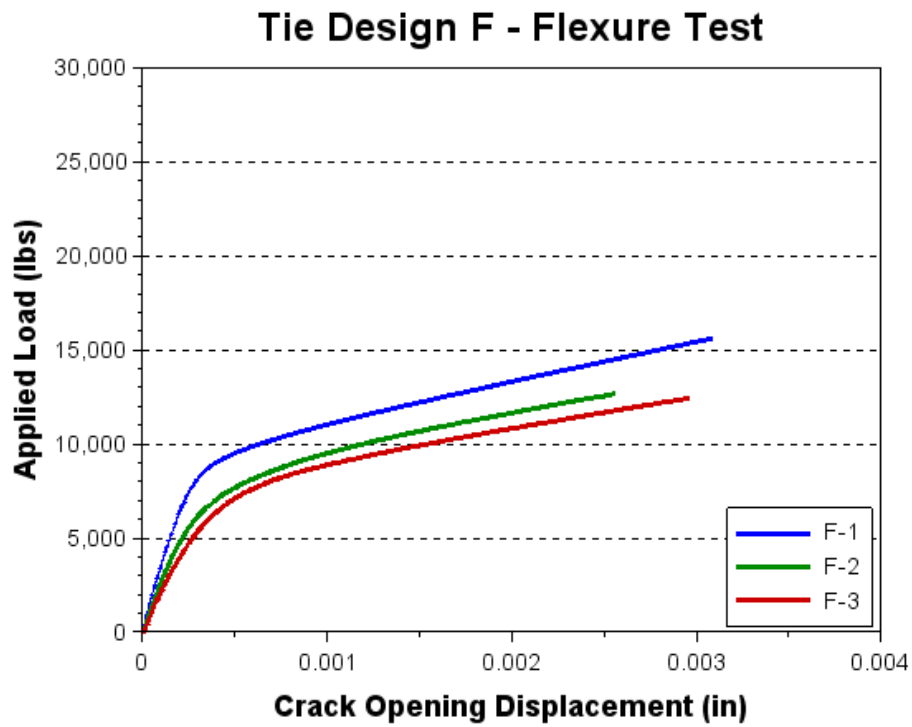


Figure 4.10 Load vs COD for tie design group F

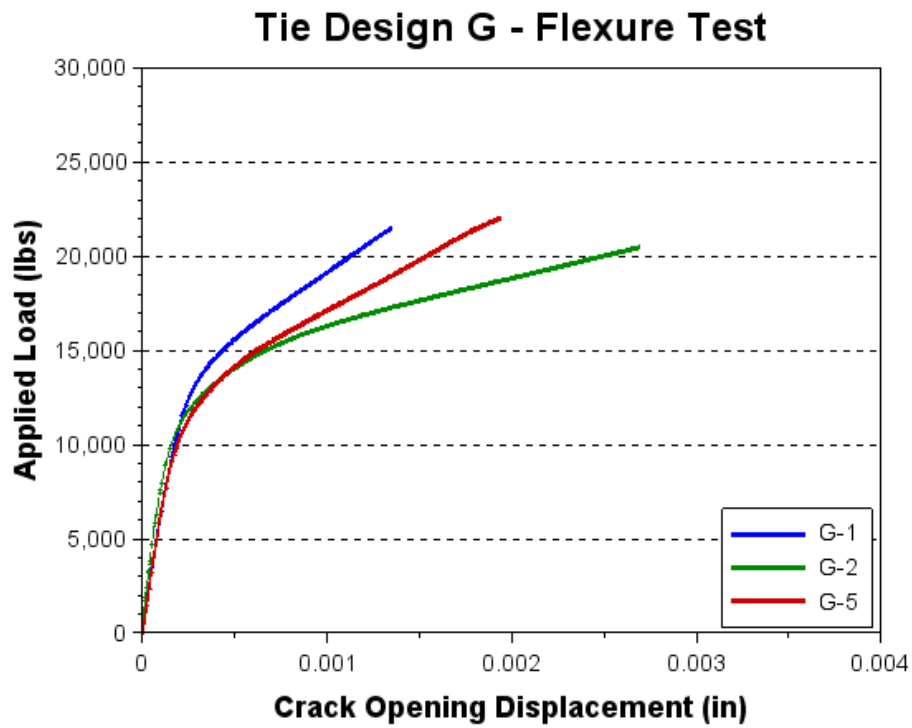


Figure 4.11 Load vs COD for tie design group G

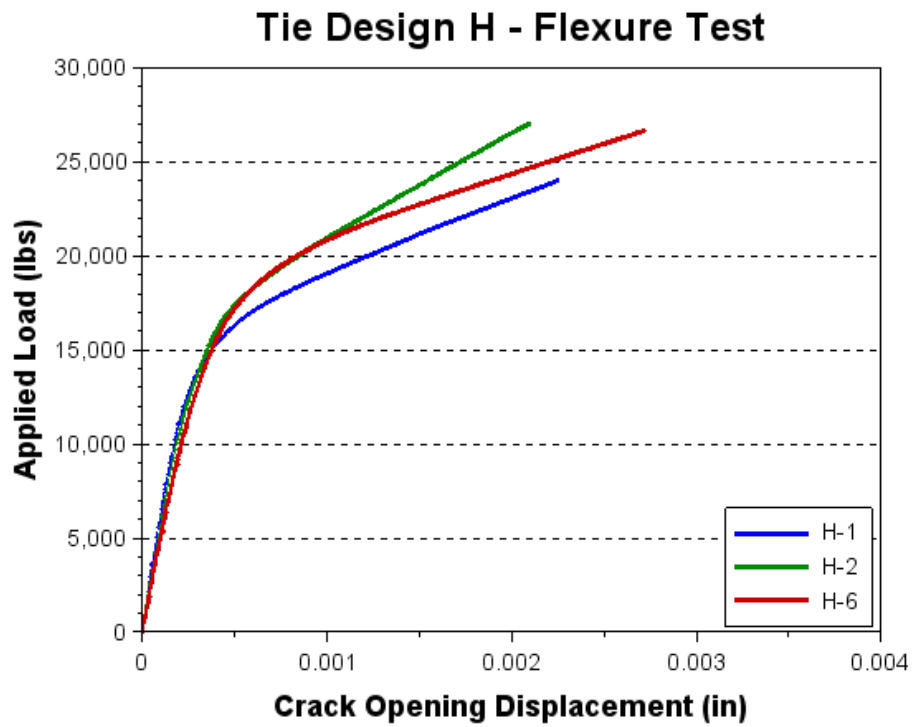


Figure 4.12 Load vs COD for tie design group H

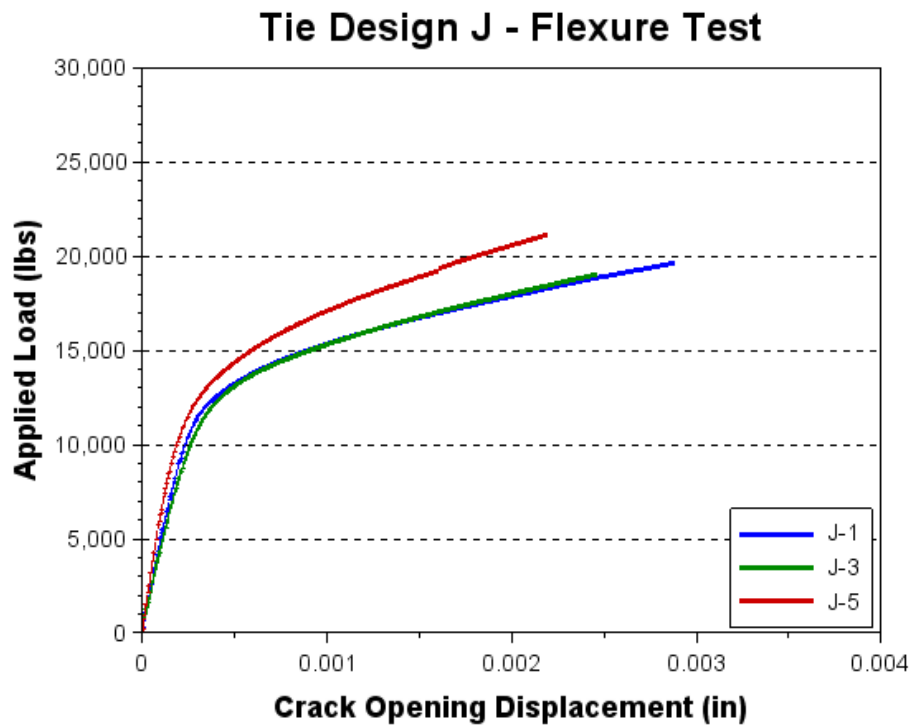


Figure 4.13 Load vs COD for tie design group J

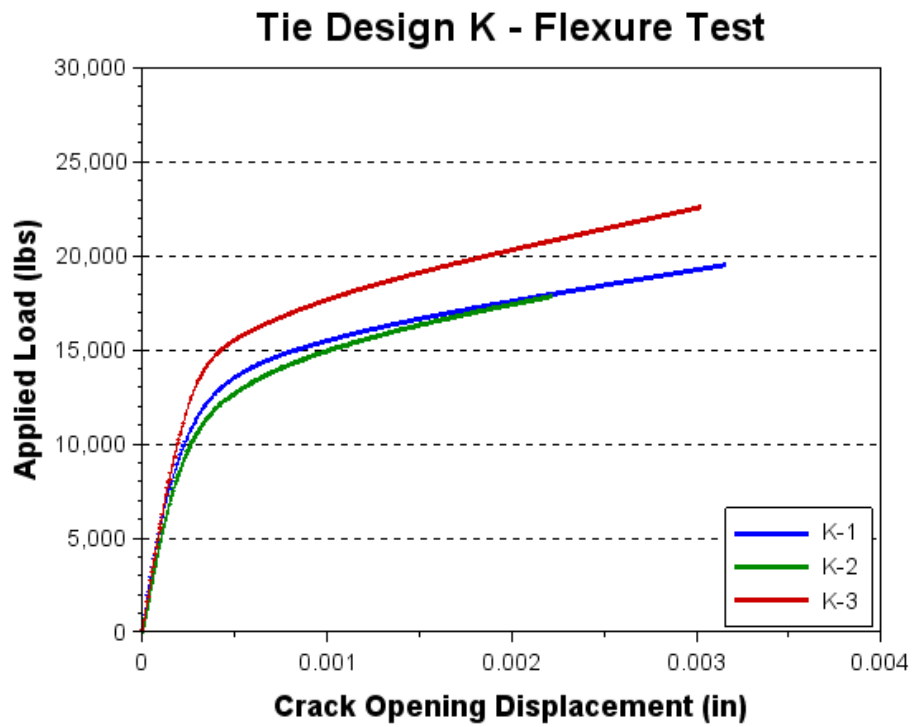


Figure 4.14 Load vs COD for tie design group K

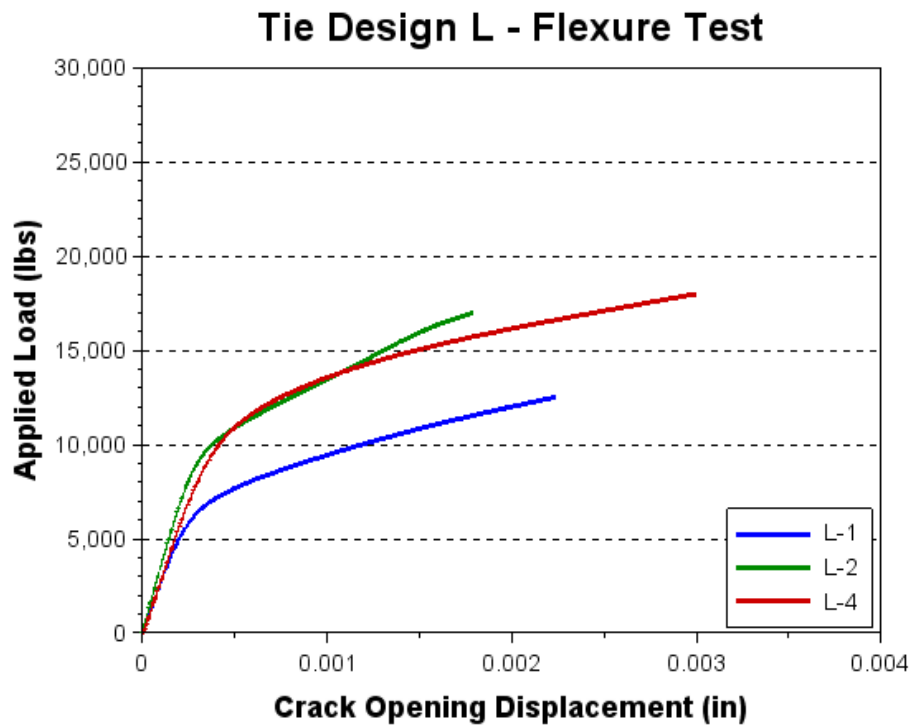
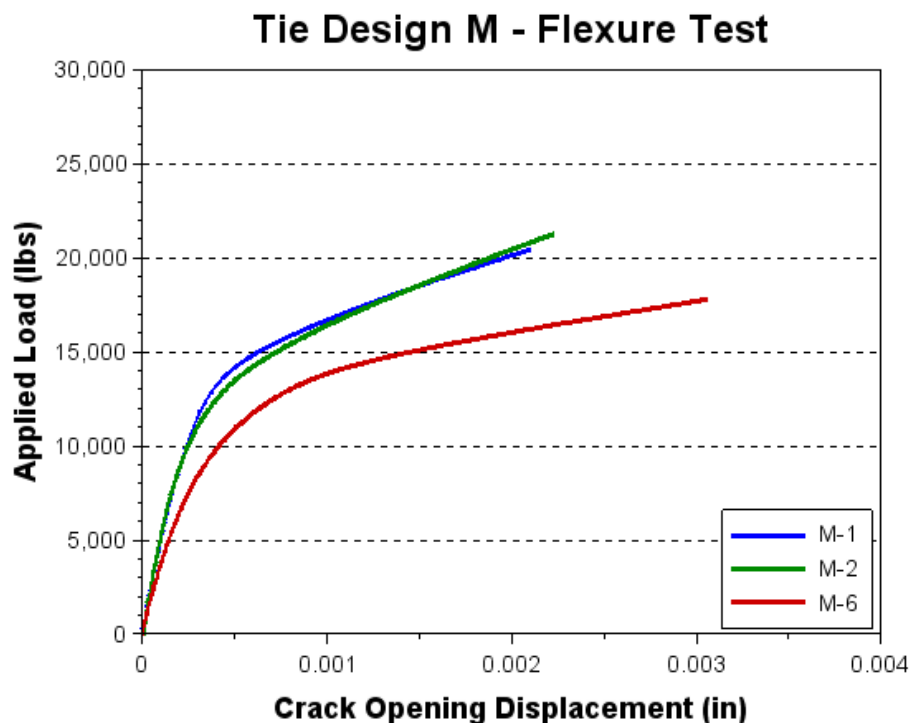


Figure 4.15 Load vs COD for tie design group L



**Figure 4.16 Load vs COD for tie design group M**

### **Determination of Crack Reopening Load**

As stated in Chapter 2, the crack reopening load is determined by either 1) using the end of linearity of the initial portion of the load versus COD curve, or 2) the intersection of the tangents for each linear portion. Observing the load versus COD curves in Figure 4.5 through Figure 4.16, the second portion of the curve is not linear, but curved. This causes the intersection point of the two tangent lines to change depending on which point on the curve the second tangent line is drawn with respect to. As such, the second method for determining the crack reopening load is not valid for this application and is not considered, and the validity of the first method for determining the crack reopening load is investigated.

To evaluate if the end of linearity accurately predicts the crack reopening load, three of the new ties instrumented with VWSGs, R-1, R-2, and R-3, were tested. The new ties were

subjected to the same flexural testing as the existing ties. VWSG readings were taken prior to the testing to evaluate the prestress force in each tie. With the prestress force known, Equation (2) was used to calculate the crack reopening load for each tie. For each of the new ties, the change in stress from initial tensioning to just prior to testing, the resulting prestress forces,  $P_e$ , and the corresponding crack reopening loads,  $P_{cr}$ , are listed in Table 4.1. The flexural test results for the new ties with the location of the crack reopening load on the curve are shown in Figure 4.17 through Figure 4.19.

**Table 4.1 Prestress force in Rocla ties prior to testing**

Tie	Initial Stress (ksi)	$\Delta$ Strain ( $\mu\epsilon$ )	$\Delta$ Stress (ksi)	Remaining Stress (ksi)	$A_{ps}$ (in <sup>2</sup> )	$P_e$ (kips)	$P_{cr}$ (kips)
R-1	204.7	-1108	-31.6	173.2	0.604	104.6	12,610
R-2	204.7	-1081	-30.8	173.9	0.604	105.1	17,510
R-3	204.7	-1050	-32.1	172.7	0.604	104.3	14,450

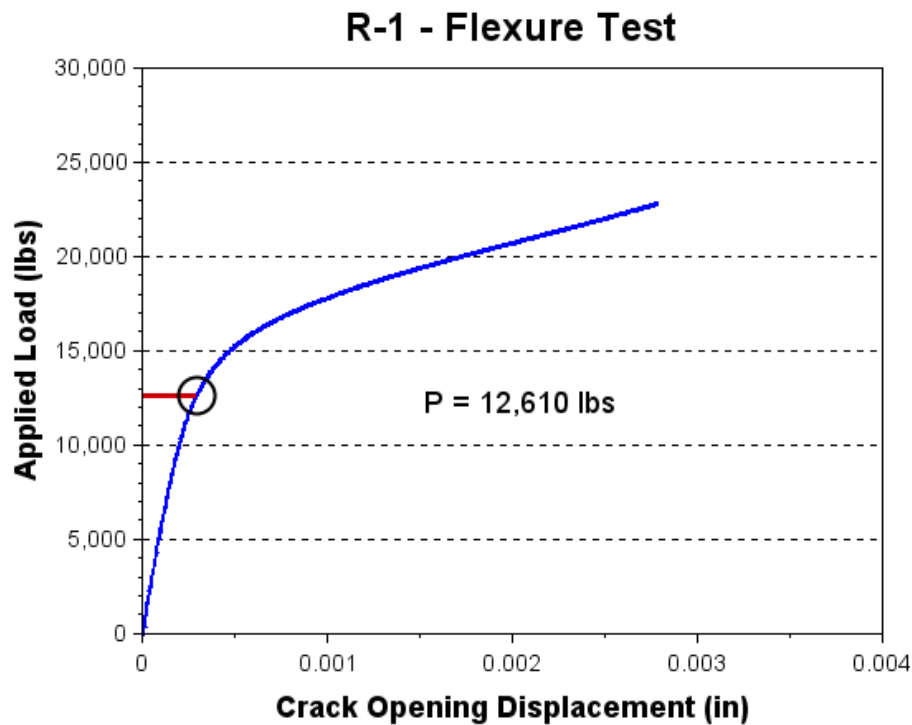


**Figure 4.17 Load vs COD for Rocla Tie 1**

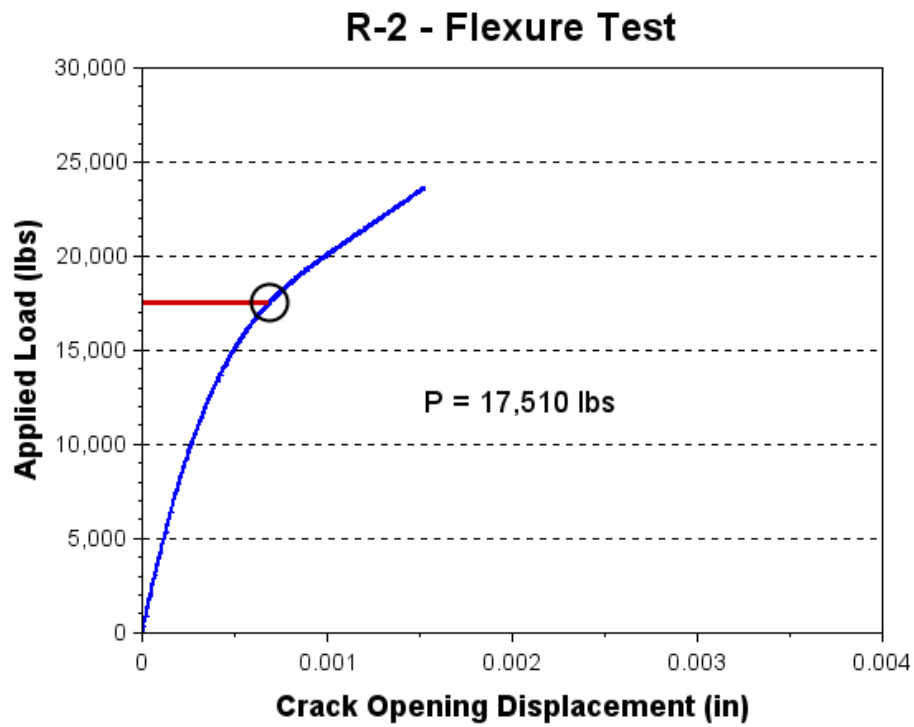


Figure 4.18 Load vs COD for Rocla Tie 2

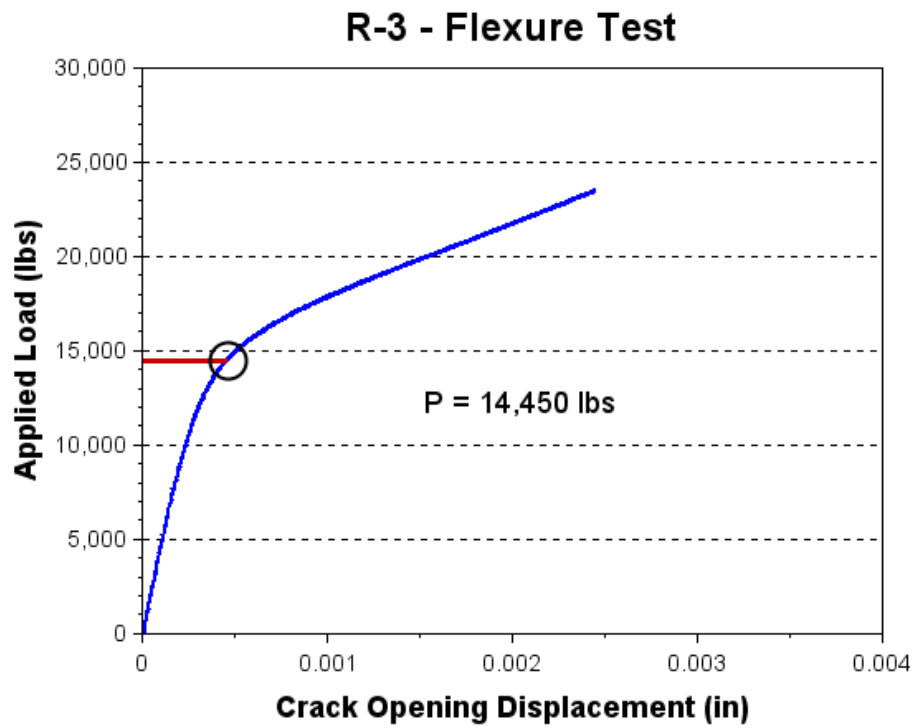


Figure 4.19 Load vs COD for Rocla Tie 3

From Figure 4.17 through Figure 4.19, it can be seen that the location of the crack reopening load for each tie is beyond the initial linear portion. This indicates that using the end of linearity to determine the crack reopening load would lead to inaccurate estimations of the prestress force.

In an attempt to develop a systematic approach to determining the crack reopening load, a third method was investigated. In the third method, the initial linear portions was offset by a certain percentage such that it intersected the crack reopening load. To measure the percentage offset, the crack opening displacement measurements on the x-axis of Figure 4.17 through Figure 4.19 were converted to strain by dividing by the 0.2 inch gage length of the clip gage. Figure 4.20 through Figure 4.22 show the offset applied to each of the Rocla ties tested.

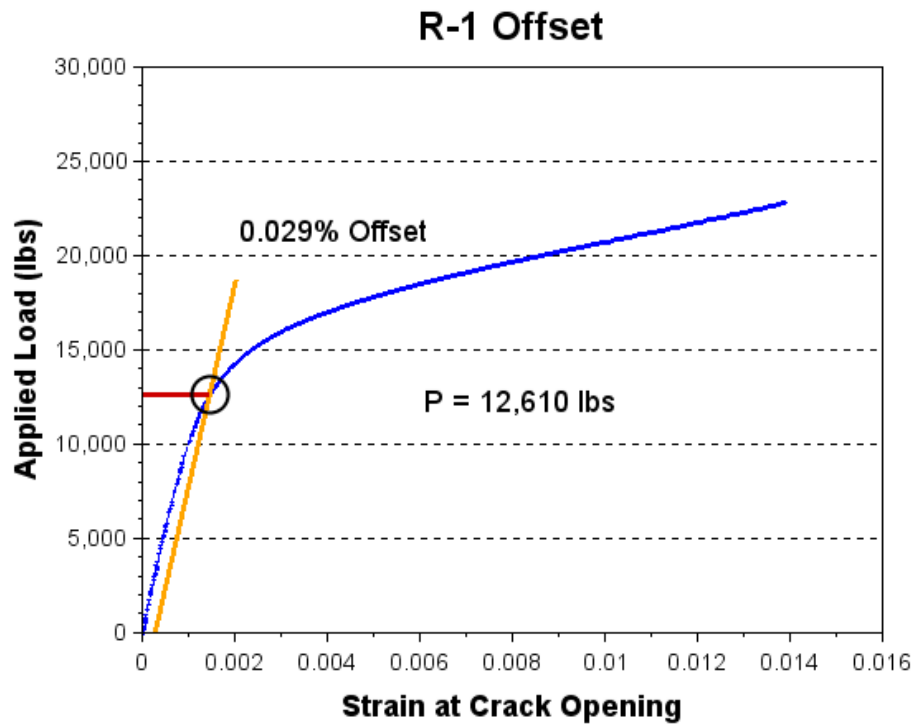


Figure 4.20 Percent offset required for Rocla Tie 1

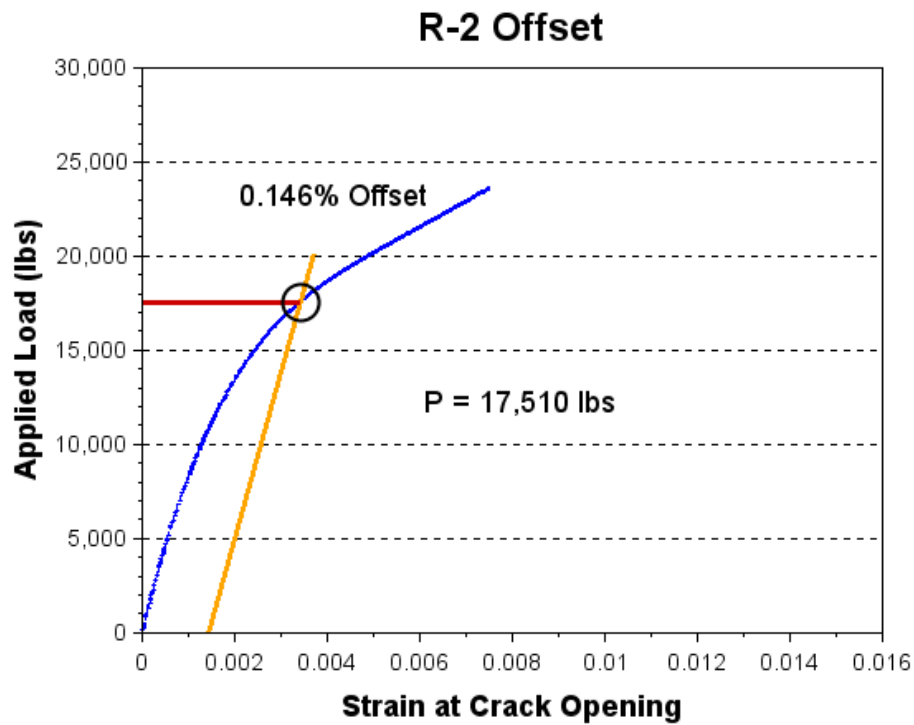


Figure 4.21 Percent offset required for Rocla Tie 2

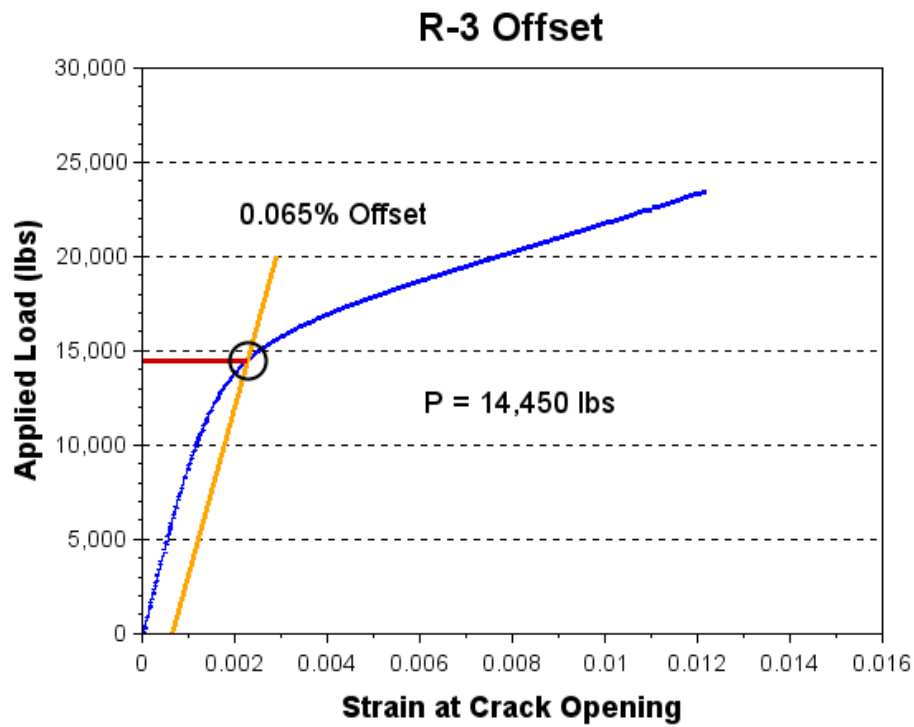
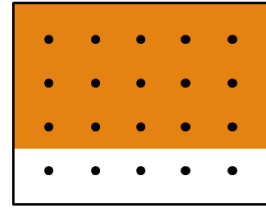


Figure 4.22 Percent offset required for Rocla Tie 3

Figure 4.20 through Figure 4.22 illustrate that the required offset varies significantly from tie to tie, indicating that applying a constant offset to each tie would not accurately determine the crack reopening load, and is not valid for estimating the prestress force.

## **Discussion**

In this investigation, neither of the two methods common in literature, nor the linear offset method, were viable for determining the crack reopening load accurately. One observation is that there is a gradual curvature of the load versus COD curves in the region where the crack is opening. In the literature, the flexural crack reopening method is typically applied to prestressed bridge girders. The prestressing tendons in these girders are typically located at the bottom of the cross section (having a large eccentricity), such that as the crack opens the stiffness transitions from the composite section to the cracked section. This causes the load vs COD curve to have a more pronounced kink when the crack opens. In the case of prestressed concrete railroad, the prestressing tendons are dispersed throughout the cross section and the eccentricity is close to zero. It was noted that a variation of 1/10" in the value used for the eccentricity resulted in a 5-15 kip change in the estimated prestress force. Additionally, for a railroad tie, as the crack propagates, the effective cross section of the tie gradually reduces, as illustrated in Figure 4.23. This results in the load versus COD curve to be more drawn out as the crack opens, and the flexural crack reopening method is therefore unable to accurately estimate the prestress force.



Effective Cross section  
Gradually Reduces

**Figure 4.23 Change of cross section as crack propagates**

## Chapter 5 - Direct Tension Test

The direct tension test method for determining the remaining prestress force in concrete railroad ties was developed to overcome the issues with flexural testing described in Chapter 4. In this method, ties are first pre-cracked at mid-span, and then loaded in direct tension. Tension is applied by encasing each end of a tie in a large reinforced concrete block and using hydraulic jacks to push the blocks apart. As load is applied, the COD of the mid-span crack is measured. For the crack to fully open, the applied load must exceed the prestress force holding the crack closed. The relation between the applied load and COD produces a curve with two distinctly linear portions. As Figure 5.1 illustrates, the first linear portion corresponds to the pre-crack-opening region, when the load is resisted by the composite action of the prestressing steel and concrete, and the second corresponding to post-crack-opening region, when the load is resisted by the prestressing steel only. When a specimen is initially loaded in tension, the bond between the prestressing tendons and concrete breaks at the crack interface. To ensure the second portion of the curve is truly linear, the specimen must be loaded a second time after the tendons have debonded. The beginning of the second linear portion indicates that the crack has fully opened, and the applied load at that point serves as an upper bound estimate of the prestress force in the tie. This chapter details the experimental program for the direct tension test from the proof-of-concept testing on small pretensioned prisms, preliminary testing on a full-scale railroad tie, and final full-scale testing of all ties. Prior to testing the existing ties, full scale testing was first conducted on new ties instrumented with VWSGs to validate the test results.

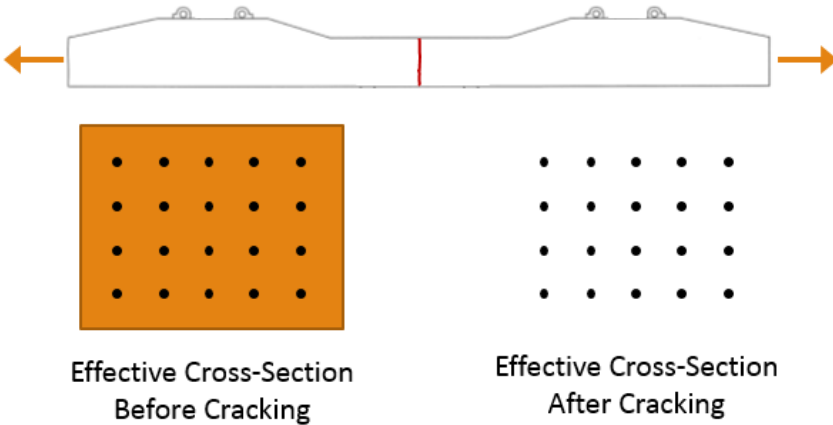


**Figure 5.1 Effective cross section of a tie in tension before and after crack opening**

### Concrete Mix Details

Two different mix designs were used for testing throughout this experiment. Mix A was used to cast blocks for the prism and the preliminary tie tests and was batched in the labs at Kansas State University. Type-III cement was used with a water-to-cementitious material ratio (w/c) of 0.3 to achieve a compressive strength of 10,000 psi prior to testing. Crushed granite was used for the coarse aggregate to provide aggregate interlock, and a local sand was used for the fine aggregate. A high range water reducer (HRWR) and a retarder were added to the mix to achieve a target slump of 6 inches for workability, and to allow for sufficient time to cast the blocks. Table 5.1 shows the materials and proportions used for Mix A.

**Table 5.1 Mix A proportions for prism and preliminary tie test**

Material	Quantity per 1.0 ft <sup>3</sup> (lbs)
Crushed Granite	52.5
Sand	52.5
Type-III Cement	28.9
Water	8.67
HRWR	varies
Retarder	varies

Mix B was used to cast blocks for the 12 full-scale tie tests. Due to the larger volume of concrete needed during this portion of testing, Mix B was batched at a ready-mix plant and transported to Kansas State University. Similar to Mix A, Mix B contained Type-III cement, crushed granite, and a local sand. Additionally, Mix B contained a second coarse aggregate, a local pea gravel, and supplemented a portion of the cement with fly ash. Mix B was designed by the batch plant with a targeted water-to-cementitious material ratio of 0.3, and a targeted slump of 6 inches. As with Mix A, Mix B included a HRWR to achieve the target slump, and a retarder to allow for time to cast the blocks. Table 5.2 shows the materials and proportions used for Mix B.

**Table 5.2 Mix B proportions for full-scale tie test**

Material	Quantity per 1.0 yd <sup>3</sup> (lbs)
Crushed Granite	1200
Pea Gravel	510
Sand	1200
Type-III Cement	650
Fly Ash	150
Water	242
HRWR	varies
Retarder	varies

### **Prism Testing**

Initial testing was conducted on smaller pretensioned prisms as a proof-of-concept for the direct tension method. Four prisms were tested, with each prism measuring 69 inches long with a 3.5-inch x 3.5-inch cross section, shown in Figure 5.2. Each prism contained four 5.32 mm type WF indented wire, as described by Bodapati et al. (2013), and had 1 inch of cover. Each wire was initially tensioned to 7,000 pounds such that each prism had an initial prestress force of

28,000 pounds. The prisms were cast in 2014 at Kansas State University and stored in lab conditions until being tested in 2017.

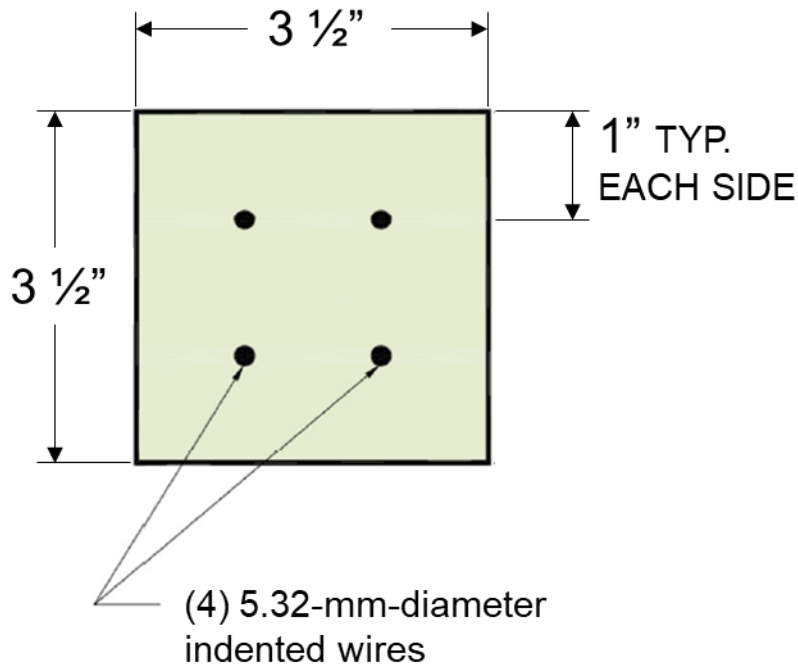


**Figure 5.2 Typical prism cross section**

### **Experimental Setup**

Prior to conducting the direct tension test, cracks were induced at the mid-span of each prism. When attempting to induce a crack while loading in direct tension at a constant loading rate, there is a risk of rupturing the prestressing tendons once the crack forms and the load is transferred to the tendons. For this reason, the prisms were first pre-cracked in flexure. To ensure the crack formed at mid-span, a  $\frac{1}{2}$  inch deep notch, shown in Figure 5.3, was cut around the prism at mid-span using a diamond blade saw. A line was drawn on prism next to the notch region to guide the saw during the notching process. The prisms were then loaded in both

positive and negative bending to initiate cracking within the notch from two opposite sides of the prism.



**Figure 5.3 Typical notch in prism**

To subject the prisms to direct tension, reinforced concrete blocks were cast around each end, with a gap left between the blocks at mid-span. Hydraulic jacks are placed in the gap and used to push the blocks apart, inducing tension into the prism. For the load to be transferred to the prism, the blocks cast around each end must be able to adequately grip the prism. Grooves were intentionally added along each end of the prism, shown in Figure 5.4, prior to casting the blocks in order to achieve adequate grip and mitigate slipping between the two surfaces.



**Figure 5.4 Typical groove in prism**

Rebar cages were cast into the blocks at the ends of the prisms to aid in gripping the prism, increase the strength of the blocks, and to arrest any cracks initiated near the bearing

surface of the jacks. The main rebar cage consisted of six #3 bars at 4-½” spacing and outer dimensions of 9-½” x 6-½”, and one slightly larger #3 stirrup was placed at the end of block near mid-span to avoid spalling at the bearing location of the jacks. The stirrups were tied to four #3 longitudinal bars, as shown in Figure 5.5. Figure 5.6 shows the prisms with end blocks after casting. Each block measured 14” x 8” by 30” long, and the two blocks were separated by an 11” gap.



**Figure 5.5 Prisms with rebar cages prior to casting blocks**



**Figure 5.6 Prisms after casting blocks**

For testing, prisms were stood in the upright position. MTS Model 632.02F-20 clip gages were installed directly over the notch at mid-span on two opposite sides and were used to measure the crack opening displacement during testing. High-precision LVDTs were instrumented spanning the gap between the two blocks on all four sides and were used to ensure that the load was being applied symmetrically during testing. The LVDTs were mounted to the bottom block and measured the displacement of an aluminum rod attached to the top block, shown in Figure 5.7 and Figure 5.8. Two 30-ton hydraulic jacks were placed between the blocks to jack the blocks apart, and apply tension to the prism. The jacks were placed on a neoprene pad, and loaded against a steel plate attached to the top block. Figure 5.8 shows the prism test setup.

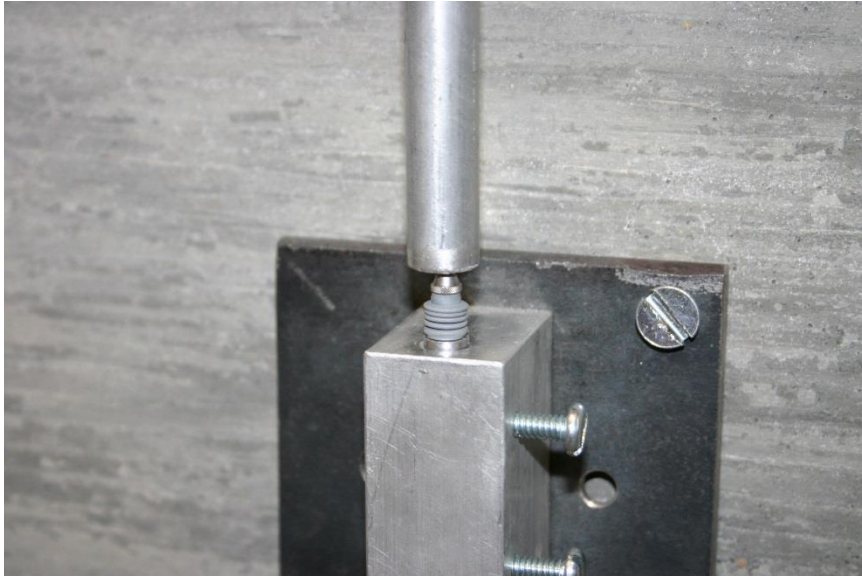


**Figure 5.7 Typical LVDT setup**



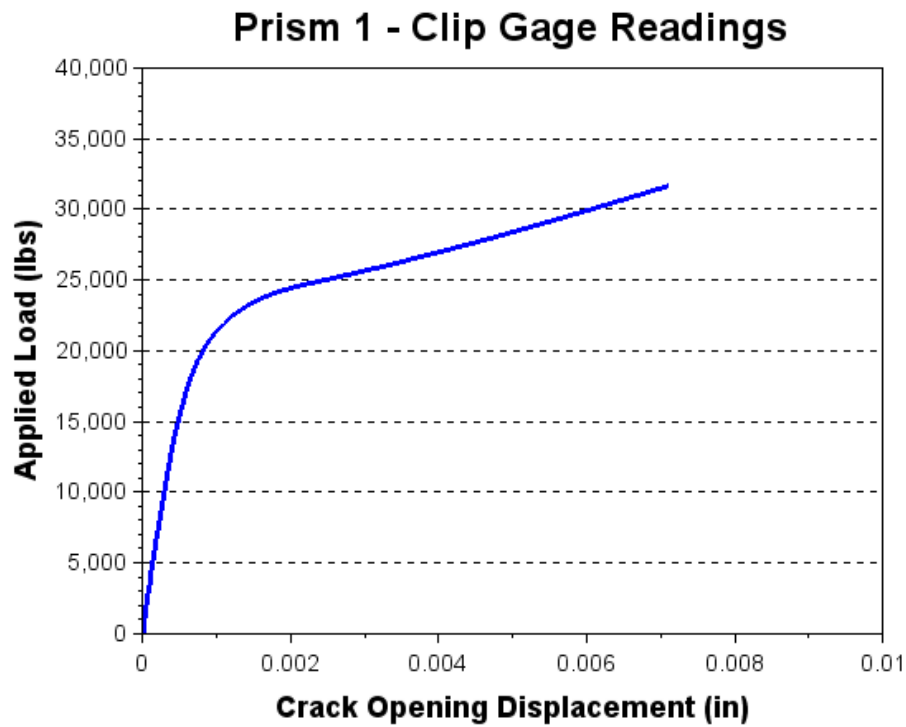
**Figure 5.8 Test configuration for prism testing**

An open-loop control system was used to apply load at a rate of 2,000 pounds per minute. A model F-25EX Forney Testing Machine was used to operate the hydraulic jacks and control the load rate. A pressure transducer affixed to the hydraulic lines of the jacks was used to

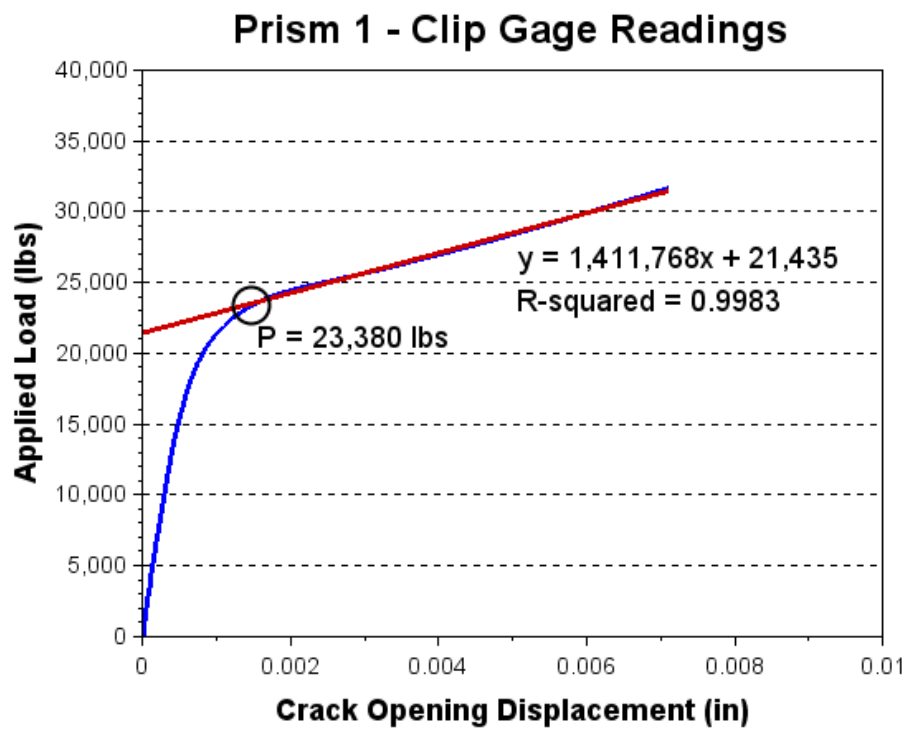
measure the load during testing. A Keithley Series 2700 data acquisition system was used to record readings of the load, two clip gages, and four LVDTs at one-second intervals.

## **Results**

Part (a) of Figure 5.9 through Figure 5.12 shows the load versus the average clip gage reading for Prisms 1 through 4, respectively. To estimate the prestress force, a best-fit line having a high coefficient of determination ( $\geq 0.998$ ),  $R^2$ , was established for the second linear portion of curve. The data point that first intersects the best-fit line marks the beginning of the post-crack opening region of the curve. The load corresponding to this point serves as an upper bound estimate for the prestress force in the prism. Part (b) of Figure 5.9 through Figure 5.12 shows the best-fit line overlaid on the test results, along with the estimated prestress force. Table 5.3 summarizes the test results for each prism and compares the remaining prestress force to the initial tensioning force.

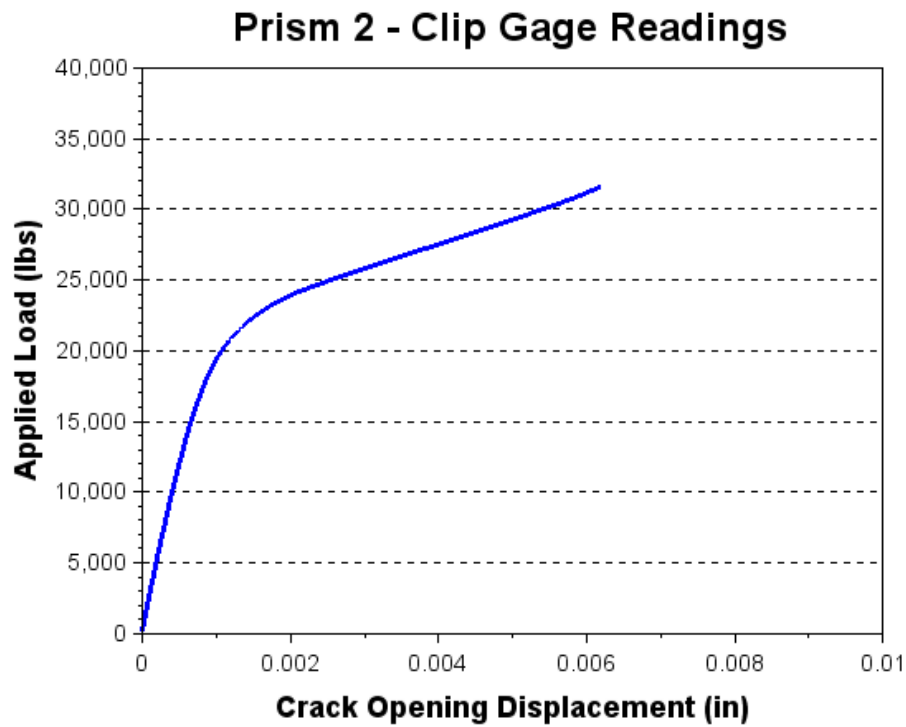


(a) Load versus average clip gage reading

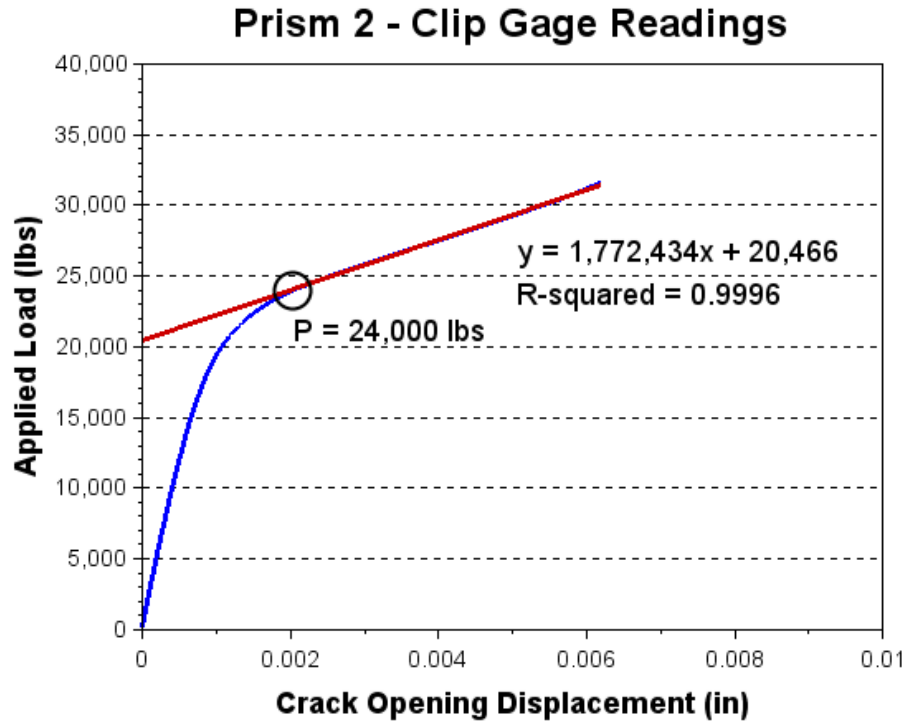


(b) Estimated prestress force from linear fit

Figure 5.9 Prism 1 test results

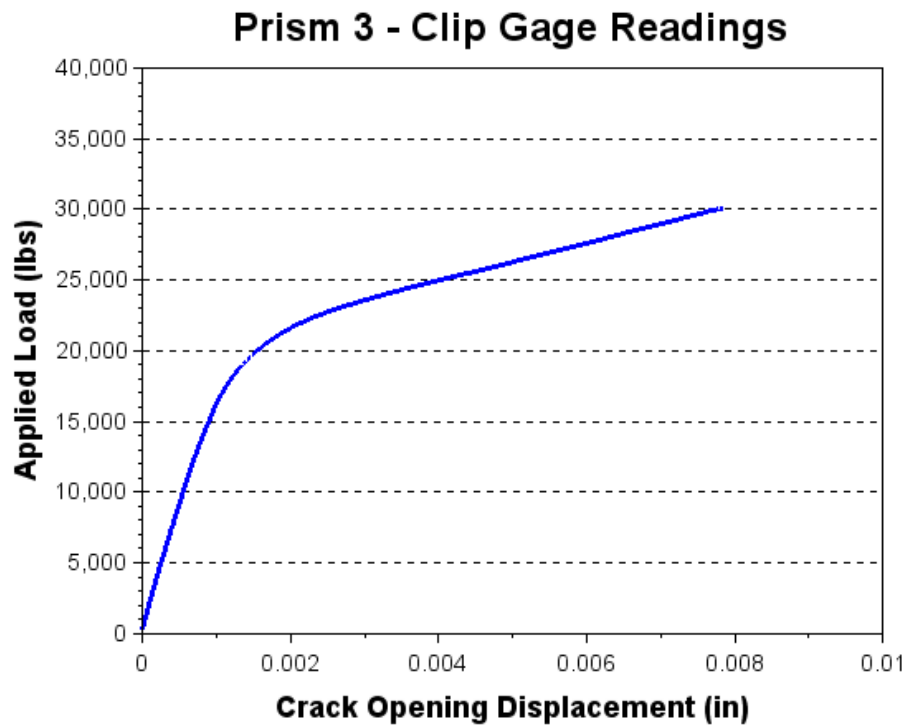


(a) Load versus average clip gage reading

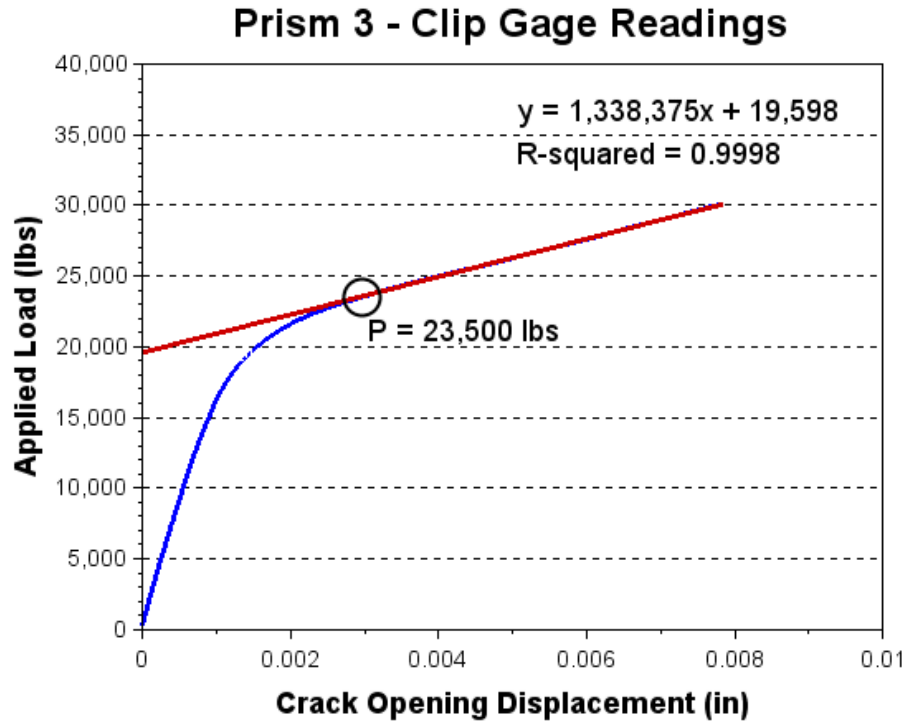


(b) Estimated prestress force from linear fit

Figure 5.10 Prism 2 test results

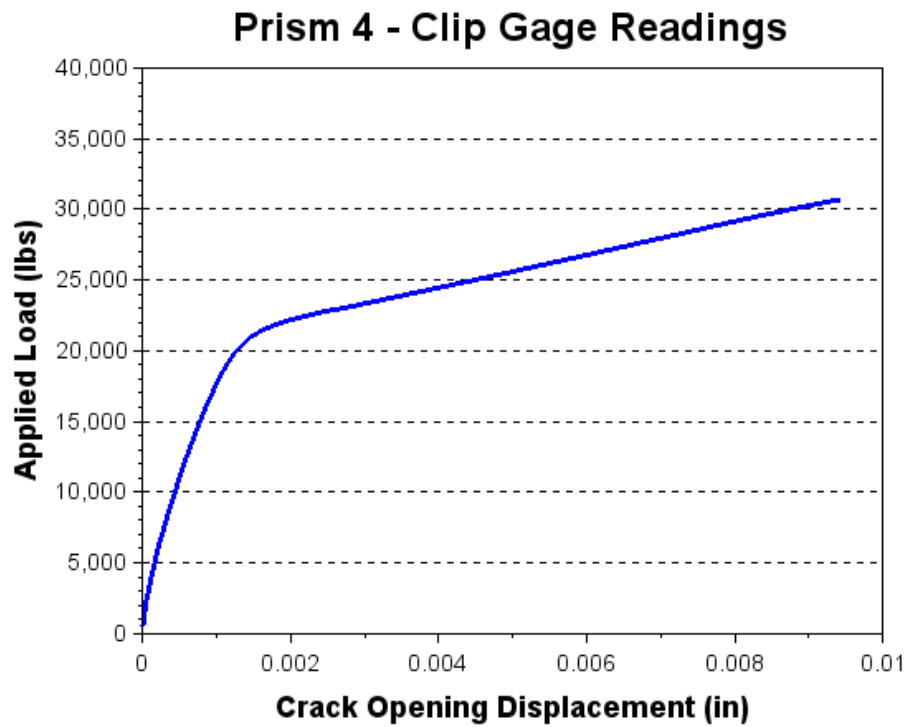


(a) Load versus average clip gage reading

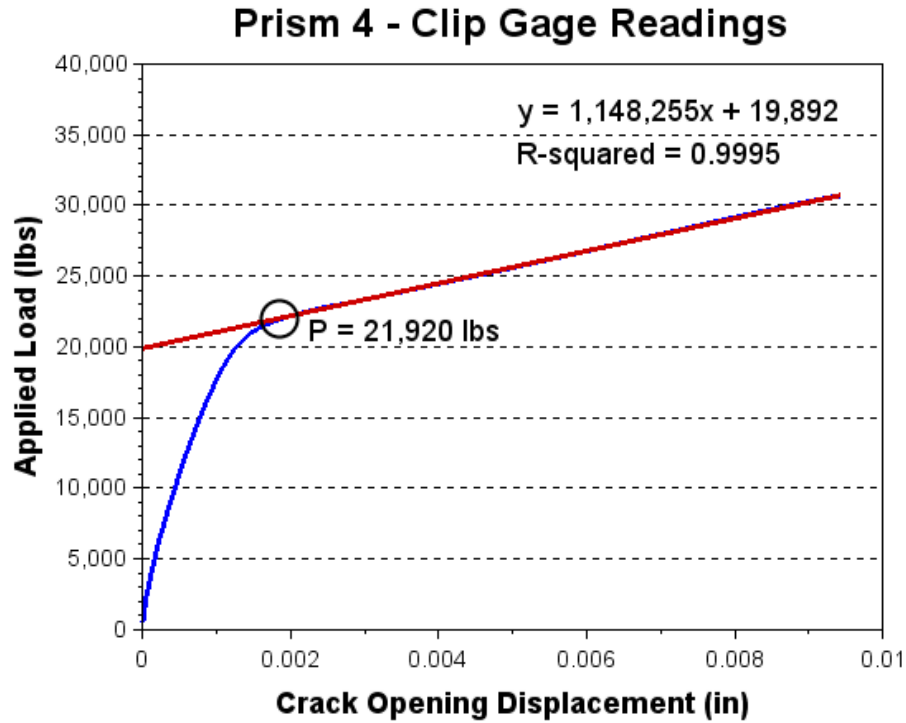


(b) Estimated prestress force from linear fit

Figure 5.11 Prism 3 test results



(a) Load versus average clip gage reading



(b) Estimated prestress force from linear fit

Figure 5.12 Prism 4 test results

**Table 5.3 Summary of prism test results**

Prism	Initial Prestress Force (kips)	Estimated Prestress Force (kips)	Estimated/Initial
1	28.0	23.4	84%
2	28.0	24.0	86%
3	28.0	23.5	84%
4	28.0	21.9	78%

Since the prisms were cast at the same time using the same concrete mix, and had the same indented wire and initial force, and stored in the same conditions since 2014, it was expected that the remaining prestress force in each prism would be similar to one another. The results for the four prisms are within a total range of 2.08 kips, and on average are estimated at 83% of the initial prestress force. With the proof-of-concept testing on prisms providing results in the expected range, the direct-tension test was adapted for preliminary testing on a full-scale railroad tie.

### **Preliminary Tie Test**

A preliminary tension test was ran on a railroad tie to verify that the test could be operated successfully on a larger scale than the prism testing. The tie used for the preliminary test was tie D-4, a Santa Fe - San Vel tie, shown in Figure 5.13. As stated in Chapter 3, tie design group D consists of eight –  $\frac{3}{8}$ ” seven-wire stress-relieved strands. The original design plans for the Santa Fe – San Vel tie were provided by Jeff McQueen and the initial prestress force was known to be 133 kips. Figure 5.14 shows a typical mid-span cross section for a group D tie.

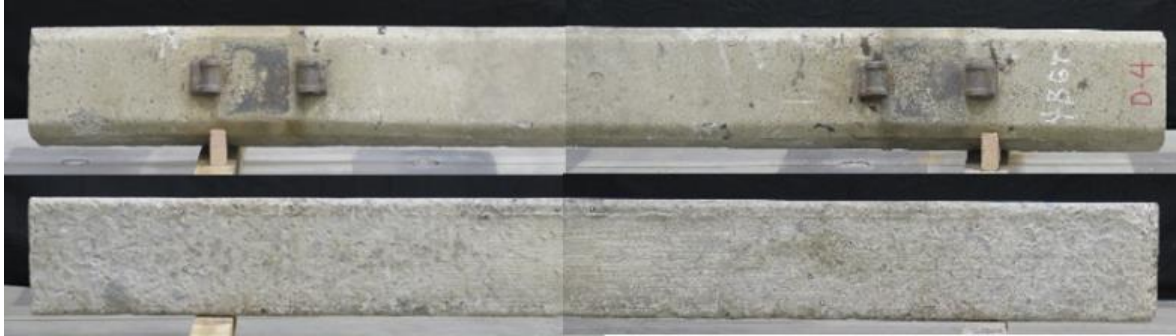


**Figure 5.13 Tie D4 used for the preliminary tie test**

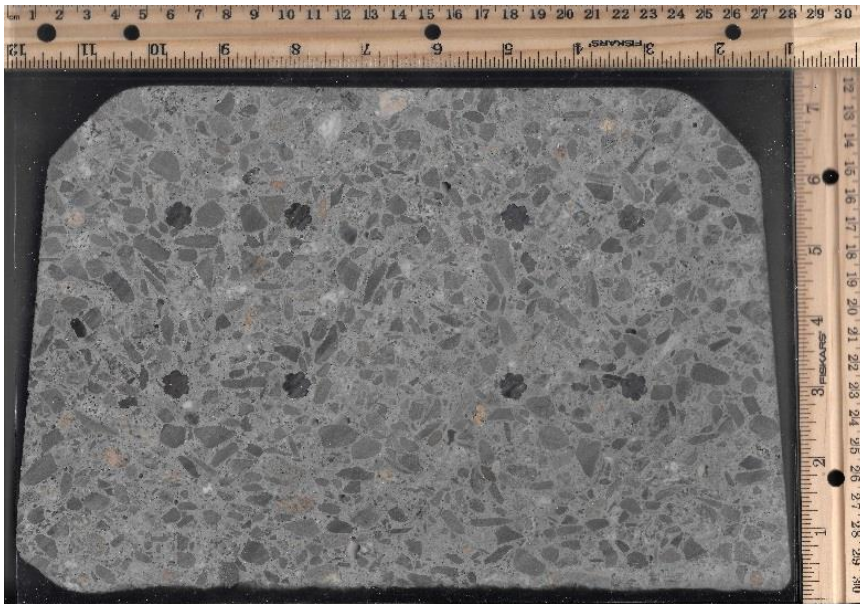


**Figure 5.14 Typical mid-span cross section of ties in design group D**

### **Experimental Setup**

As with the prism testing, the tie was first notched at mid-span, shown in Figure 5.15. The depth of notch varied on each side of the tie such that there was a  $\frac{1}{2}$ " of cover remaining on each side of the strands. The box in Figure 5.16 depicts the cross section remaining in the tie after the notch was cut. The tie is then loaded in both positive and negative bending to initiate cracking within the notch on the top and bottom surfaces of the tie. While pre-cracking the tie, cracks from both sides did not propagate far enough to join in the middle, but enough to significantly reduce the section of concrete to be cracked in tension, and reduce the risk of

rupturing the tendons when loading in direct tension. This method of pre-cracking also allows for the crack to be perpendicular to the applied tensile loading and provides smoother readings during the direct tension test.



**Figure 5.15 Notch cut at mid-span of tie D4**

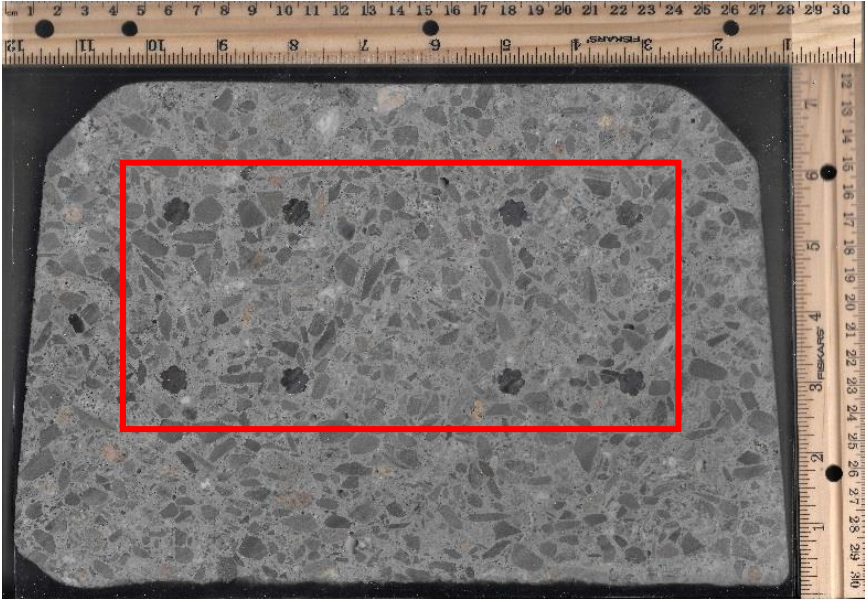


**Figure 5.16 Reduced cross section at notch location**

Existing tie features such as the varying section geometry, and the presence of the rail clips, aid the gripping between the existing tie surface and the blocks being cast around the ends. Similar to the prisms, the grooves in Figure 5.17 were intentionally added to further increase the gripping between the two surfaces and mitigate potential slipping.



**Figure 5.17 Grooves added at ends of tie**

The blocks were reinforced with rebar cages shown in Figure 5.18. The main rebar cage consisted of four #3 longitudinal bars and a #3 rectangular spiral with a  $2\frac{1}{4}$ " pitch and outer dimensions of  $15\frac{3}{4}$ " x  $19\frac{1}{4}$ ". Additional 6" diameter spirals with a  $2\frac{1}{4}$ " pitch were added to the corner of the cages to strengthen the blocks near the bearing surface of the hydraulic jacks to arrest any cracks formed during loading and prevent spalling on the blocks. Each block is 36" x  $18\frac{1}{2}$ " and  $43\frac{1}{4}$ " long, and the two blocks are separated by a  $21\frac{1}{2}$ " gap. The blocks cured until a minimum compressive strength of 10,000 psi was achieved (typically 7 days) prior to testing.



**Figure 5.18 Rebar caging used for preliminary tie testing**

The tie was tested while standing in an upright position. MTS Model 632.02F-20 clip gages were installed directly over the notch at mid-span, shown in Figure 5.19, on the top and bottom surfaces of the tie, and LVDTs were instrumented spanning the gap between the two blocks on all four sides. The tie was loaded using four 30-ton hydraulic jacks controlled by a model F-25EX Forney Testing Machine. Jacks were placed in the gap between the two blocks on a steel stand, with a neoprene pad between the stand and the bottom block. The jacks applied load to a steel plate attached to the top block. The jacks were initially set up symmetrically about the tie, and fine adjustments were made to eliminate eccentricities in the loading and ensure an even load was applied. Figure 5.20 shows the test configuration with the instrumentation and jack placement.



**Figure 5.19** Clip gage instrumented over the notch

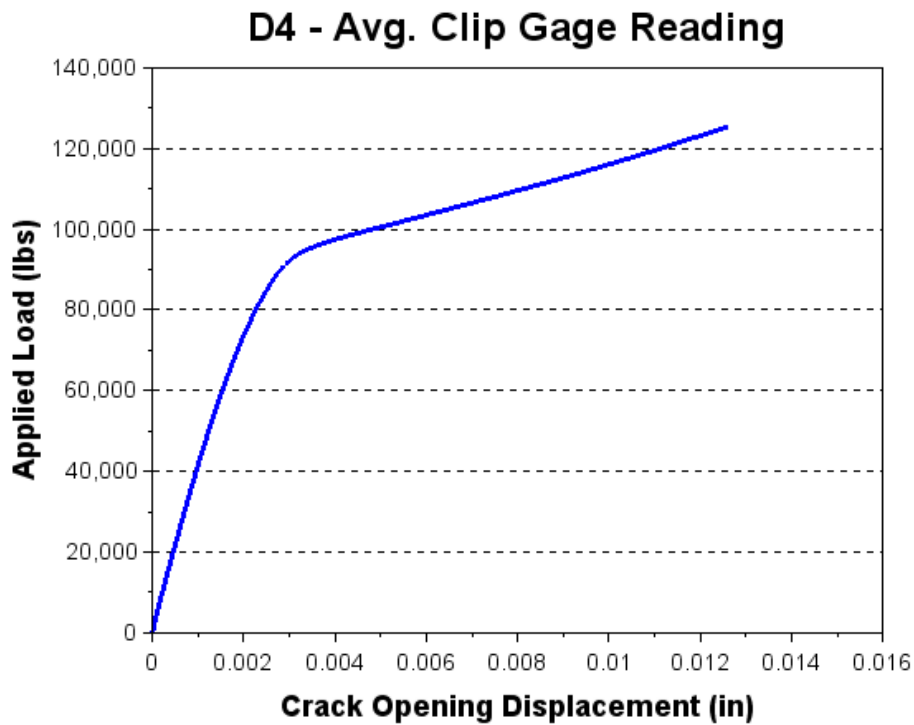


**Figure 5.20 Test configuration for preliminary tie test**

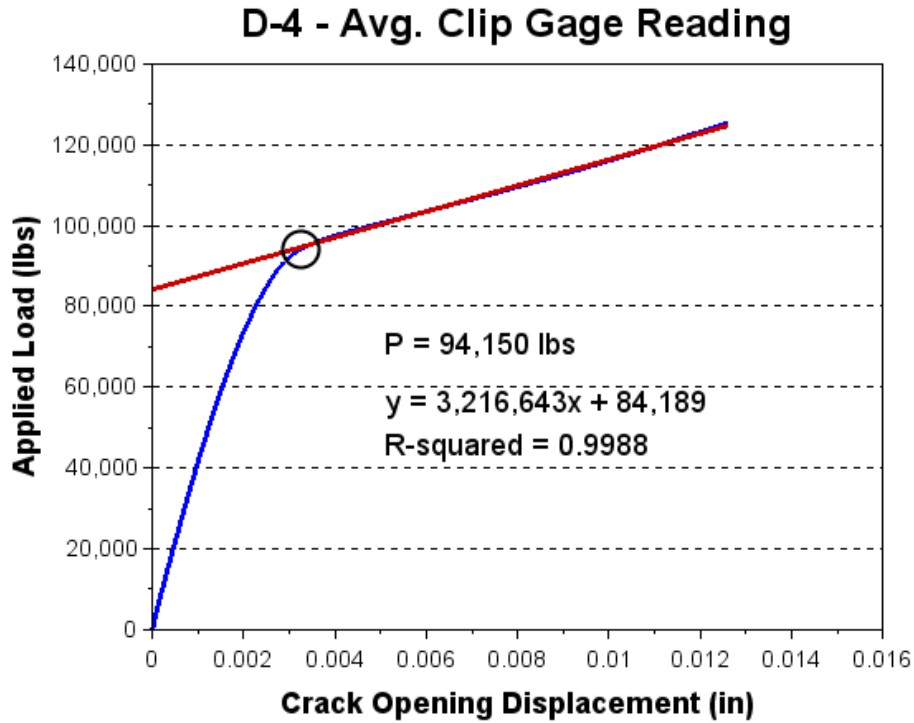
Load was applied at a rate of 15,000 pounds per minute. A Keithley Series 2700 Data Acquisition system was used to take readings of the load, the two clip gages, and the four LVDTs at one-second intervals.

## Results

Testing data for the preliminary tie test is presented in Figure 5.21 (a). The line of best fit calculated for the post-crack linear region of the curve had a strong correlation to the data with an  $R^2$  of 0.9988, shown in part (b) of Figure 5.21. Following the same method used with the prisms, an upper bound for the remaining prestress force in the tie is estimated to be 94,150 pounds.



(a) Load versus average clip gage reading



(b) Estimated prestress force from linear fit

Figure 5.21 Preliminary tie test results

## Discussion

To verify that the slope of the second linear region of the curve represents the stiffness of the strands only, it is compared to the theoretical slope of steel with a modulus of elasticity (MOE) of 28,500,000 psi. A theoretical stress strain curve of steel was converted to a load-displacement curve by multiplying the stress by the area of prestress steel, 0.688 in<sup>2</sup>, and the strain by various gage lengths (GL). As previously discussed, when the strands are initially loaded in tension, they debond from the concrete on either side of the crack. The total length of unbonded strand on either side of the crack represents the gage length of the strand, and is unknown during testing. Figure 5.22 shows the theoretical force-displacement curves and corresponding slopes of steel with gage lengths of 5, 6, and 7 inch, and the second linear portion of the curve in Figure 5.21. The slope of the actual test results closely matches the theoretical slope of steel with a six inch gage length. This implies that the crack is fully open and the strands which have debonded approximately three inches on either side of the crack.

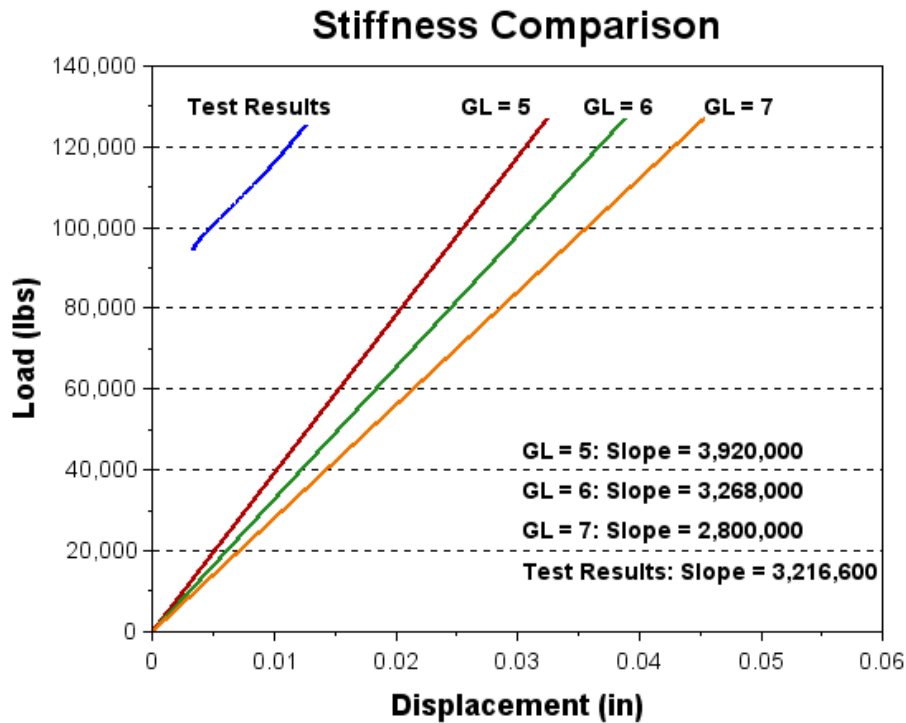


**Figure 5.22 Comparison of actual and theoretical load-displacement curves for steel at various gage lengths ( $E = 28,500,000$  psi)**

For the testing described in this section, it is important to note the following:

- 1) A large amount of cross-sectional area was removed at the mid-span of the tie when the notch was cut. This area reduction theoretically creates elastic shortening at the notched section, causing the internal prestress force of the tie to decrease once the notch is cut and causing the test to under-estimate the internal prestressing force.
- 2) For the crack to fully open, the applied load must exceed not only the prestress force in the tie, but the self-weight of the tie and block above the crack as well. Due to the large size of the blocks cast on the end of the tie, neglecting the weight of the block would cause this method to over-estimate the internal prestress force.

The net effect of these two issues, calculated in Appendix C, resulted in an under-estimation of the prestress force in tie D-4 by 2,560 pounds, for a total error of 2.7%. Adjusting the prestress force to account for this error would increase estimated prestress force to 96,700 pounds. While the effect of the weight of the block on the final results is apparent and can be easily calculated, there remains uncertainty to the degree of which the elastic shortening is taking place. The extent to which elastic shortening occurs due to notching the tie is investigated using ties instrumented with VWSGs during the full-scale testing stage.

## **Full-Scale Tie Testing**

Upon successful preliminary testing of a full-scale railroad tie, further testing on existing ties commenced. This section addresses the modifications made to the tension test prior to testing additional ties. Additional tests were conducted on new ties to validate the direct tension method prior to testing the existing ties. To validate the tension test, testing was conducted on the new ties R-4, NT-1, and CXT-1, where R-4 and NT-1 were instrumented with VWSGs. Test results for the new ties are compared to the prestress forces determined from the VWSG readings, and the estimated prestress force remaining after losses. The existing ties investigated in this section include ties from design groups A, B, D, F, H, K, and L. Additionally, the effects of elastic shortening mentioned in the previous section are investigated. For the ties instrumented with VWSGs, readings were taken before and after notching the tie at mid-span to evaluate the total strain change incurred from notching the tie.

### **Experimental Setup**

For the full-scale testing, the notch depth and end block dimensions were reduced from the preliminary testing stage. The new notch consist of a ½” deep cut around the tie at mid-span

to reduce the cross-section as shown in Figure 5.23. The notch depth was changed such that flexural pre-cracking would still initiate within the notch and reduce the effects of elastic shortening described in the previous section.

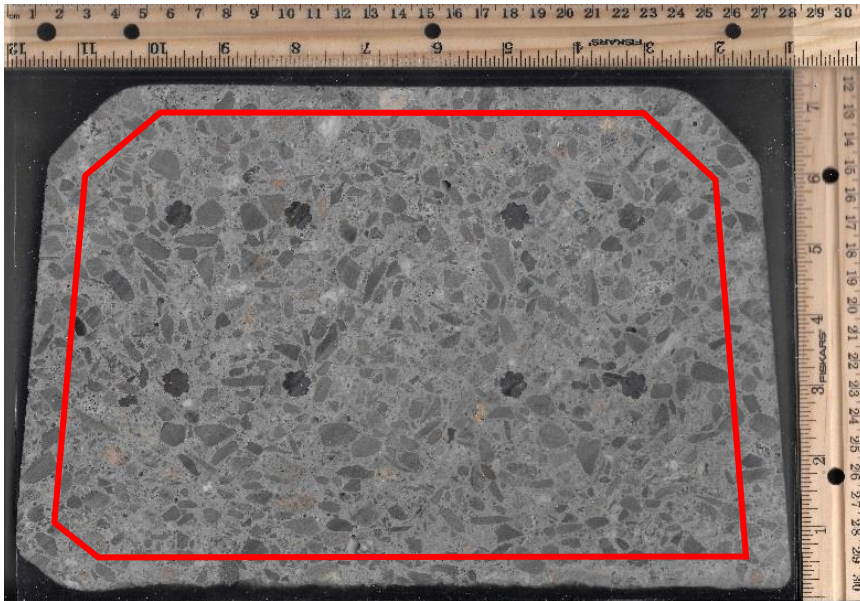


**Figure 5.23 Reduced cross section at notch location**

The dimensions of the blocks were reduced to 22" x 18" by 46" long, with a 13" gap between the two blocks. The rebar cage consisted of four #3 longitudinal bars and a #3 rectangular spiral with a 2 ½" pitch and outer dimensions of 15 ¾" x 19 ¼", shown in Figure 5.24. The 6" spirals used in the preliminary test were removed. As with the preliminary testing, grooves were intentionally added along the ends of the ties prior to casting the blocks to improve the grip between the existing tie surface and newly cast block.



**Figure 5.24 Typical rebar cage**

The ties were tested standing in an upright position, shown in Figure 5.25. MTS Model 632.02F-20 clip gages were instrumented across the notch on both the top and bottom faces of the tie to measure the COD. LVDTs were instrumented spanning the gap between the two blocks on each side to ensure that the load was applied symmetrically. Load was applied using four 30-ton hydraulic jacks controlled by a Forney Testing Machine. The jacks were placed in the gap between the two blocks on a neoprene pad, and loaded on a steel plate attached to the top block. The typical instrumentation setup and jack placement is shown in Figure 5.26. To capture more data during testing, the load rate was reduced from the preliminary testing to a rate of 10,000 pounds per minute. For tie design A the load rate was further reduced to 6,000 pounds per minute. As design A is a post-tensioned tie, the crack opening occurs more suddenly, and the reduced load rate allowed more data to be recorded during testing. Load, clip gage, and LVDT readings were recorded at one-second intervals using a Keithley Series 2700 Data Acquisition system.



**Figure 5.25 Test configuration for tension test of all ties except D-4**



**Figure 5.26 Typical instrumentation configuration for tension test**

### Results for new ties

To validate the results obtained from the direct tension test, three new tie designs with known initial prestressing force were tested. The new ties consisted of tie R-4, NT-1, and CXT-1, with the Rocla and Nortrak ties containing internal vibrating-wire strain gages and having a known prestress force prior to testing.

To estimate the prestress force, a best-fit line having an  $R^2 \geq 0.998$  was established for the second linear portion of curve and the data point that first intersects the best-fit line marks the beginning of the post-crack opening region of the curve. The load corresponding to this point serves as an upper bound estimate for the prestress force in the prism. Figure 5.27 - Figure 5.29 show the load vs COD curves for ties R-4, NT-1, and CXT-1, respectively, along with the established best-fit line and estimated prestress force.

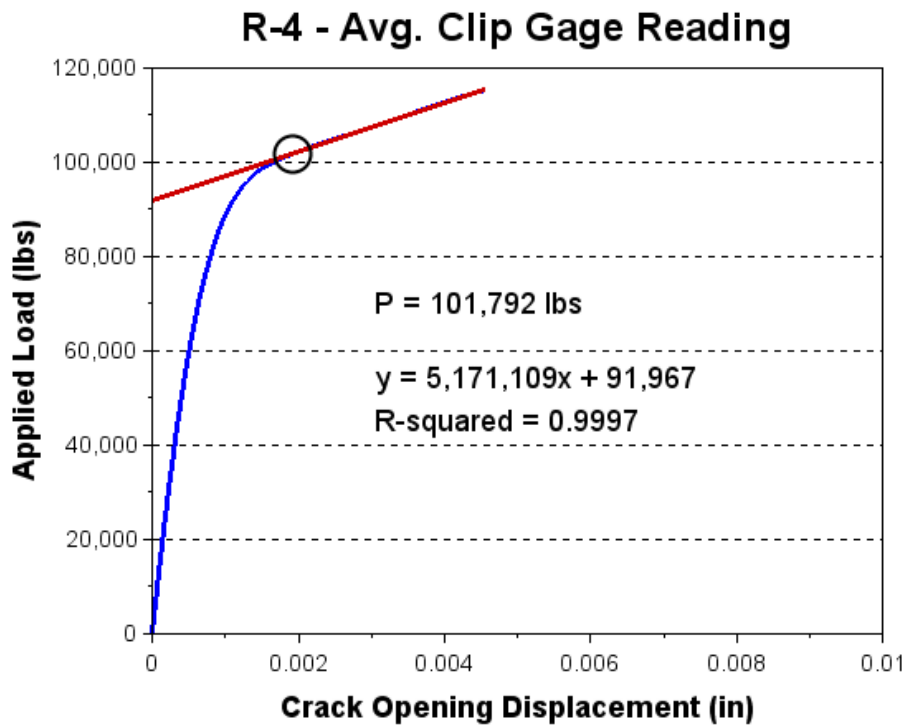


Figure 5.27 Tension test results for tie R-4

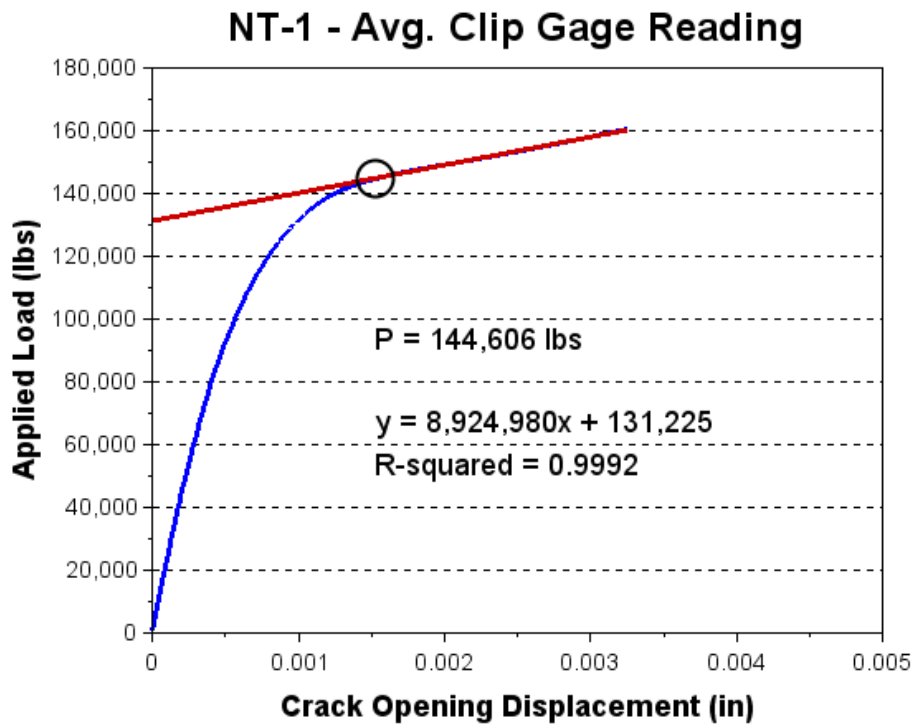


Figure 5.28 Tension test results for tie NT-1

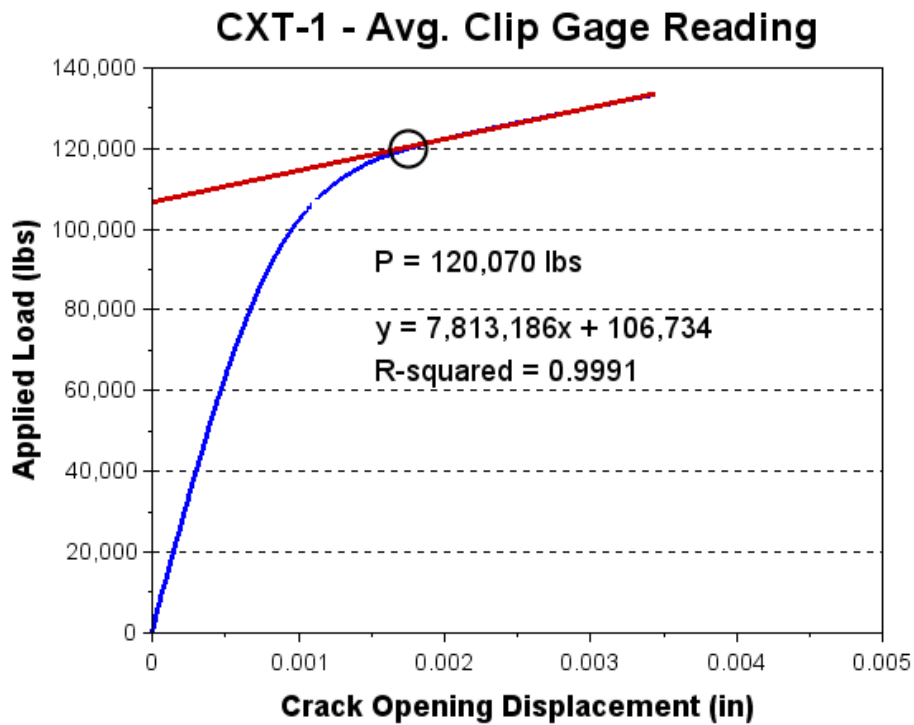


Figure 5.29 Tension test results for tie CXT-1

As noted in the preliminary test discussion, the effects of elastic shortening and the weight of the top block on the prestress force estimation need to be considered. To evaluate the effect of elastic shortening on the prestress force, the total strain change after notching the tie was measured on tie R-4. The strain change due to notching was also measured on tie R-6, though R-6 was not included in the tension testing due to flexural cracking initiating outside the notch. VWSG readings were taken for each tie just prior to cutting the notch, and again afterwards. Table 5.4 lists the VWSG readings and total strain and stress change due to notching. Since notching the tie only changed the strain by a magnitude of 9-12  $\mu\epsilon$ , the effects of elastic shortening are assumed to be negligible and were not calculated for the final prestress force estimates.

**Table 5.4 VWSG readings before and after notching tie**

Tie	Before Notch		After Notch		$\Delta$ Strain ( $\mu\epsilon$ )	$\Delta$ Stress (ksi)
	R <sub>0</sub> ( $\mu\epsilon$ )	T <sub>0</sub> (°C)	R <sub>1</sub> ( $\mu\epsilon$ )	T <sub>1</sub> (°C)		
R-4	2498.4	27.6	2489.9	27.2	-9.2	-0.26
R-6	2222.5	19.8	2202.2	23.5	-11.8	-0.34

To account for the weight of the block, the entire specimen was weighed using a digital crane scale and the weight of the tie and block above the crack is assumed to be half of the total weight. After adjusting for the weight, the final prestress force estimates for ties R-4, NT-1, and CXT-1 are 100.2 kips, 142.9 kips, and 118.5 kips, respectively. Table 5.5 lists the weights of the top half and the adjusted prestress force estimates.

**Table 5.5 Adjusted prestress force estimates**

Tie	Initial Prestress Force Estimate (kips)	Weight of Top Half (kips)	Adjusted Prestress Force (kips)
R-4	101.8	1.63	100.2
NT-1	144.6	1.67	142.9
CXT-1	120.1	1.62	118.5

For each of the new tie designs, the prestress force after losses was estimated following the method outlined in the PCI Design Handbook (2010). VWSG readings were taken prior to the direct-tension testing to determine the prestress for comparison to the test results. Table 5.6 summarizes the prestress force estimates after accounting for losses, determined from the VWSG readings, and from the tension test results. The tension test results coincide with the prestress force determined from VWSG readings, with a difference of 0.6 kips for tie R-4 and 1.2 kips for tie NT-1. These results validate that the direct tension test is a suitable method for evaluating the prestress force in a railroad tie. The estimated prestress force after losses tends to provide results lower than the other two methods. This is to be expected as the loss estimation is used for design and intended to be conservative.

**Table 5.6 Comparison of prestress force results for new tie designs**

Tie	Theoretical Prestress Force After Calculated Losses (kips)	Prestress Force Determined from VWSG Readings (kips)	Prestress Force Determined from Direct Tension Test (kips)
R-4	97.4	102.6	101.8
NT-1	136.9	143.4	144.6
CXT-1	106.4	-	120.1

## Results for existing ties

With the test results of the new ties verifying that the direct tension test provided accurate estimates of the prestress force, testing on the existing ties began. The existing ties investigated in this section were ties A-6, B-7, D-2, D-7, D-8, F-6, H-3, K-5, and L-6. Four ties from group D were tested to examine how consistent the remaining prestress force was in various ties of the same design, and to get a typical value of the prestress force for a design with a particularly good performance in track.

The same regression criterion for the new tie results was applied to the existing tie results, with the exception of A-6. Since A-6 was a post-tensioned tie, when the crack opened the COD increased significantly and less data was captured for the post-crack opening region. Figure 5.30 - Figure 5.38 show the tension test results for ties A-6, B-7, D-2, D-7, D-8, F-6, H-3, K-5, and L-6, respectively.

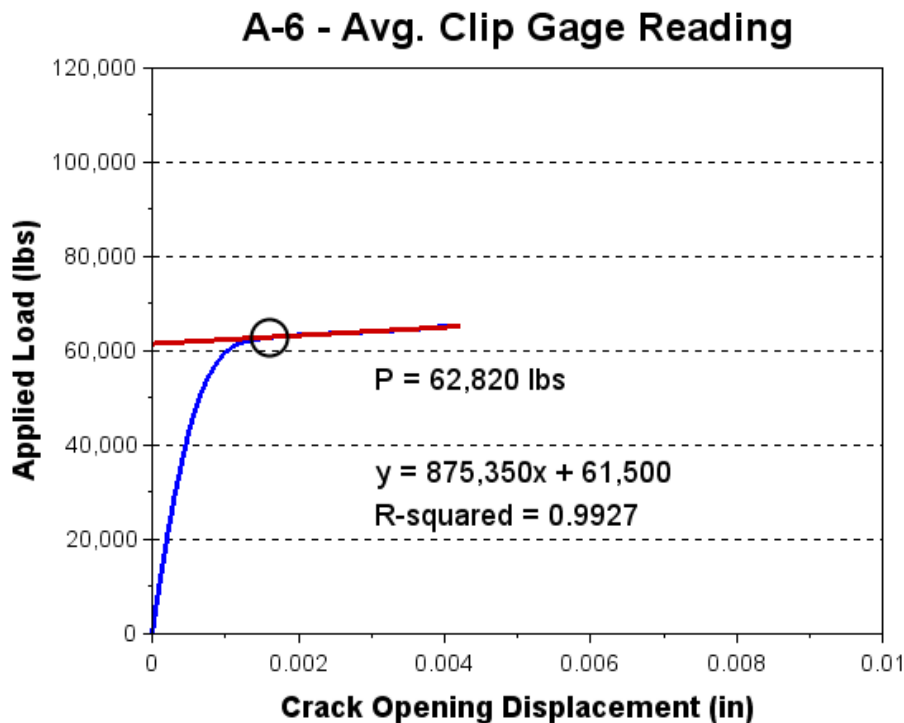


Figure 5.30 Tension test results for tie A-6

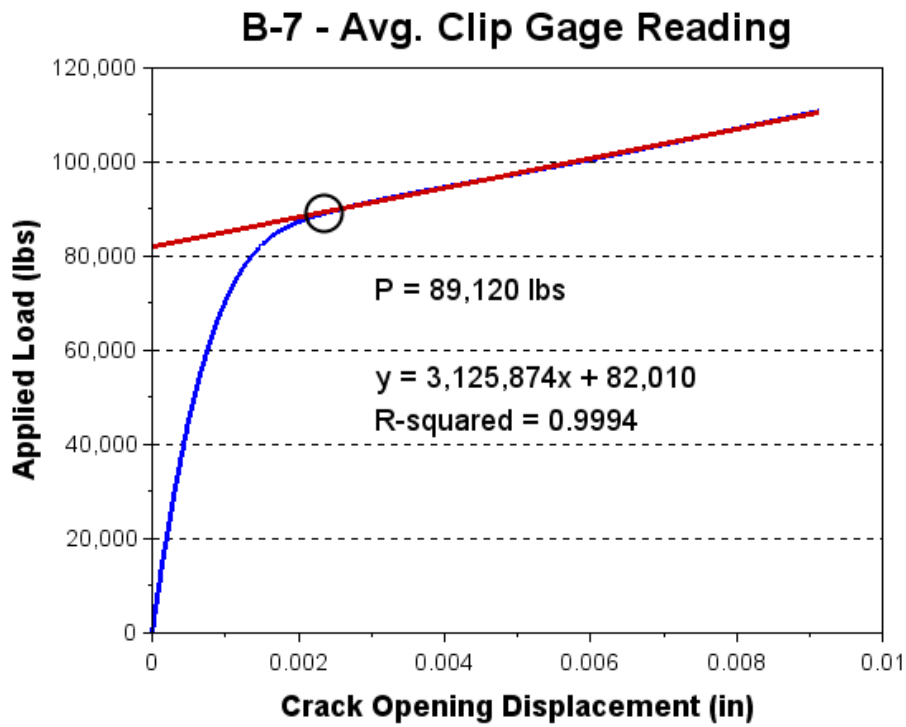


Figure 5.31 Tension test results for tie B-7

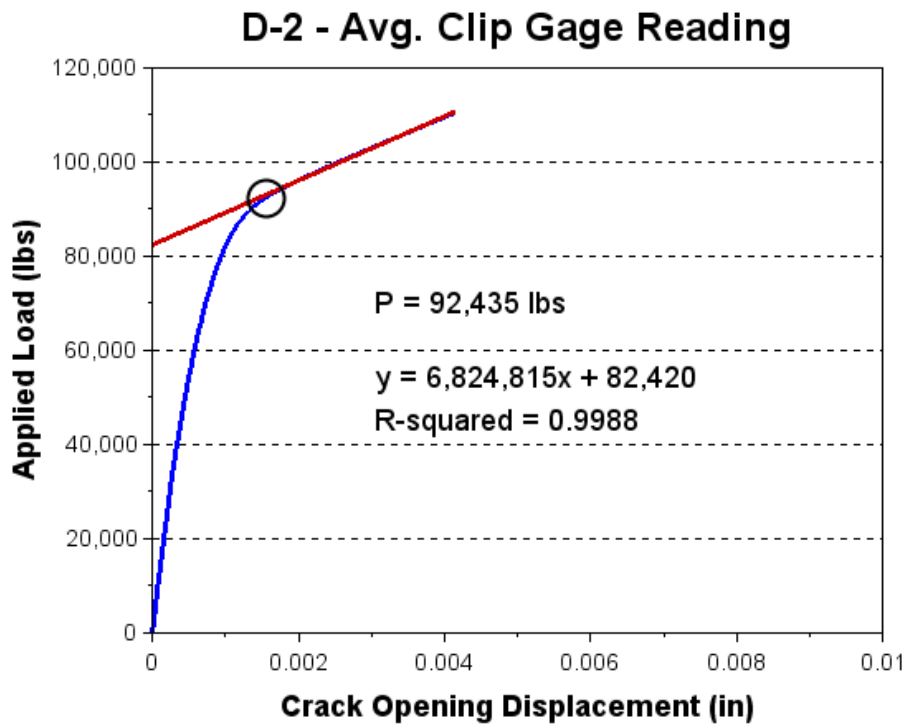


Figure 5.32 Tension test results for tie D-2

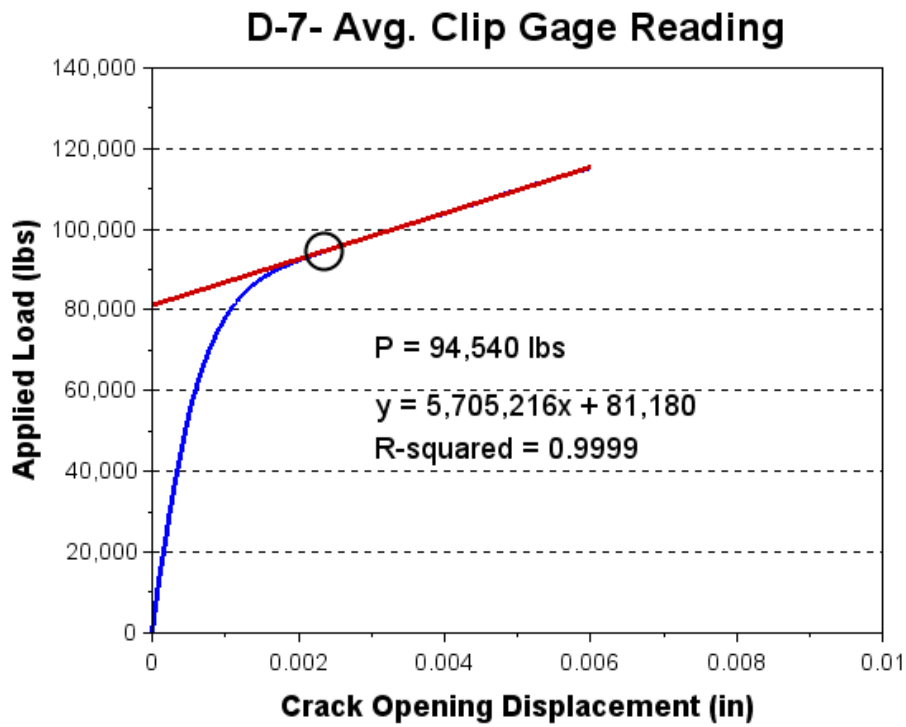


Figure 5.33 Tension test results for tie D-7

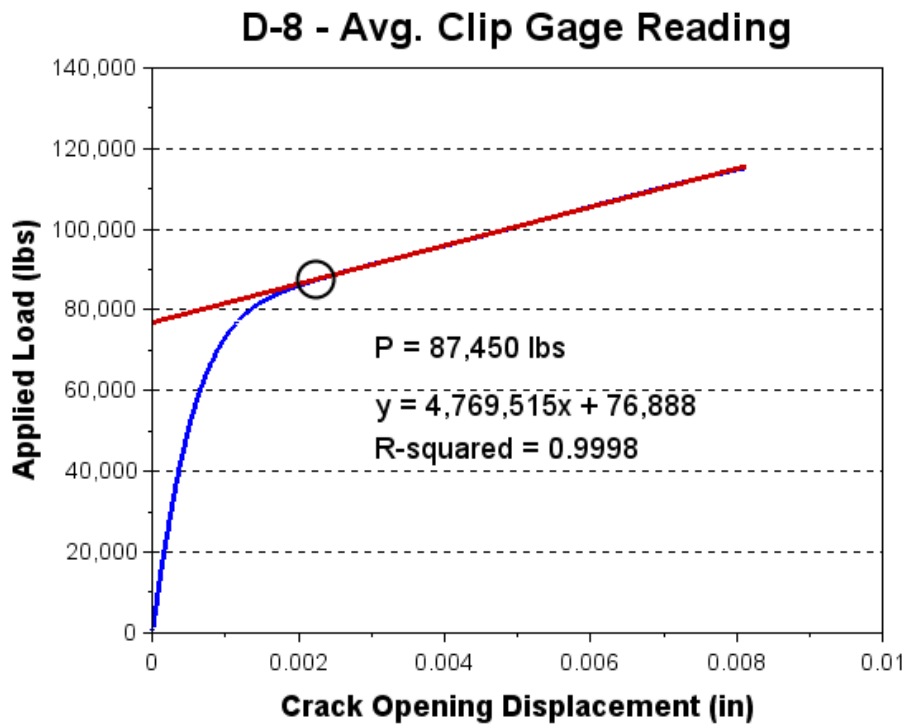


Figure 5.34 Tension test results for tie D-8

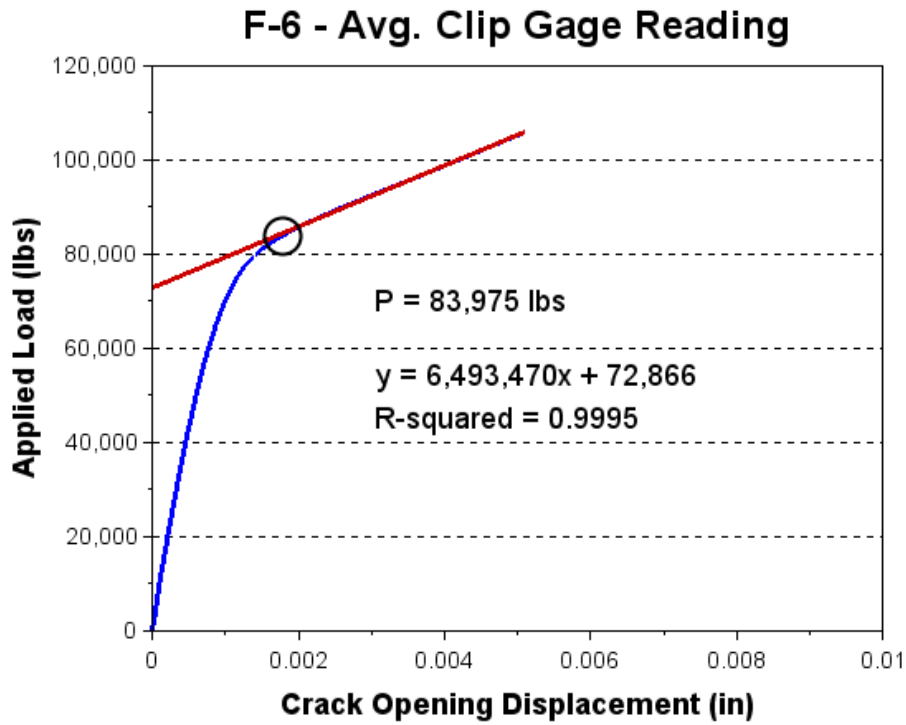


Figure 5.35 Tension test results for tie F-6

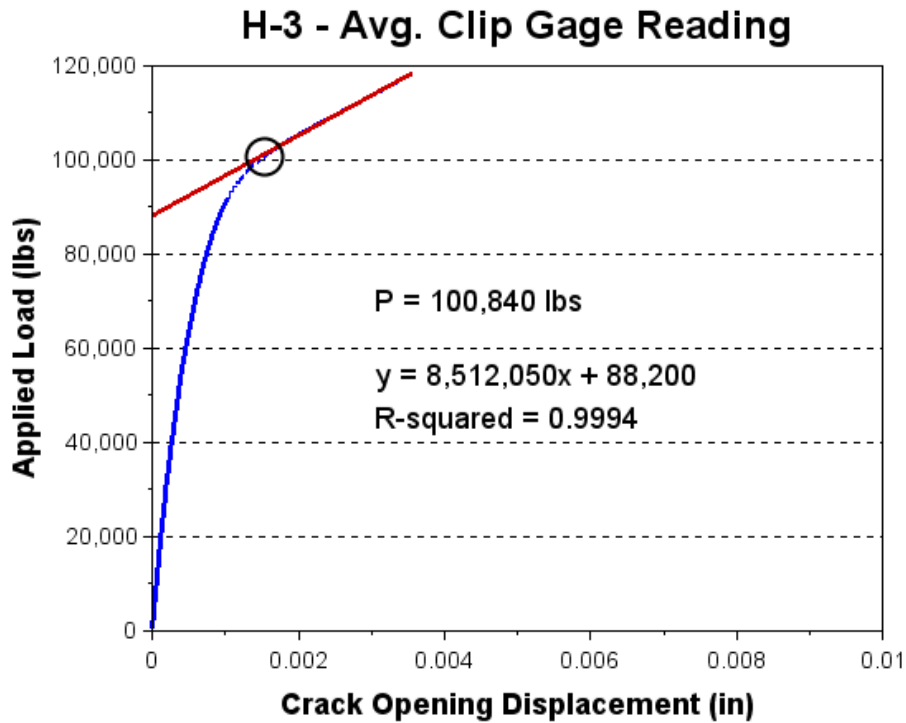


Figure 5.36 Tension test results for tie H-3

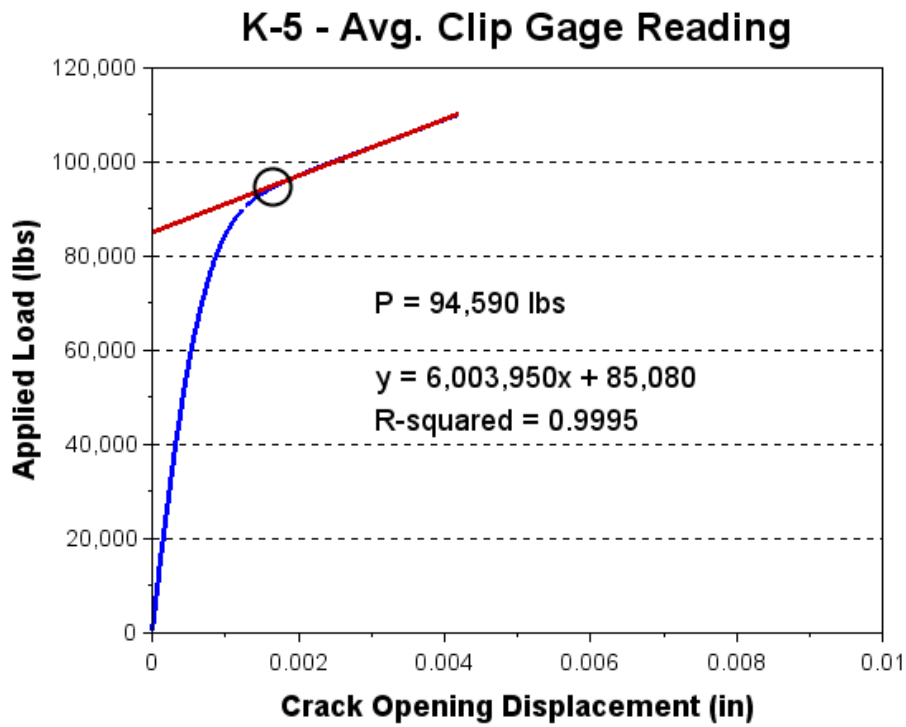


Figure 5.37 Tension test results for tie K-5

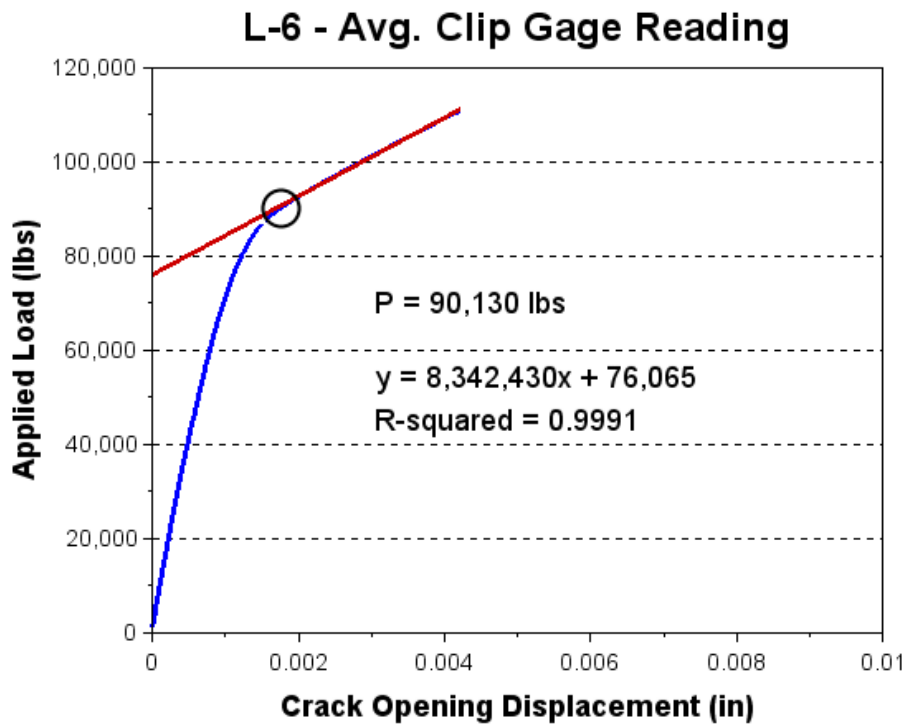


Figure 5.38 Tension test results for tie L-6

Each test specimen was weighed using a digital crane scale after testing to increase the accuracy of the direct tension test results. The weights and adjusted prestress force for each tie are listed in Table 5.7. All but two of the tie designs have a prestress force in the 82-93 kip range. Design A, the post-tensioned tie has a significantly lower prestress force of 61.2 kips, and design H is the highest with just under 100 kips. When comparing the estimated prestress force of existing ties presented in Table 5.7 to the prestress force of the new tie designs listed in Table 5.5, the existing ties tend to have a lower prestress force than the new ties.

**Table 5.7 Summary of prestress force estimates for existing ties**

Tie	Initial Prestress Force Estimate (kips)	Weight of Top Half (kips)	Adjusted Prestress Force (kips)
A-6	62.8	1.62	61.2
B-7	89.1	1.63	87.5
D-2	92.4	1.61	90.8
D-4	94.2	2.50	91.7
D-7	94.5	1.57	92.9
D-8	87.5	1.57	85.9
F-6	84.0	1.60	82.4
H-3	100.8	1.57	99.2
K-5	94.6	1.62	93.0
L-6	90.1	1.63	88.5

## **Chapter 6 - Strain Gage Method**

This chapter details the use of the strain gage method described in Chapter 2 to estimate the prestress force in ties R-5, NT-1, and CXT-2. In this method, concrete cover is first removed to expose a prestressing tendon and then a strain gage is installed on the tendon. The tendon is then cut and the change in strain is measured. Multiplying the strain change by the modulus of elasticity of the prestressing tendon results in the stress change of the wire. As the final stress after cutting is zero, the stress change corresponds to the stress in the wire prior to cutting. The force in the tendon is determined by multiplying the stress times the area of the wire. The total prestress force is then extrapolated by multiplying the force per tendon by the number of tendons.

As a result of the manufacturing process of indented prestressing wire, the wires tend to have a bow when in an unstressed state. When cutting the tensioned wire in this method, the wire will go back to its original shape, and may cause the strain gage to detect additional strain due to the curvature of the wire in the unstressed state. To evaluate the effect that the bow of the wire in the unstressed state has on the strain gage readings, a separate test was conducted on a wire tensioned to a known value in the laboratory.

### **Experimental Program**

Cover was removed to expose two wires at mid-span for all three ties. The mid-span location was selected to ensure that the wire was fully stressed at the section being tested. Figure 6.1 through Figure 6.3 show the typical amount of cover removed from tie R-5, NT-1, and CXT-1, respectively.



**(a) Length**



**(b) Width**



**(c) Depth**

**Figure 6.1 Typical dimensions of removed cover on tie R-5**



**(a) Length**



**(b) Width**



**(c) Depth**

**Figure 6.2 Typical dimensions of removed cover on tie NT-1**



**(a) Length**



**(b) Width**



**(c) Depth**

**Figure 6.3 Typical dimensions of removed cover on tie CXT-1**

After the wires were exposed, high precision linear strain gages (SGD-5/350-LY11 from Omega) were instrumented to the prestressing tendons. The gages had an active gage length of 4.5 mm (0.177 inch) and carrier dimensions of 9.8 mm x 5.2 mm (0.386 inch x 0.205 inch). The strain gages were attached with M-Bond AE-10, a high-strength adhesive with elongation capabilities of 6-10%. As the tendons in tie R-5 are 5.25 mm (0.207 inch) indented wire, and 5.32 mm (0.209 inch) indented wire for both NT-1 and CXT-1, there was not a large enough surface to adhere the strain gage to. To create an even surface to apply the strain gage to, an initial layer of M-Bond AE-10 was applied to the wire to fill the indents, and allowed to cure. Once cured, the excess adhesive was sanded down to create a smooth surface for the strain gage to bond to. For the two wires exposed on each tie, one wire was instrumented with two strain gages, and the other wire was instrumented with one strain gages, and labeled Gage 1, 2, and 3. The gage arrangement on tie R-5, NT-1, and CXT-1 are shown in Figure 6.4 - Figure 6.6, respectively.

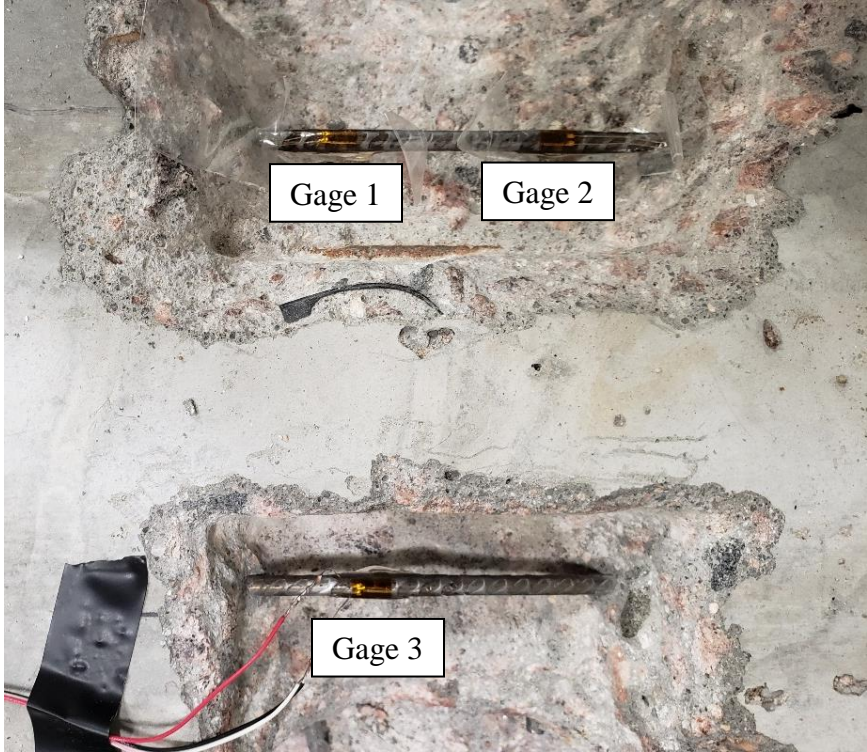


**Figure 6.4 Gage placement on tie R-5**

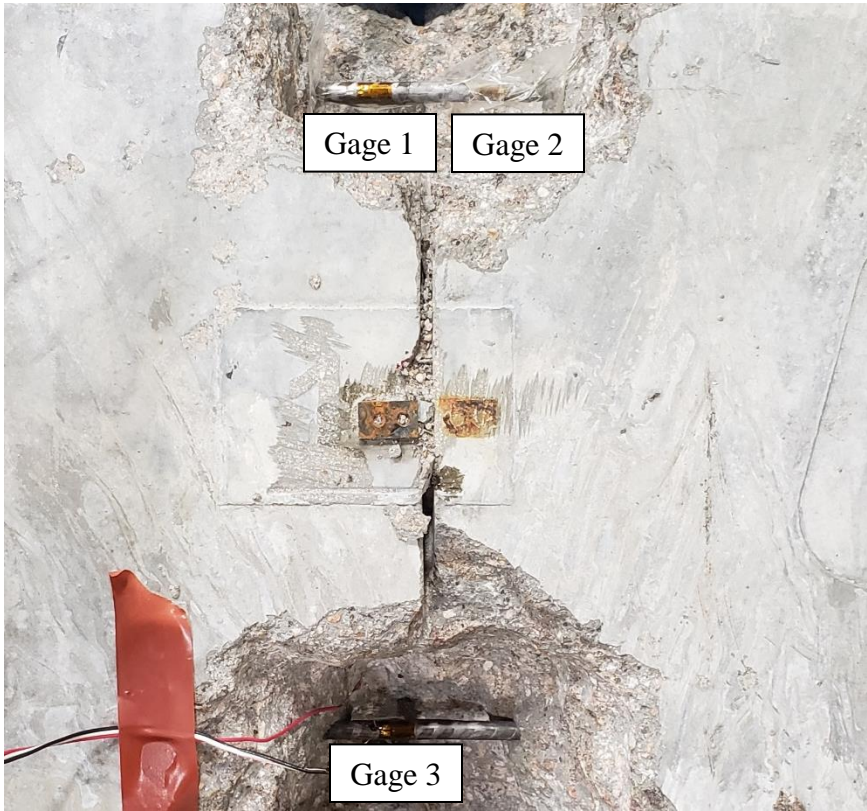


**Figure 6.5 Gage placement on tie NT-1**

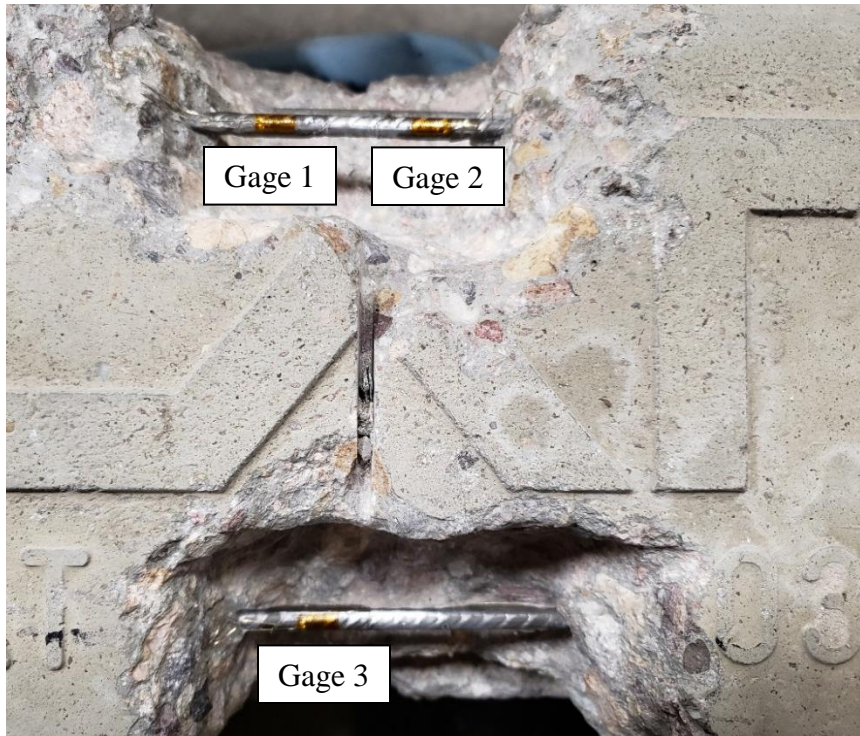


**Figure 6.6 Gage placement on tie CXT-1**

After the strain gages were attached to the wires and the adhesive had cured, they were connected to a Vishay System 7000 data acquisition system. The strain gages were used in a quarter-bridge circuit with an excitation voltage of 5V. Calibration of the strain gages was completed using the internal 10,000 $\mu\epsilon$  shunt calibration on the System 7000. During testing, strain measurements were captured at a rate of 2,000 Hz.

For ties R-5 and NT-1, the VWSG readings were taken after each step the measure the strain change associated with the removal of cover and cutting of the wires. Measurements were taken before and after the removal of cover, and after the wires had been cut.

## **Results**

Table 6.1 lists the VWSG readings and the total change in strain and stress from before the removal of cover to each step. The strain changes of 241.4 $\mu\epsilon$  and 31.5 $\mu\epsilon$  for ties R-5 and NT-

1, respectively, are both smaller than would be expected for the amount of cross-sectional area lost and the cutting of two wires. While the strain change in tie NT-1 is small and has a minimal effect on the internal prestress force, the strain change in tie R-5 is larger and may result in a more significant loss of prestress force. It is possible that the measured strain changes include the result of a slight camber induced in the tie from the changing centroidal location and wire eccentricities associated with removing cover and cutting wires. As NT-1 was previously tested using the direct tension method and has the large blocks on each end, it would be less susceptible to camber, resulting in smaller strain changes at each step.

**Table 6.1 VWSG readings at each stages of testing**

Tie	Step	R ( $\mu\epsilon$ )	T ( $^{\circ}\text{C}$ )	$\Delta$ Strain ( $\mu\epsilon$ )	$\Delta$ Stress (ksi)
R-5	Before cover removal	2466.3	21.8	-	-
	After cover removal	2409.5	23.1	-52.8	-1.5
	After cutting wires	2223.3	20.3	-241.4	-6.9
NT-1	Before cover removal	2407.1	26.4	-	-
	After cover removal	2396.8	26.7	-9.3	-0.3
	After cutting wires	2388.7	20.2	-31.5	-0.9

Figure 6.7 plots the strain measurements from the three gages on tie R-5 during the cutting process. When the wires were cut, they vibrated briefly before coming to a rest in an unstressed state. The average measured strain of the three wires was approximately 4,440 microstrain. Using Hooke's Law with an assumed modulus of elasticity of 28,500 ksi, the average stress per wire was calculated to be 126.5 ksi. For each tendon, having an area of 0.0336

in<sup>2</sup>, the average force per wire is 4.25 kips. With 18 total wires, the strain gage method estimates the total prestress force in tie R-5 to be 76.5 kips.

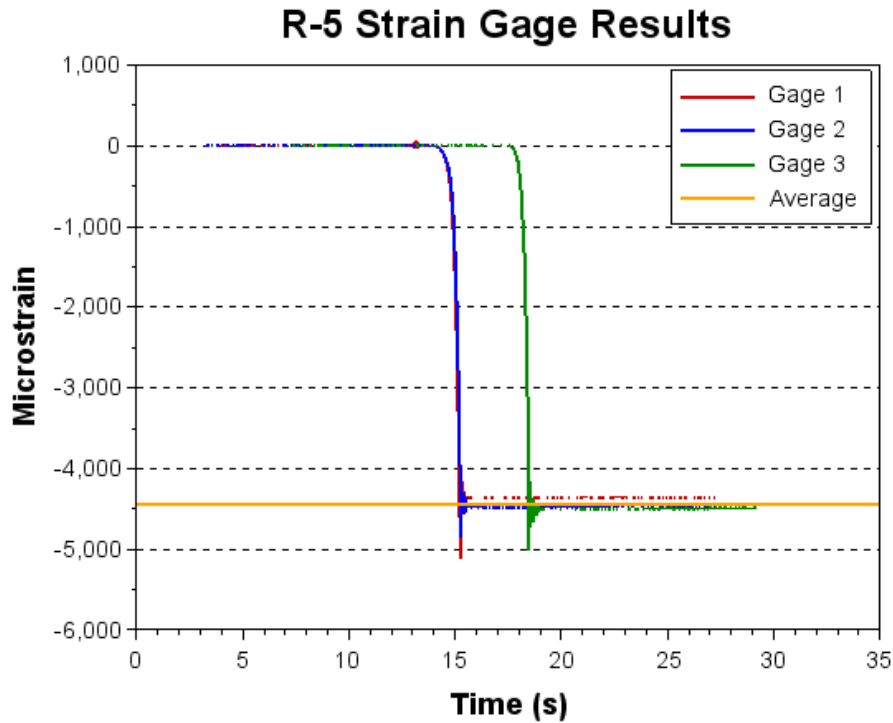


**Figure 6.7 Strain measurements of wires cut on tie R-5**

Several issues were encountered during the testing of tie NT-1. As shown in Figure 6.8, the strain measurements for gages 1 and 2 were not captured throughout the entire test. Since the final strain measurement of wire in the unstressed state is used to calculate the force per wire, the final strain measurements were recorded directly from the computer channels actively monitoring the strain gages. Screenshots of the computer screen with the final measurements of gages 1 and 2 are shown in Figure 6.9 and Figure 6.10, respectively. Additionally, it was noted that gage 2 was installed at an orientation that was skewed on the wire, shown in Figure 6.11, causing the final measurement to slightly underestimate the true axial strain in the wire.

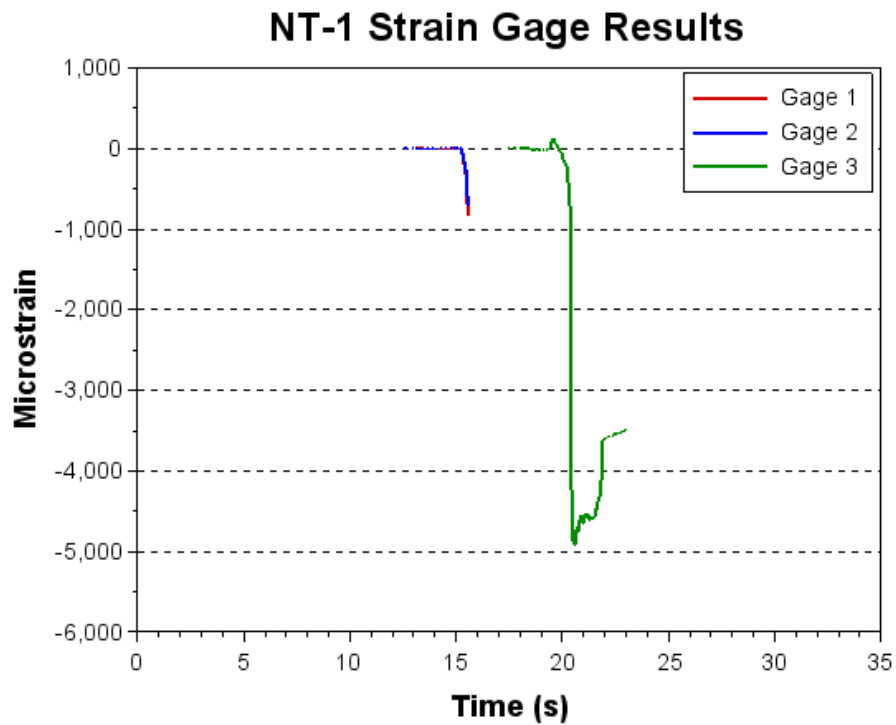


Figure 6.8 Strain measurements of wires cut on tie NT-1

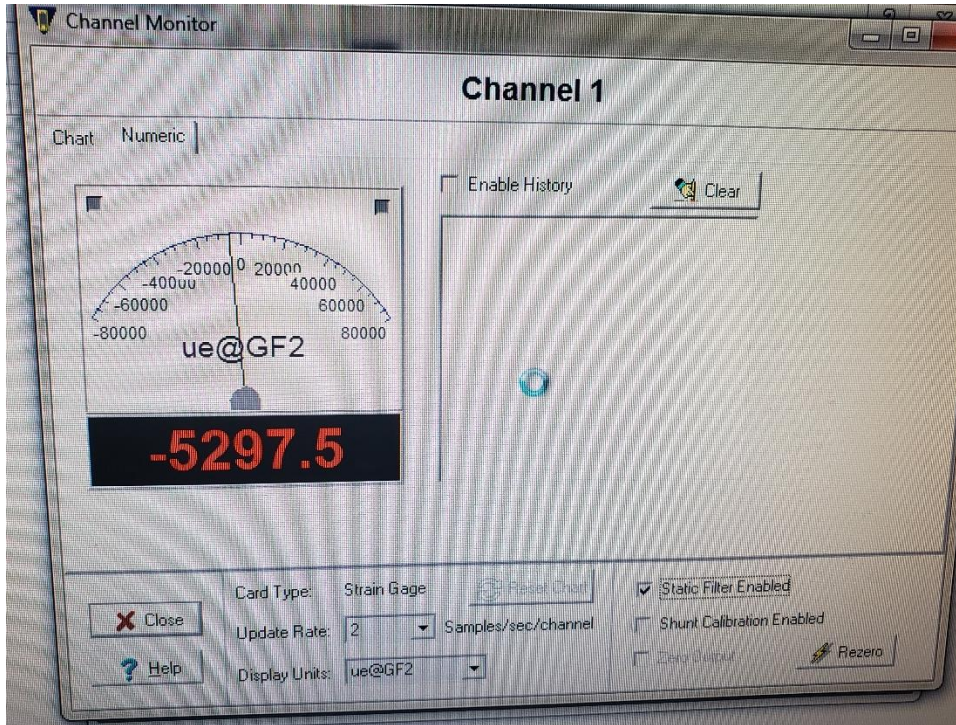
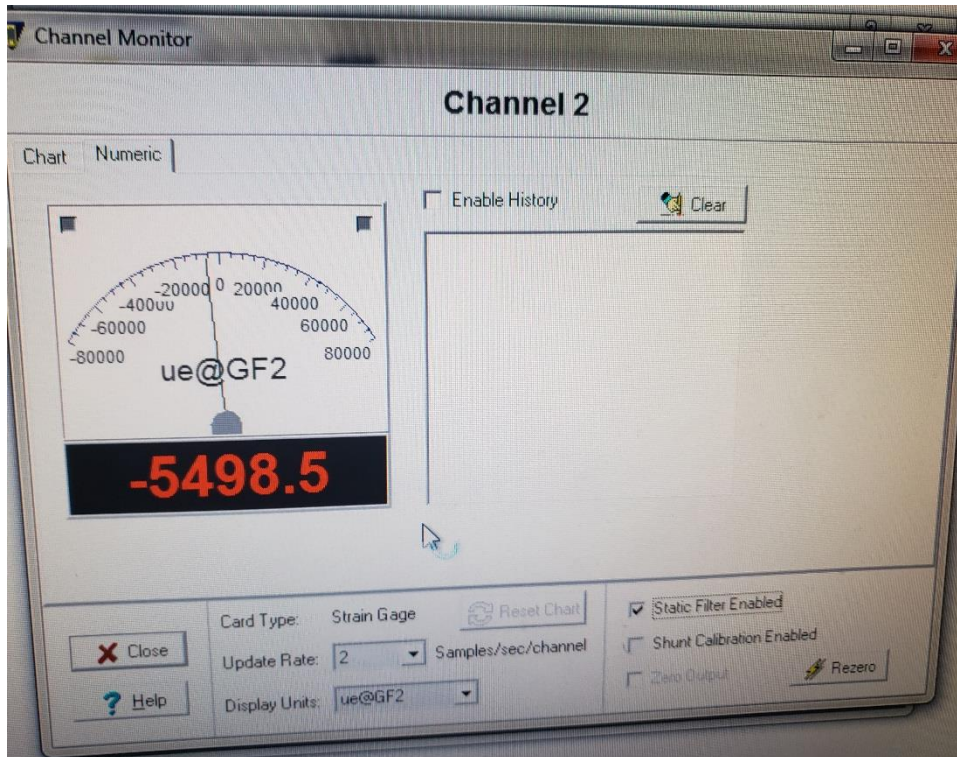


Figure 6.9 Final strain measurement for gage 1 of tie NT-1



**Figure 6.10 Final strain measurement for gage 2 of tie NT-1**



**Figure 6.11 Close up of gages 1 and 2 on tie NT-1**

Additional issues occurred when cutting the second wire containing gage 3. As seen in Figure 6.8, the strain measurement did not reach a steady state. During the cutting process, the wire on the left side of the cut was bent downward, and got caught on the wire to the right of the cut, causing a reduction in the strain measurements captured during testing. Figure 6.12 shows

one side of the wire caught on the other at the cut location. The wire was straightened out, shown in Figure 6.13, by pushing it back into place, and the final strain measurement was recorded from the computer channel actively monitoring the strain gage readings. A screenshot of the final strain measurement is shown in Figure 6.14.



**Figure 6.12 Wire in bent position after cutting**



**Figure 6.13 Wire straightened out after cutting**

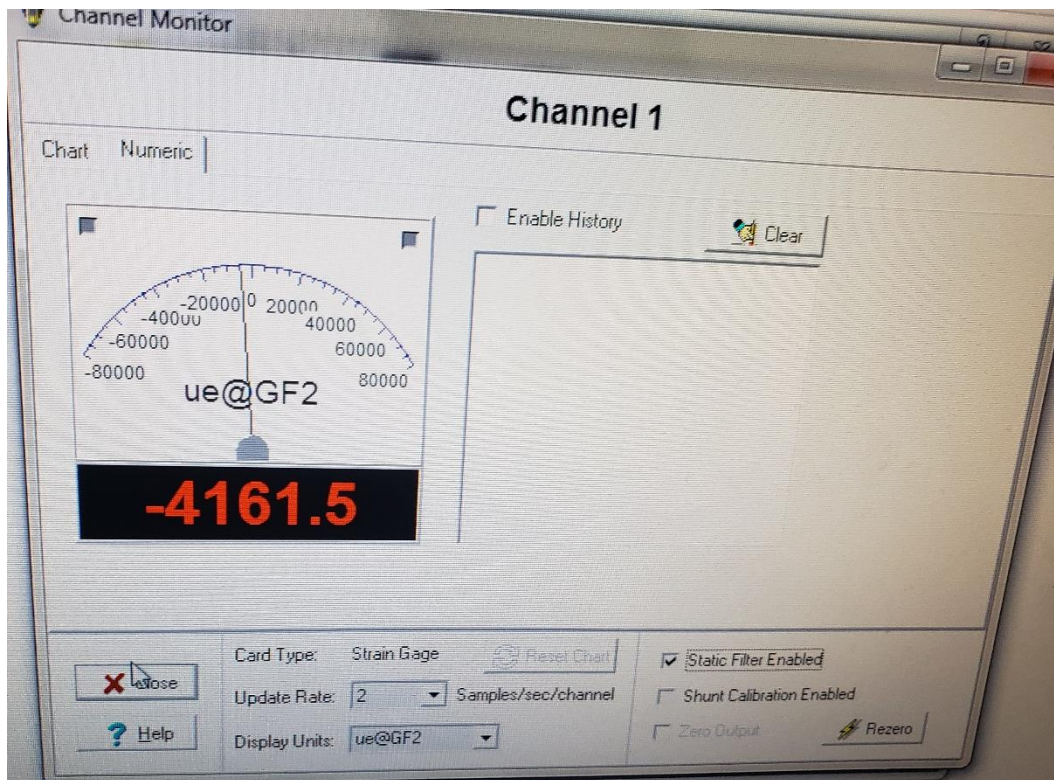


**Figure 6.14 Final strain measurement for gage 3 of tie NT-1**

The average measured strain of the three wires in tie NT-1 was approximately 4,986 microstrain. Using an assumed modulus of elasticity of 28,500 ksi, the average stress per wire was calculated to be 142.1 ksi. For each tendon, having an area of 0.0345 in<sup>2</sup>, the average force per wire is 4.9 kips. With 24 total wires, the total prestress force in tie NT-1 is estimated to be 117.6 kips. It should be noted there was a difference in the two wires of approximately 1,200 microstrain. This error could have been caused by slight delamination of the strain gage or it may indicate that the assumption that all wires have the same prestress force is wrong and cause inaccurate estimations of the prestress force.

The strain measurements from the three gages on tie CXT-2 are displayed in Figure 6.15. Gage 1 is seen to initially reach a steady strain, then magnitude begins to decrease. This could be the result of the strain gage partially debonding from the wire after the cut was made. To

determine the average strain value in the wires, the strain during the initial steady period after cutting the wire was used for gage 1. The average measured strain of the three gages was 4,380 microstrain. Multiplying the average strain by an assumed modulus of elasticity of 28,500 ksi, the average stress per wire was calculated to be 124.8 ksi. For each tendon, having an area of 0.0345 in<sup>2</sup>, the average force per wire is 4.31 kips. With 20 total wires in CXT-1, the estimated prestress force is 86.1 kips.

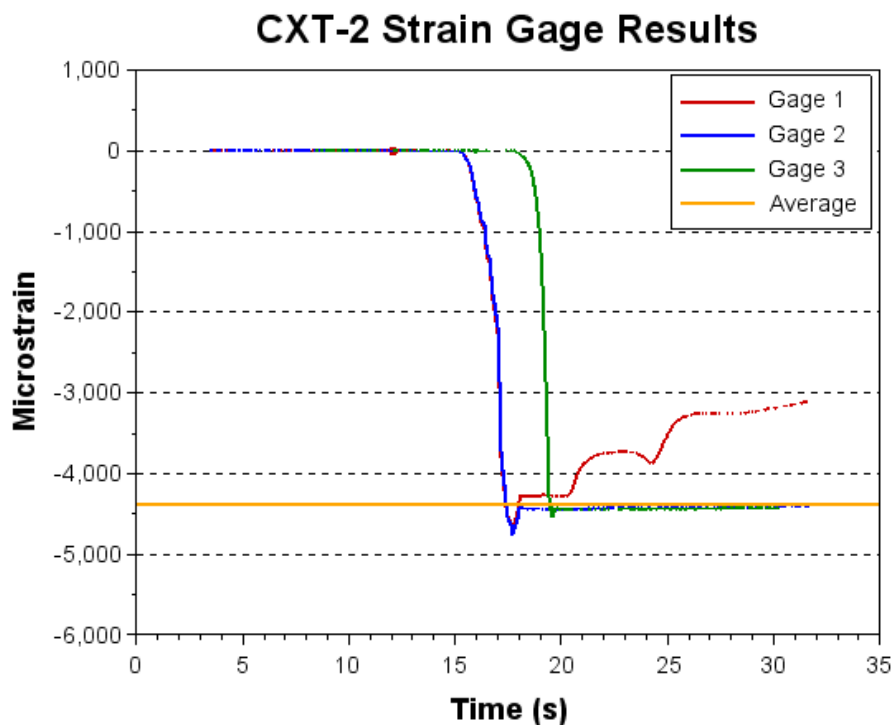


**Figure 6.15 Strain measurements from CXT 505S tie test**

A summary of the average stress and strain per wire, and corresponding prestress forces for ties R-5, NT-1, and CXT-2 are listed in Table 6.2. Additionally, for ties R-5 and NT-1, the prestress force was calculated from VWSG readings prior to any testing and is compared to the strain gage results in Table 6.3.

**Table 6.2 Prestress force estimates from the strain gage method**

Tie	Average Strain per Wire ( $\mu\epsilon$ )	Average Force per Wire (kips)	Number of Wires	Prestress Force (kips)
R-5	4,440	4.25	18	76.5
NT-1	4,986	4.90	24	117.6
CXT-2	4,380	4.31	20	86.1

**Table 6.3 Comparison of prestress force, in kips, from strain gage method and VWSG readings**

Tie	Strain Gage Method	VWSG	Net Difference
R-5	76.5	103.5	27.0
NT-1	117.6	143.4	25.8

For all three ties the prestress force estimated using the strain gage method were significantly lower than expected prestress force. For the case of ties R-5 and NT-1, the strain gage method underestimated the prestress force by 27 and 25.8 kips, respectively, when compared to the prestress force determined from VWSG readings. This results in the strain gage method estimating the prestress force with an error in the range of 18-26%. As previously noted, due the manufacturing process of the wires, they have a bowed shape when in an unstressed state. An additional test was conducted on a wire in a lab setup to evaluate how much the bow of the wire contributed to the overall error.

### **Test for Bowing of Wire**

To test for effects of the bow in an unstressed wire, a separate test was ran on the wire shown in Figure 6.16. Prior to testing, the expected strain difference between the outer and inner face of curve was calculated. The wire, containing a bow of 3/32 inches for the 19 inch long span, was calculated to have a radius of curvature,  $\rho$ , of 481 inches. Using basic mechanics, the expected strain,  $\epsilon$ , due to the curvature of the wire is calculated using Equation (5), where  $y$  is the

distance from the neutral axis, shown in Figure 6.17. From Equation (5), the total expected strain difference between the outer and inner edges of the bend was calculated to be approximately 435 microstrain.

$$\varepsilon = \frac{\pm y}{\rho} \quad (5)$$



**Figure 6.16 Bow in unstressed wire**

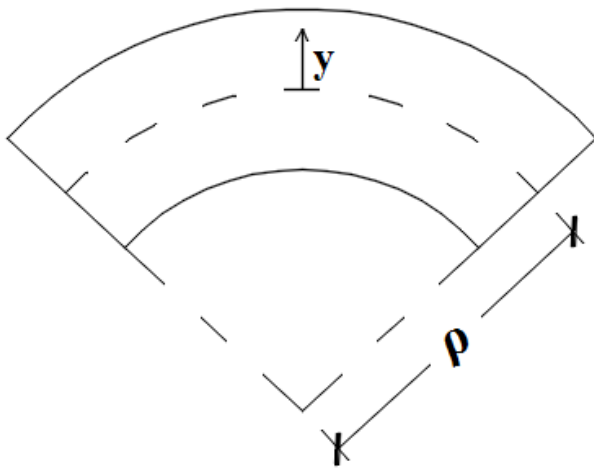


**Figure 6.17 Curvature of a wire**

The wire was tested using a Schimadzu Universal Testing machine with the setup shown in Figure 6.18. The wire was initially tensioned to 7,000 pounds. After allowing for relaxation loss, the final force in the wire was 6,776 pounds. Strain gages were then instrumented on the outer and inner faces of the bend in the wire while the wire was held in tension. The same process described above was used to instrument the strain gages, where an initial layer of M-

Bond AE-10 is applied the wire. The excess adhesive was sanded down to provide a smooth surface to attach the gages to. Figure 6.19 shows the strain gages instrumented to the wire, where Gage 1 is on the inner edge of the bend, and Gage 2 is on the outer edge.



**Figure 6.18** Wire bow test setup



**Figure 6.19 Strain gages instrumented on opposite faces of wire**

The wire was connected to the Vishay System 7000 for data acquisition during testing, and strain measurements were recorded at a rate of 2,000 Hz. The wires were then cut with a grinding wheel. The test results for the bow test are shown in Figure 6.20, where it can be observed that Gage 1 recorded a larger magnitude of strain than Gage 2. This is to be expected as Gage 1 was on the inner edge of the bend, so when the wire returns to its bowed shape in the unstressed state, Gage 1 would experience additional compressive strains, while Gage 2 would experience tensile strains, reducing the overall magnitude of the reading.

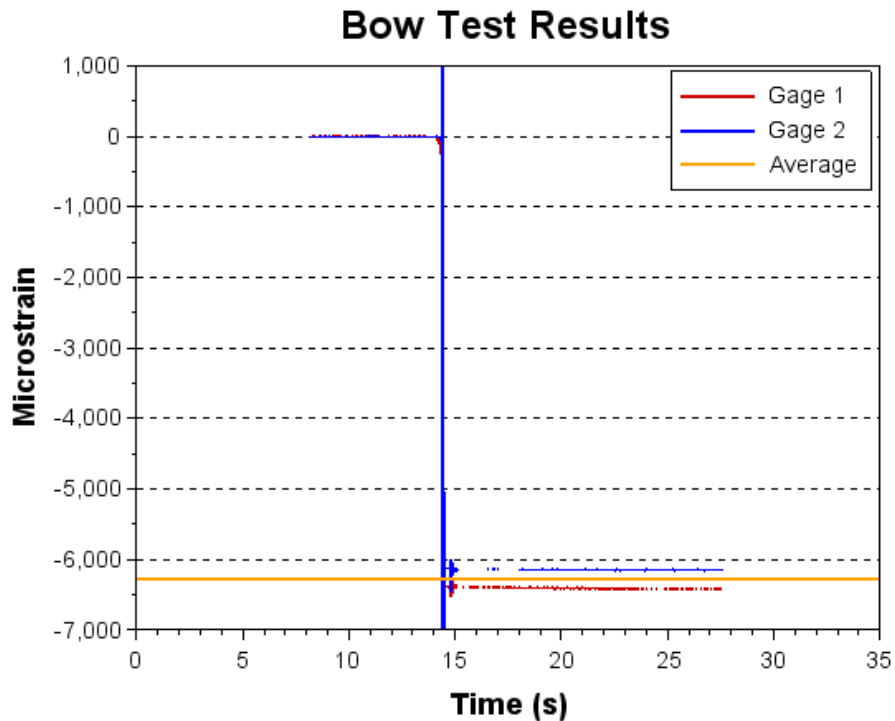


**Figure 6.20 Strain measurements from wire bow test**

The final strain readings for gages 1 and 2 were 6,400 and 6,130 microstrain, for a difference of 270 microstrain. The difference in microstrain is between the two gages is less than 435 microstrain calculated using the radius of curvature. Using the average strain value of the two gages, the strain in the wire is 6,265 microstrain. With an assumed modulus of 28,500 ksi and an area of  $0.0345\text{in}^2$ , this results in an estimated force of 6,160 pounds in the wire, resulting in a total error of 9.1% from the actual force in the wire. While the bow of the wire had some effect on the strain gage readings, the magnitude of strain error due to wire curvature is much lower than the error noted when attempting to estimate the total prestress force in ties.

## Chapter 7 - Length Change of Extracted Wire

This chapter details the use of the wire extraction method to estimate the prestress force in a tie. In the wire extraction method, the change in length of wires extracted from a tie were measured. Equation (6) can be used to solve for the force,  $P$ , in the wire, where  $E$  is the modulus of elasticity of the wire and is assumed to be 28,500 ksi,  $A$  is the area of the wire, and  $L_0$  is initial gage length. The prestress force in the tie can then be estimated by multiplying the force per wire by the number of wires in the tie.

$$\Delta L = \frac{PL_0}{AE} \quad (6)$$

Ties R-5 and CXT-2 were investigated in this section using two separate methods to measure the change in length of the extracted wire. In method 1, the full length of the wire is measured prior to extraction. In method 2, cover is removed to expose the wire at two locations 60 inches apart, and the wire is marked to create an initial gage length of 60 inches over which the length change is measured.

### Method 1: Full Length Measurement

In the Method 1, the prestress force is estimated using Equation (6), where  $\Delta L$  is measured over the whole length of wire in the tie. Because the prestress force is not fully developed in the tie until a distance of  $L_T$  (the transfer length) on each end, the length of the wire in the tie cannot be used as the initial gage length,  $L_0$ . To account for the distance on each end of the tie where the tendon stress is transitioning from unstressed to fully stressed, the initial gage length, calculated in Equation (7), is taken as the length of the wire in the tie minus half of the transfer length from each side (minus 1 transfer length total). Figure 7.1 illustrates the tendon

stress levels along the length of the tie and value used as the initial gage length. Since the actual value of the transfer length was unknown for both ties, and a typical value of 10 inches was assumed for calculation of the initial gage length.

$$L_0 = L_w - L_T \quad (7)$$

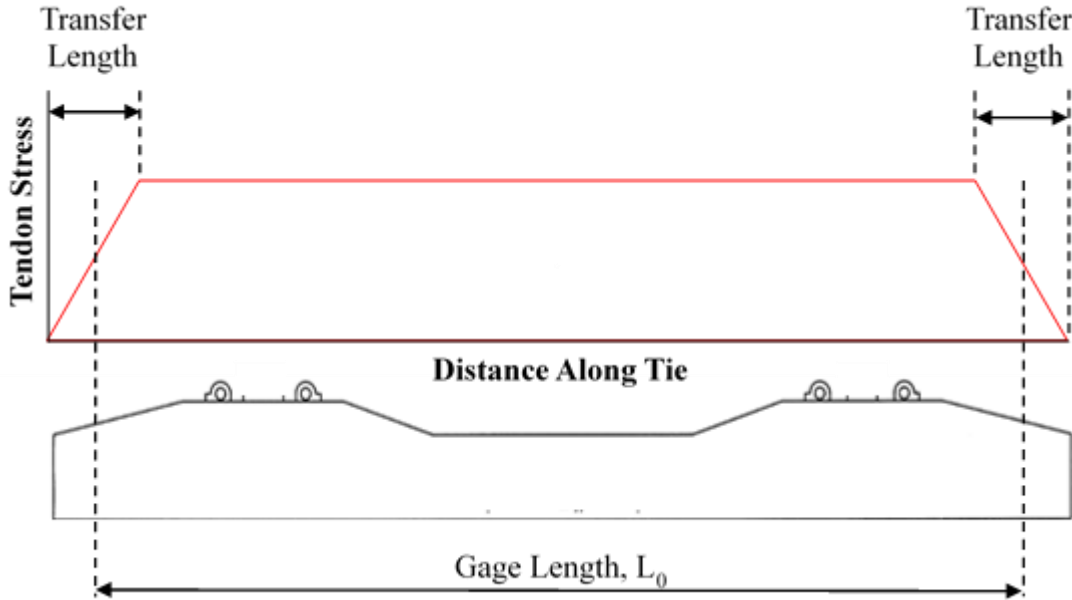


**Figure 7.1 Initial gage length,  $L_0$ , for Method 1 measurement**

To measure the length of the wire both prior to extraction and afterwards, the apparatus in Figure 7.2 was fabricated. This device consist of a conical insert on one end for centering on a wire end, and a micrometer with a resolution of 0.00005 inches on the other end for taking measurements. A #9 rebar with a length of 101-9/16 inches, shown in Figure 7.3, was used as a reference gage block. With the micrometer zeroed when fully retracted, a measurement taken on the rebar was -0.3383, indicating a total reference length of 101.9008 inches. Subsequent measurements were subtracted from the reference length to determine the wire length.



**Figure 7.2 Wire measuring apparatus**



**Figure 7.3 Length of rebar used as gage block**

In cases where the wires stuck out from the end of the tie, the wire was ground down to create a smooth surface for taking measurements. Figure 7.4 shows a row of wires that have been

ground down prior to being measured. In Figure 7.5, the apparatus is set up along a tie for wire measurements. In Figure 7.6 and Figure 7.7, the conical end is lined up at the end of a tie, and centered on the end surface of a wire, respectively. The micrometer is lined up with the other end of the wire and a measurement is taken, shown in Figure 7.8.



**Figure 7.4 Smoothened wire surfaces for length measurement (bottom row)**



**Figure 7.5 Measurement of wires in tie**



**Figure 7.6 Conical end piece at end of tie**



**Figure 7.7 Conical piece centered on the end of a wire**



**Figure 7.8 Micrometer measuring wire length**

After initial wire lengths were measured and recorded, the wires were extracted from the tie by removing the concrete cover, shown in Figure 7.9. Special care was taken to ensure the wires were not damaged during the extraction process. The wires extracted from ties R-5 and CXT-2 are shown in Figure 7.10 and Figure 7.11, respectively. These figures show that the wires are not straight when in the unstressed state. To ensure the wires were straight for post-extraction length measurements, they were clamped to a 5" x 3" x 1/4" aluminum I-beam at the 90 degree bend, shown in Figure 7.12. Once clamped, the wire length was measured using the same measuring apparatus, where the conical end piece and micrometer were centered on the wire, shown in Figure 7.13 and Figure 7.14, respectively.



**Figure 7.9** Extraction of wires from tie

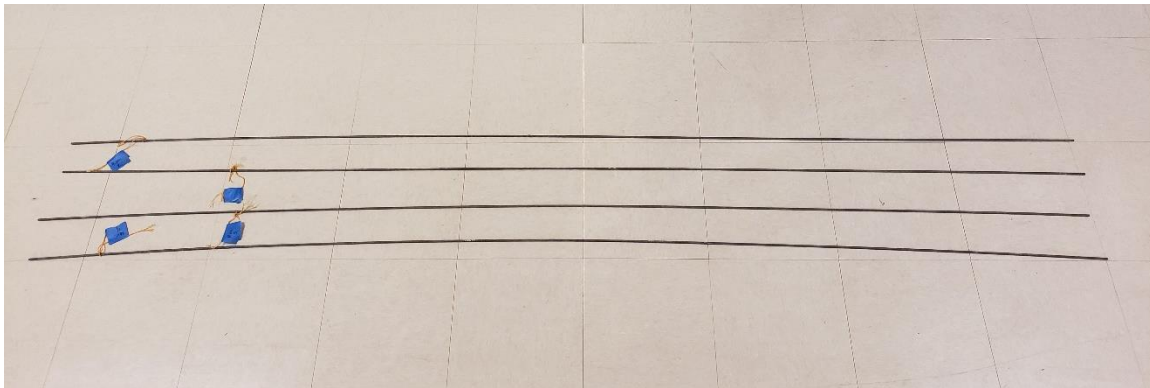


**Figure 7.10** Wires extracted from tie R-5

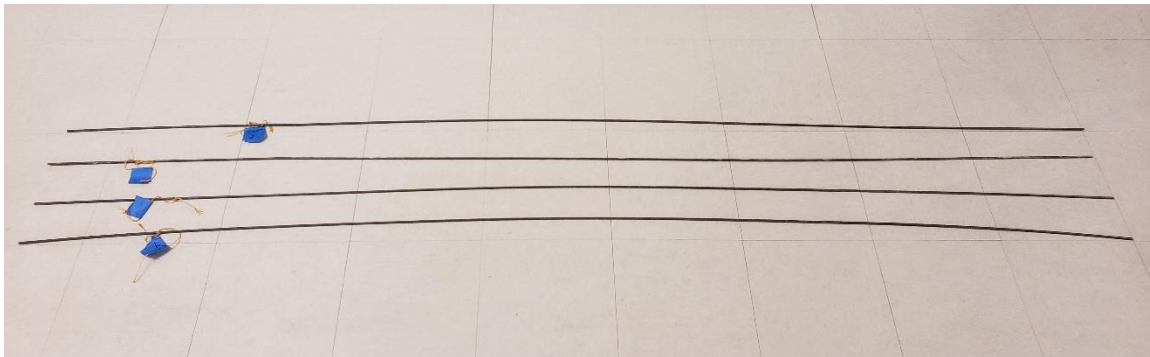


**Figure 7.11** Wires extracted from tie CXT-2



**Figure 7.12 Clamping used to keep wires straight**



**Figure 7.13 Conical end piece centered on wire**



**Figure 7.14 Micrometer centered on wire**

### Method 1 Results

Four wires from the bottom row of each tie were measured and extracted to determine the average force per wire. The measurements taken for the tie R-5 are presented in Table 7.1 along with the calculated average force per wire. To calculate the force per wire, the area of a single wire is taken as  $0.0336 \text{ in}^2$ , and value of 28,500 ksi is assumed for the modulus of elasticity of the wire. With tie R-5 having 18 wires and an average force per wire of 5.23 kips, listed in Table 7.1, the total prestress force is estimated to be 94.14 kips.

**Table 7.1 Method 1 results for tie R-5**

Wire	Pre-Extraction Measurement (in)	Implied Total Length (in)	Gage Length $L_0^*$ (in)	Post-Extraction Measurement (in)	$\Delta L$ (in)	Force in Wire (kips)
1	-0.2328	101.6680	91.6680	-0.7281	0.4953	5.17
2	-0.2906	101.6102	91.6102	-0.7910	0.5004	5.23
3	-0.3167	101.5841	91.5841	-0.8295	0.5128	5.36
4	-0.3040	101.5968	91.5968	-0.7953	0.4913	5.14

\*Assumes Transfer Length of 10 inches

Average = 5.23

The measurements taken for tie CXT-2 are presented in Table 7.2 along with the calculated average force per wire. To calculate the force per wire, the area of a single wire is taken as 0.0345 in<sup>2</sup>, and value of 28,500 ksi is assumed for the modulus of elasticity of the wire. With tie CXT-2 having 20 wires and an average force per wire of 5.42 kips, listed in Table 7.2, the total prestress force is estimated to be 108.4 kips.

**Table 7.2 Force per wire results from Method 1 for CXT 505S tie**

Wire	Pre-Extraction Measurement (in)	Total Length (in)	Gage Length L <sub>0</sub> (in)	Post-Extraction Measurement (in)	ΔL (in)	Force in Wire (kips)
1	-0.01225	101.8886	91.8886	-0.52075	0.5085	5.44
2	-0.04015	101.8807	91.8807	-0.54460	0.5045	5.40
3	-0.00165	101.8892	91.8892	-0.50765	0.5060	5.41
4	-0.00320	101.8976	91.8976	-0.50950	0.5063	5.42
Average =						5.42

The average force per wire and total prestress force estimates determined from Method 1 are summarized in Table 7.3. For tie R-5, when compared to the prestress force of 103.5 kips determined from the vibrating-wire strain gage, the error in the estimated prestress force is 9%. This indicates that it is feasible to estimate the prestress force using this method, but not make an accurate prediction.

**Table 7.3 Summary of results from Method 1**

Tie	Average Force per Wire (kips)	Number of Wires	Estimated Prestress Force (kips)
R-5	5.23	18	94.14
CXT-2	5.42	20	108.4

## Method 2: 60 Inch Gage Length

In Method 2, the prestress force was again estimated using Equation (6), where an initial gage length,  $L_0$ , of 60 inches is used. The gage length was set by removing the concrete cover to expose a wire at two locations separated by 60 inches, as illustrated in Figure 7.15. A small mark was scribed into the wire at each location using the wire scriber shown in Figure 7.16. The wire scriber consisted of a steel tube with two scribers mounted at a fixed distance of 60 inches apart. After the wire was extracted from the tie, a tape measure was used to measure the distance between the two marks to the nearest  $1/32$ " to determine the change in length,  $\Delta L$ , used to calculate the force per wire,  $P$ , in Equation (6). By using a set gage length of 60 inches, the tendons were assumed to be fully stressed throughout the measured length. This eliminates the need in Method 1 to estimate the transfer length in order to calculate the initial gage length. Figure 7.17 shows a tie where the cover has been removed to expose a wire at two locations along the bottom surface. A typical wire mark made by the scriber is shown in Figure 7.18.

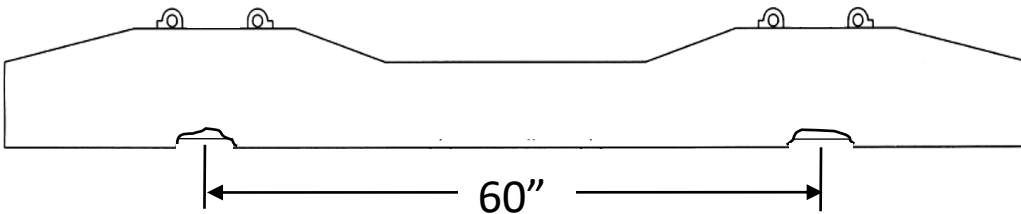


**Figure 7.15 Wires exposed on bottom surface of tie**

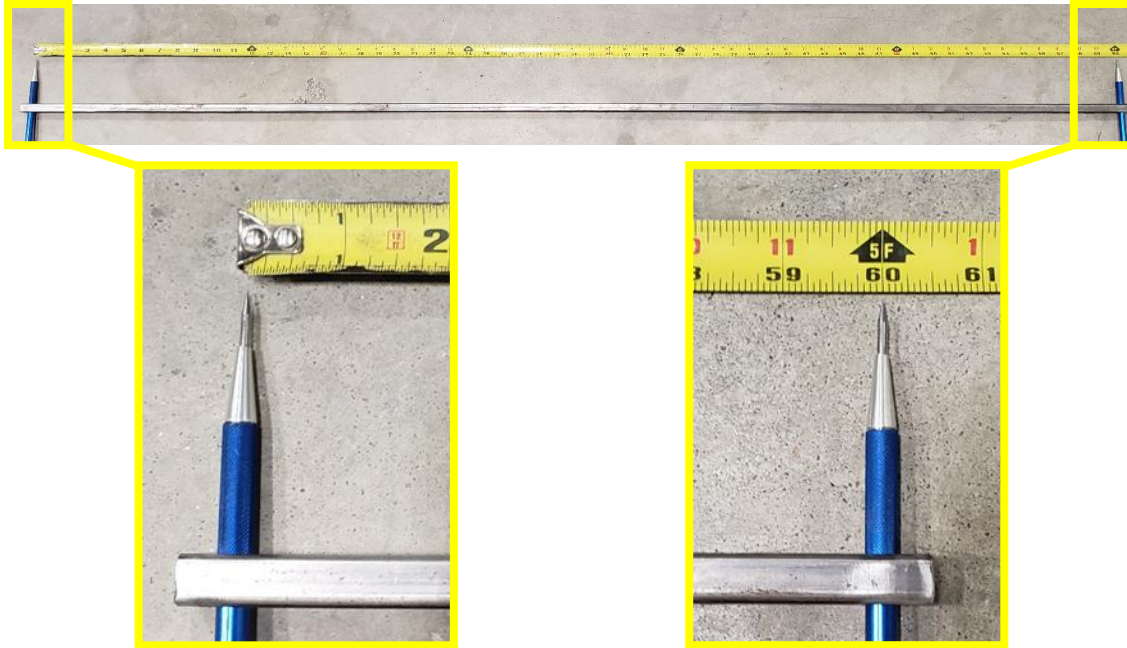


**Figure 7.16 Wire scriber with a set 60" gage length**



**Figure 7.17 Wired exposed on tie for marking 60 inch gage length**



**Figure 7.18 Typical mark from wire scribe**

### **Method 2 Results**

Due to the difficulty of removing cover to access the wires, only the two corner wires (wires 1 and 4) on the bottom surface from each tie were used for measurements in Method 2. The measurements taken for tie R-5 are presented in Table 7.4, along with the calculated average force per wire. The force per wire was calculated the same way as in Method 1, where the area of a single wire is  $0.0336 \text{ in}^2$ , and the modulus of elasticity is assumed to be 28,500 ksi. The total prestress force is likewise calculated the same way as in Method 1, where the force per wire is multiplied by the total number of wires. With tie R-5 having 18 wires and an average force per wire of 4.23 kips, listed in Table 7.4, the total prestress force is estimated to be 76.1 kips.

**Table 7.4 Force per wire results from Method 2 for Rocla tie**

Wire	$L_0$ (in)	Post-Extraction Length (in)	$\Delta L$ (in)	Force in Wire (kips)
1	60	59.75	0.25	3.99
4	60	59.72	0.28	4.47

Average = 4.23

The measurements taken for tie CXT-2 are presented in Table 7.5, along with the calculated average force per wire. To calculate the force per wire, the area of a single wire was taken as 0.0345 in<sup>2</sup>, and value of 28,500 ksi is assumed for the modulus of elasticity of the wire. With tie CXT-2 having 20 wires and an average force per wire of 4.10 kips, listed in Table 7.5, the total prestress force is estimated to be 82.0 kips.

**Table 7.5 Force per wire results from Method 2 for CXT 505S tie**

Wire	L <sub>0</sub> (in)	Post-Extraction Length (in)	ΔL (in)	Force in Wire (kips)
1	60	59.69	0.31	5.08
4	60	59.81	0.19	3.11

Average = 4.10

The average force per wire and total prestress force estimates determined from Method 2 are summarized in Table 7.6. The prestress force estimated using Method 2 was lower for both ties than the results from Method 1. Since the transfer length estimation was not needed in Method 2, the estimated prestress forces were expected to be larger (closer to actual values) than in Method 1. However, for tie R-5, the estimated prestress force of 76.1 kips results in an error of 26% when compared to the prestress force of 103.5 kips determined from the VWSG readings. Wires may have been damaged while removing cover to make the initial marks for the 60 inch gage length, which may have reduced the prestress force.

In Method 1 where ΔL was approximate ½”, the micrometer used for measurements had a precision of 0.01%, whereas in Method 2 where ΔL was approximately 1/3”, the precision of the tape measure used was 9.5%. The difference between the precision of the measuring devices for each method had a significant contribution to the difference in error between the two methods.

**Table 7.6 Summary of results from Method 2**

Tie	Average Force per Wire (kips)	Number of Wires	Estimated Prestress Force (kips)
R-5	4.23	18	76.1
CXT-2	4.10	20	82.0

## Chapter 8 - Center negative Cracking Moment

In this chapter, the center negative cracking moments are investigated for the existing tie designs. For the ties investigated in Chapter 5, the theoretical cracking moment is calculated using the prestress force results from the direct tension test. Additionally, the experimental cracking moments for each tie design group are determined and compared to the current requirements of the AREMA Chapter 30 center negative bending test.

### Theoretical Cracking Moments

For the tie designs investigated in Chapter 5, the theoretical center negative cracking moments were calculated using the prestress force results from the direct tension method. For group D, the average prestress force of all the type D ties tested with the direct tension method was used to calculate the theoretical center negative cracking moment. The theoretical cracking moment is calculated using Equation (2) in Chapter 4, and solving for M. The term  $\sigma_t$  in Equation (2) is calculated as the modulus of rupture using (8) below from ACI-318 (American Concrete Institute, 2014), assuming a long term concrete compressive strength of 10,000 psi.

$$f_r = 7.5\sqrt{f'_c} \quad (8)$$

To calculate the theoretical moments, the section properties listed in Chapter 3 for each tie were used, where  $y_{top}$  is simply the height of the section at the center minus  $y_b$ . The cross-section properties, prestress force, and theoretical cracking moments are listed in Table 8.1.

**Table 8.1 Section properties and theoretical cracking moments**

	A (in <sup>2</sup> )	y <sub>top</sub> (in)	I (in <sup>4</sup> )	e (in)	P (kips)	Theoretical M <sub>cr</sub> (kip-in)
A	58.9	3.57	235	-0.05	61.2	121
B	70.6	3.77	293	-0.17	87.5	169
D	73.0	3.53	298	-0.43	89.9	206
F	52.0	2.68	126	0.40	82.4	76.8
H	68.3	3.42	273	-0.21	99.2	197
K	71.0	3.60	274	-0.03	93.0	154
L	57.4	3.03	169	-0.14	88.5	115

### Experimental Cracking Moments

The pre-cracking phase of the flexural crack reopening method described in Chapter 3 was used to evaluate the experimental cracking moment of the ties and is described in more detail in this chapter. For each design group, three ties were loaded in flexure to determine the center negative cracking moment, M<sub>cr</sub>. Ties were tested upside-down and simply supported at the rail seat. The ties were loaded in four-point bending using a 15 inch spreader beam, shown in Figure 8.1, creating a region of constant moment at mid-span in which flexural cracking is initiated. Two LVDTs (one on each side) were used to measure mid-span deflection during testing - as shown in Figure 8.2.

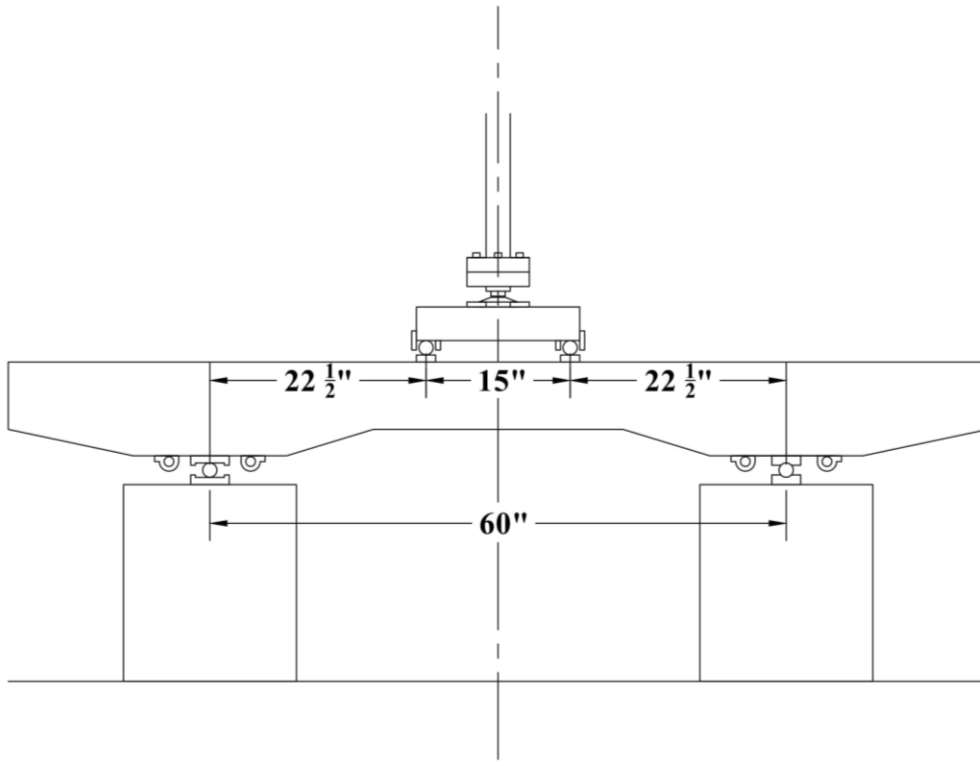


**Figure 8.1 Center negative bending test schematic**



**Figure 8.2 Flexural test setup**

A 50-kip-capacity hydraulic actuator and MTS servo-hydraulic controller were used to apply load at a rate of 1,000 pounds per minute. Load was applied until flexural cracking within the constant moment region was observed visually. The load corresponding to first cracking was recorded as the cracking load,  $P_{cr}$ , and used to calculate the cracking moment using Equation (4) in Chapter 4. The experimental cracking moments for each tie and the corresponding average cracking moments for each design group are summarized in Table 8.2. It was noted that the experimental cracking moments were larger than the theoretical cracking moments in Table 8.1. Since the flexural cracks of prestressed member are very small, the use of visual inspection typically results in overestimating the cracking moments.

**Table 8.2 Average center negative cracking moments**

Tie	P <sub>cr</sub> (lbs)	M <sub>cr</sub> (kip-in)	Avg. M <sub>cr</sub> (kip-in)
A-1	17,000	191	170
A-3	14,000	158	
A-4	14,300	161	
B-1	21,750	245	247
B-2	21,190	238	
B-3	22,550	254	
B-4	22,400	252	
C-1	16,400	185	179
C-2	14,300	161	
C-3	17,000	191	
D-1	25,200	284	284
D-3	25,350	285	
D-4	25,100	282	
E-1	18,000	203	200
E-4	17,700	199	
E-5	17,500	197	
F-1	13,000	146	127
F-2	10,350	116	
F-3	10,550	119	
G-1	21,900	246	250
G-2	22,600	254	
G-5	22,200	250	
H-1	24,400	275	284
H-2	25,800	290	
H-6	25,400	286	
J-1	19,400	218	221
J-3	19,800	223	
J-5	19,800	223	
K-1	21,800	245	249
K-2	21,600	243	
K-3	23,100	260	
L-1	14,100	159	178
L-2	14,800	167	
L-4	18,500	208	
M-1	16,800	189	198
M-2	18,500	208	
M-6	17,400	196	

When compared to the theoretical cracking moments in Table 8.1, the experimental values are consistently higher. These differences may be caused by theoretical moments being calculated using an estimation of the tensile strength of concrete. The actual tensile strength is unknown, and is likely different from the value used in calculation. Additionally, the average cross-section properties were used for each design group, but properties vary between individual ties, such that each tie would have different theoretical cracking moments.

### **AREMA Center negative Test Comparison**

The AREMA center negative bending test is the current standard used to evaluate the center negative moment capacity of new tie designs. To compare the experimental cracking moments of the ties to the AREMA test, the factored center negative bending-moment capacity is first calculated for each tie design using the procedure outlined in AREMA Chapter 30. In AREMA Chapter 30, the factored center negative bending-moment is determined from Equation (9) below.

$$M_{C-} = B_{C-} \times V \times T \quad (9)$$

Where:

$M_{C-}$  = factored center negative bending-moment (kip-in)

$B_{C-}$  = unfactored center negative bending-moment (kip-in)

V = speed factor

T = tonnage factor

The unfactored center negative bending-moment,  $B_{C-}$ , is calculated according to Equation (10) below.

$$B_{c-} = -\frac{1}{2}R \left[ -\frac{L^2 - (1-a)c^2}{2(L - (1-a)c)} - g \right] \quad (10)$$

Where:

R = design rail seat load (kips)

L = tie length (in)

g = rail center-to-center spacing (in)

c = 2g - L = center reaction section (in)

a = center reaction factor

The unfactored bending-moments for each tie were calculated using the recommended 82 kip axel load, and an assumed center-to-center spacing of 24 inches. A speed factor of 0.8 and a tonnage factor of 1.0 were chosen, corresponding to a speed of 40 mph and annual tonnage of 60 million gross tons (MGT), respectively. The factored center negative moments for each design group are listed in Table 8.3, where the difference between design types is due to the length of ties.

**Table 8.3 Factored center negative bending-moments**

Tie Design	Factored Center Negative Moment (kip-in)
A	202
B	191
C	160
D	191
E	191
F	202
G	191
H	191
J	202
K	191
L	202
M	202

The AREMA center negative bending-moment test states that load should be applied at a rate no greater than 5 kips per minute until the load required to produce the center negative design moment is reached. The load is then held for three minutes and if no cracking is observed, the tie passes. The setup for the AREMA Chapter 30 center negative test, shown in Figure 8.3, is similar to the experimental setup in Figure 8.1, where the AREMA test calls for a 6 inch gap between the two point loads, rather than the 15 inch used. While the experimental test procedure varied slightly from the procedure in the AREMA center negative test, the cracking moments can still be compared to the design moment capacities. Table 8.4 shows the design moments from AREMA, the experimental cracking moments, and whether or not they meet the requirements of the AREMA center negative test. It can be seen that 8 of the 12 existing tie designs investigated would meet the requirements of the current AREMA test, despite all 12 having performed well in track for over 25 years with no signs of center negative cracking.

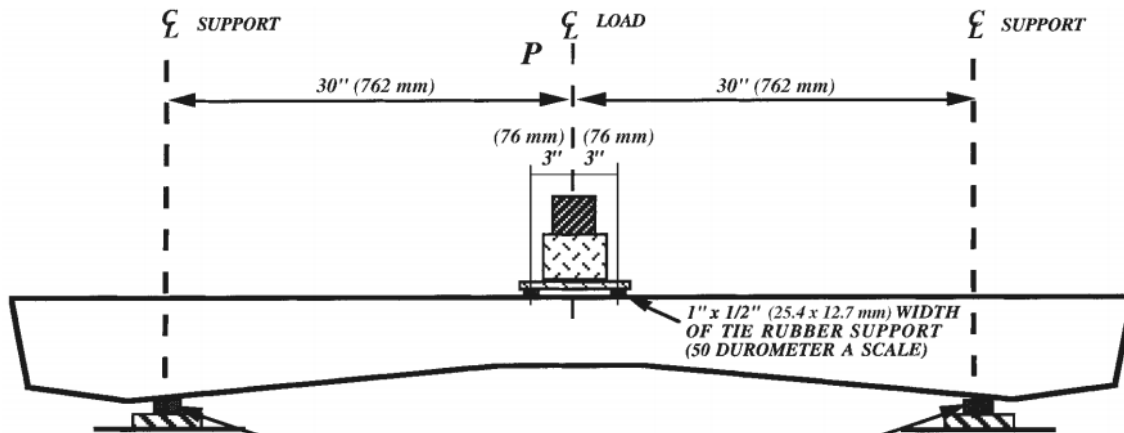


Figure 8.3 AREMA center negative test setup (ARMEA, 2017)

**Table 8.4 AREMA center negative test results**

Tie	Experimental Cracking Moment (kip-in)	AREMA Design Moment (kip-in)	Center negative Bending Test
A	170	202	Fail
B	247	191	Pass
C	179	160	Pass
D	284	191	Pass
E	200	191	Pass
F	127	202	Fail
G	250	191	Pass
H	284	191	Pass
J	221	202	Pass
K	249	191	Pass
L	178	202	Fail
M	198	202	Fail

## Chapter 9 - Conclusions

This section details the conclusions drawn from the testing conducted on prestressed concrete railroad ties throughout this research.

1. The flexural crack reopening test was conducted on the existing ties to attempt to determine the remaining prestress force. In this test, the crack reopening load is determined from the load versus COD curves by either using the end of the initial linear portion, or the intersection of the tangent lines. Testing on ties instrumented with VWSGs revealed that neither the end of linearity or the tangent intersection methods would accurately predict the crack reopening load, and in turn the prestress force. A third method of determining the crack reopening load was investigated, where an offset is applied to the initial linear portion of the curve, but ultimately was unable to predict the prestress force accurately. Since this test has predominantly been used on prestressed bridge girders where the cross-section is larger and the prestress force is concentrated at the bottom of the section, with a much greater eccentricity, this method was determined to not be applicable to railroad ties, where the prestress force is dispersed through a smaller cross-section
2. To improve upon the shortcomings of the flexural crack reopening test, the direct tension test method was developed to determine the prestress force in a railroad tie experimentally. In this method, a more global approach is taken to evaluate the ties than the methods that measure flexural cracks or individual wires. This approach eliminates the need to make assumptions about the concrete strength, the prestressing steel modulus of elasticity, and that all tendons have the same amount of stress. Testing conducted on ties instrumented with VWSGs showed the method provides

accurate estimations of the prestress force in a railroad tie, with a maximum error of only 2%. The test was then applied to existing ties to evaluate the remaining prestress force after being removed from track. A majority of the existing ties had prestress forces in the range of 82-93 kips, with the post-tensioned tie having a prestressed force of 61.2 kips. These forces are significantly lower than level of prestress force that modern tie designs (100-144 kips for new ties investigated in this study).

3. The strain gage method was investigated as a way to determine the average force in an individual wire, and extrapolate the prestress force in the tie from that force. Several issues arose throughout the application of this method. In this method it is assumed that the prestress force is the same in all wires. Testing conducted on multiple wires from the same tie indicated that this assumption is likely not correct. Additionally, a value for the modulus of elasticity of steel is assumed to convert the measured strain values to stresses, introducing error into the final prestress force estimation. Further issues associated with implementing this test method increased the error and uncertainty in the final results, including gage misalignment during installation, and having to fill the wire indents with adhesive prior to instrumenting the gages. It remains unknown to what degree the final readings were impacted by filling the wire indents with adhesive. Further error occurs due the wires having a bow shape while in an unstressed state, which was seen to have a measureable effect when testing an individual wire. Since the direction of the bow is unknown on a tensioned wire in a railroad tie, it is difficult to compensate for this effect during testing. When testing was conducted on ties instrumented with VWSGs, the error of the prestress force estimations was in the range of 18-26%. The high error involved

- with the strain gage method from the aforementioned sources, this method was not used for estimating the prestress force in the existing ties.
4. Method 1 of the wire extraction method was shown to be a feasible method for estimating the prestress force, having a 9% error when compared with the VWSG measurements. As the transfer length and modulus of the tendons were assumed in this calculation, the error associated with this method could be reduced when these values have been measured. Method 2, where a 60 inch initial gage length is used, proved be less effective, with an error of 26% when compared to VWSG measurements. In this method, any damage incurred on the wire during the removal of the cover could reduce the force in the tendon and result in a lower estimated prestress force. Additionally, the use of tape measure to measure the post-extraction length was less accurate than the micrometer used in Method 1, and induced further error. In both Method 1 and 2, the assumption is made that the force in every tendon is roughly the same, using an average force per tendon to estimate the total prestress force. As previously mentioned, this is not the actual case, and contributes some of the error in the final estimate.
  5. Vibrating-wire strain gages were used periodically throughout the testing conducted in this research program and provided beneficial insight on strain associated with section loss and loss of prestress force in prestressed members. Throughout the strain gage method and wire extraction method, ties with VWSGs had wires at mid-span exposed and cut. Readings taken at different stages showed that the strain associated with the inflicted damage, in the range of 30-240 microstrain, were much smaller than anticipated. This indicates that while VWSGs are good for evaluating the prestress

force in an undamaged member, they may not detect the full extent of damage done to a prestressed member, and the readings in a damaged member may lead to inaccurate estimates of the prestress force.

6. The experimental center negative cracking moments were determined for the existing ties and compared to the AREMA Chapter 30 center negative bending test. This testing was beneficial in comparing tie designs that are known to have performed well in track to current design standards. For the 12 different existing tie designs investigated, where all had performed well in track for over 25 years, only 8 of the designs would meet the current requirements of the AREMA center negative bending test. Combined with the knowledge that many of these ties have lower level of prestress forces than modern designs, this indicates that new ties can be designed with lower prestress forces to mitigate splitting propensity, but still meet design standards and provide a durable long-term performance in track.

## References

- AASHTO. (2012). AASHTO LRFD Bridge Design Specifications. Washington, D.C.: American Association of State Highway and Transportation Officials.
- Abraham, M. A., Park, S., & Stubbs, N. (1995, April). Loss of prestress prediction based on nondestructive damage location algorithms. In *Smart Structures and Materials 1995: Smart Systems for Bridges, Structures, and Highways* (Vol. 2446, pp. 60-68). International Society for Optics and Photonics.
- American Concrete Institute. (2014). Building Code Requirements for Structural Concrete (ACI 318-14): Commentary on Building Code Requirements for Structural Concrete (ACI 318R-14): an ACI Report. American Concrete Institute. ACI.
- AREMA (American Railway Engineering and Maintenance-of-Way Association). "Manual for railway engineering." (2017).
- Arnold, M. L., Peterman, R. J., Bodapati, N. N. B., Beck, B. T., & Wu, C. H. J. (2013, April). Development of a standard bond test for indented prestressing wires. In 2013 Joint Rail Conference. American Society of Mechanical Engineers.
- Baran, E., Shield, C. K., & French, C. E. (2005). A comparison of methods for experimentally determining prestress losses in pretensioned prestressed concrete girders. *Special Publication*, 231, 161-180.
- Bodapati, N. N. B., Peterman, R. J., Beck, B. T., & Wu, C. H. J. (2014, April). Effect of concrete properties on transfer lengths in concrete railroad ties. In 2014 Joint Rail Conference. American Society of Mechanical Engineers.
- Bodapati, N. N. B., Zhao, W., Peterman, R. J., Wu, C. H. J., Beck, B. T., Haynes, M., & Holste, J. R. (2013, April). Influence of indented wire geometry and concrete parameters on the transfer length in prestressed concrete crossties. In 2013 Joint Rail Conference. American Society of Mechanical Engineers.
- de Vries, M., Arya, V., Meller, S., Masri, S. F., & Claus, R. O. (1997). Implementation of EFPI-based optical-fiber sensor instrumentation for the NDE of concrete structures. *Cement and concrete composites*, 19(1), 69-79.
- Geokon, Incorporated. (2018). Instruction Manual: Model 4200 Series Vibrating-wire Strain Gage. [https://www.geokon.com/content/manuals/4200-4202-4204-4210\\_Strain\\_Gages.pdf](https://www.geokon.com/content/manuals/4200-4202-4204-4210_Strain_Gages.pdf)

- Gross, S. P., & Burns, N. H. (1995). Transfer and development length of 15.2 mm (0.6 in.) diameter prestressing strand in high performance concrete: results of the Hoblitzell-Buckner beam tests (No. FHWA/TX-97/580-2). University of Texas at Austin. Center for Transportation Research.
- Halsey, J. T., & Miller, R. (1996). Destructive testing of two forty-year-old prestressed concrete bridge beams. *PCI journal*, 41(5).
- Hanna, A. (1979). Prestressed concrete ties for North American railroads—a state of the art report. *J. Prestressed Concr. Inst*, 24, 32-61.
- Holste, J. R., Haynes, M., Peterman, R. J., Beck, B. T., & Wu, J. C. H. (2014, April). Tensioned pullout test used to investigate wire splitting propensity in concrete railroad ties. In 2014 Joint Rail Conference. American Society of Mechanical Engineers.
- Holste, J. R., Peterman, R. J., Bodapati, N. N. B., Beck, B. T., & Wu, C. H. J. (2013, October). Transfer bond test used to predict transfer length of concrete railroad ties. In ASME 2013 Rail Transportation Division Fall Technical Conference. American Society of Mechanical Engineers.
- Kaar, P. H., La Fraugh, R. W., & Maas, M. A. (1963). Influence of concrete strength on strand transfer length. Portland Cement Association, Research and Development Laboratories.
- Kim, J. T., Yun, C. B., Ryu, Y. S., & Cho, H. M. (2004). Identification of prestress-loss in PSC beams using modal information. *Structural Engineering and Mechanics*, 17, 467-482.
- Labia, Y., Saiidi, M. S., & Douglas, B. (1997). Full-scale testing and analysis of 20-year-old pretensioned concrete box girders. *Structural Journal*, 94(5), 471-482.
- Larson, K. H., Peterman, R. J., & Rasheed, H. A. (2005). Strength-fatigue behavior of fiber reinforced polymer strengthened prestressed concrete T-beams. *Journal of Composites for Construction*, 9(4), 313-326.
- Law, S. S., & Lu, Z. R. (2005). Time domain responses of a prestressed beam and prestress identification. *Journal of sound and vibration*, 288(4-5), 1011-1025.
- Lu, Z. R., Liu, J. K., & Law, S. S. (2008). Identification of prestress force in a prestressed Timoshenko beam. *Structural Engineering and Mechanics*, 29(3), 241-258.

- Lundqvist, P. (2012). Assessment of long-term losses in prestressed concrete structures- application for nuclear reactor containments. Lund University
- Murphy, R., Zhao, W., Peterman, R., Beck, T., & Center, M. A. T. (2012). Determining the transfer length in prestressed concrete railroad ties produced in the United States (No. MATC-KSU: 453). Mid-America Transportation Center.
- Otter, J. R. H., Cassell, A. C., Hobbs, R. E., & POISSON. (1966). Dynamic relaxation. *Proceedings of the Institution of Civil Engineers*, 35(4), 633-656.
- PCI. (2010). *PCI Design Handbook: Precast and Prestressed Concrete (7th ed.)*. Chicago, Illinois: Precast/Prestressed Concrete Institute.
- Pessiki, S., Kaczinski, M., & Wescott, H. H. (1996). Evaluation of effective prestress force in 28-year-old prestressed concrete bridge beams. *PCI journal*, 41(6), 78-89.
- Peterman, R. J., Ramirez, J. A., & Olek, J. (2000). Influence of flexure-shear cracking on strand development length in prestressed concrete members. *PCI journal*, 45(5), 76-94.
- Rabbat, B. G. (1984). 25-Year-Old Prestressed Concrete Bridge Girders Tested. *PCI JOURNAL*, 29(1), 177-179.
- Remennikov, A. M., & Kaewunruen, S. (2014). Determination of prestressing force in railway concrete sleepers using dynamic relaxation technique. *Journal of Performance of Constructed Facilities*, 29(5), 04014134.
- Saiidi, M., Douglas, B., & Feng, S. (1994). Prestress force effect on vibration frequency of concrete bridges. *Journal of structural Engineering*, 120(7), 2233-2241.
- Savic, A. (2019). Developing a prism qualification test to ensure adequate splitting resistance in pretensioned concrete railroad ties (Doctoral dissertation).
- Swartz, B. D. (2010). Time-dependent analysis of pretensioned concrete bridge girders. (Doctoral dissertation, Pennsylvania State University).
- Tadros, M. K., Al-Omaishi, N., Seguirant, S. J., & Gallt, J. G. (2003). NCHRP Report 496: Prestress losses in pretensioned high-strength concrete bridge girders. Washington D.C.: Transportation Research Board.

Tadros, M. K., Ghali, A., & Bilger, W. H. (1977). Time-dependent analysis of composite frames. *Journal of the Structural Division*, 103(ASCE 12893 Proceeding).

Xuan, F. Z., Tang, H., & Tu, S. T. (2009). In situ monitoring on prestress losses in the reinforced structure with fiber-optic sensors. *Measurement*, 42(1), 107-111.

Yu, H. (2017b). Causes and prevention of splitting/bursting failure of concrete cross-ties: a computational study. *The AREMA 2017 Annual Conference*

Zia, P., H. K. Preston, N. L. Scott, and E. B. Workman. 1979. Estimating prestress losses. *Concrete International*, V. 1, No. 6 (June).

## Appendix A - Pictures of Existing Ties and Mid-span Cross-sections



Figure A.1 Typical side and top view of tie type A

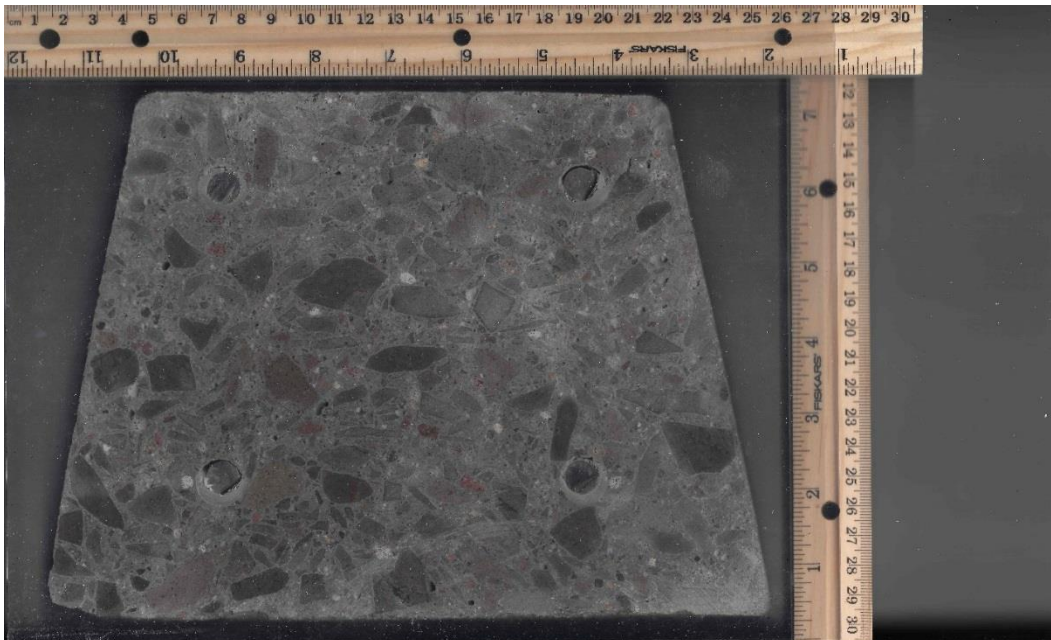
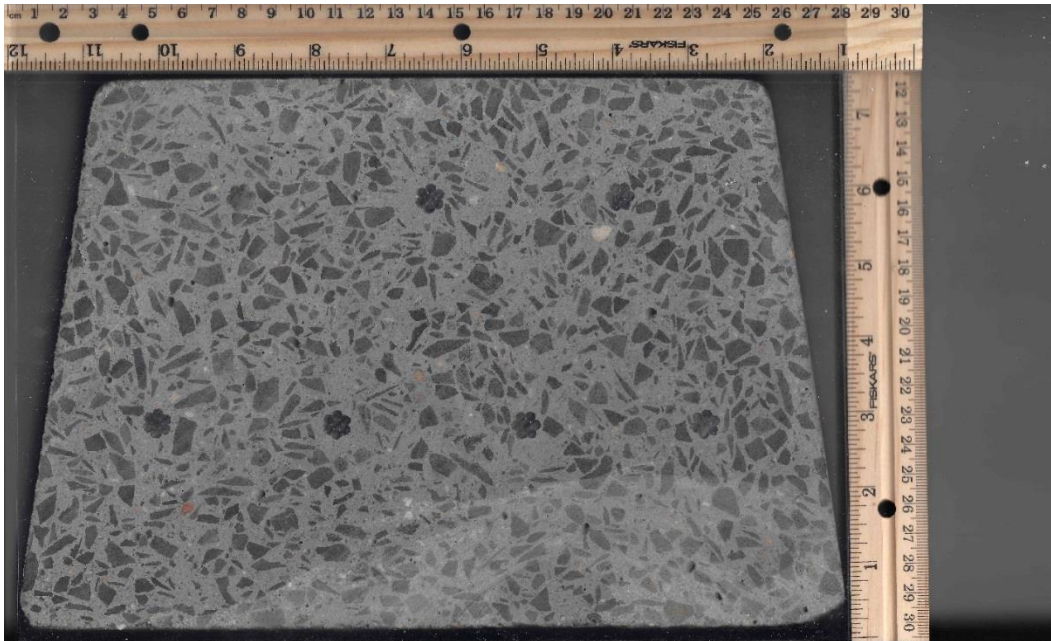


Figure A.2 Typical mid-span cross-section of tie type A



**Figure A.3 Typical side and top view of tie type B**



**Figure A.4 Typical mid-span cross-section of tie type B**



**Figure A.5 Typical side and top view of tie type C**



**Figure A.6 Typical mid-span cross-section of tie type C**



**Figure A.7 Typical side and top view of tie type D**

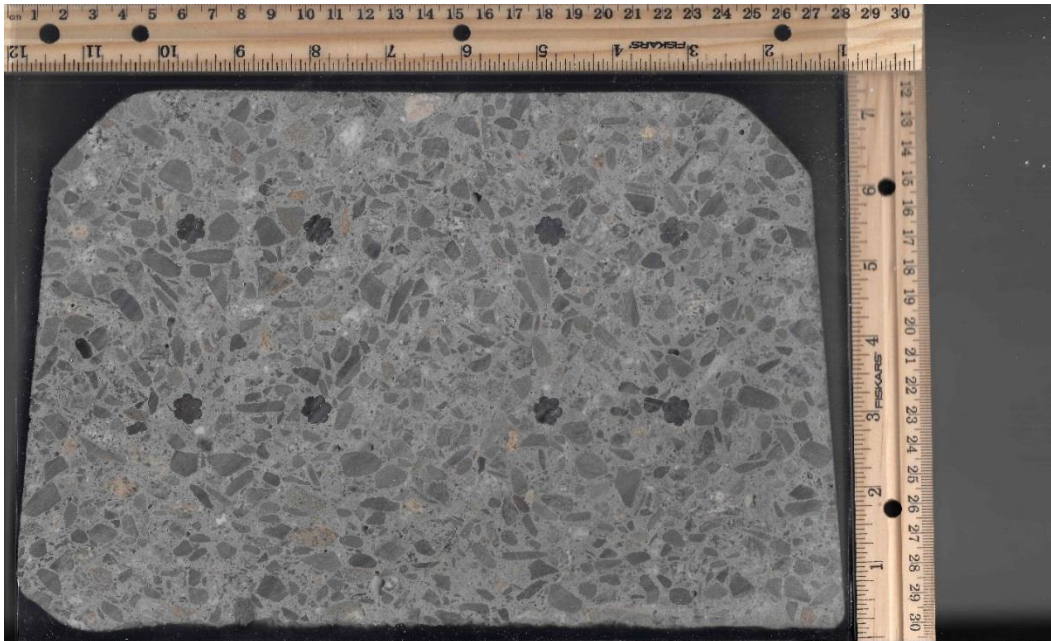


**Figure A.8 Typical mid-span cross-section of tie type D**



**Figure A.9 Typical side and top view of tie type E**



**Figure A.10 Typical mid-span cross-section of tie type E**



**Figure A.11 Typical side and top view of tie type F**

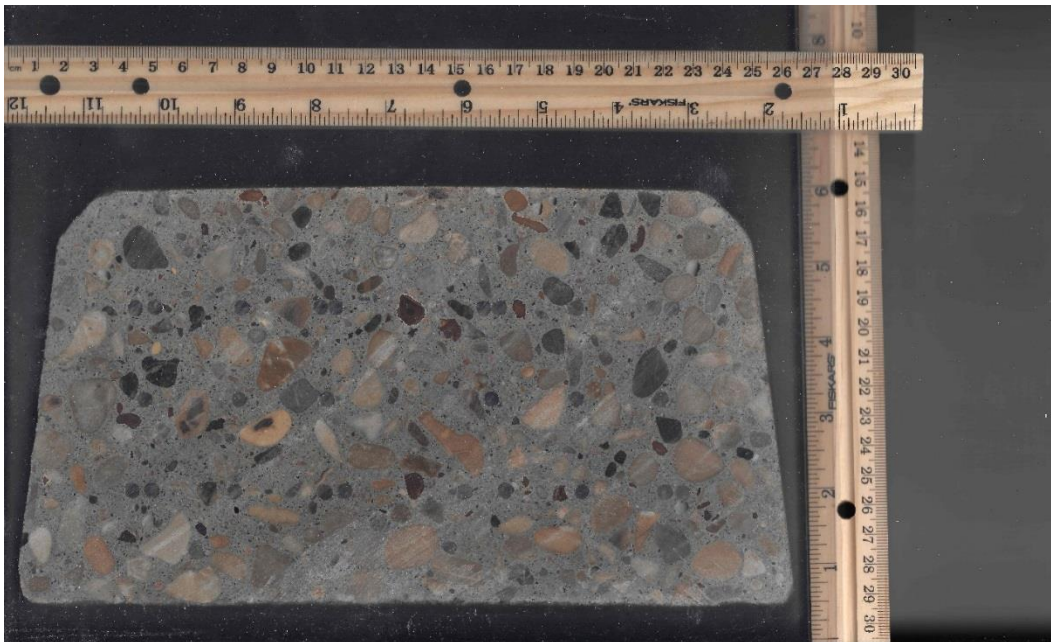


**Figure A.12 Typical mid-span cross-section of tie type F**



**Figure A.13 Typical side and top view of tie type G**

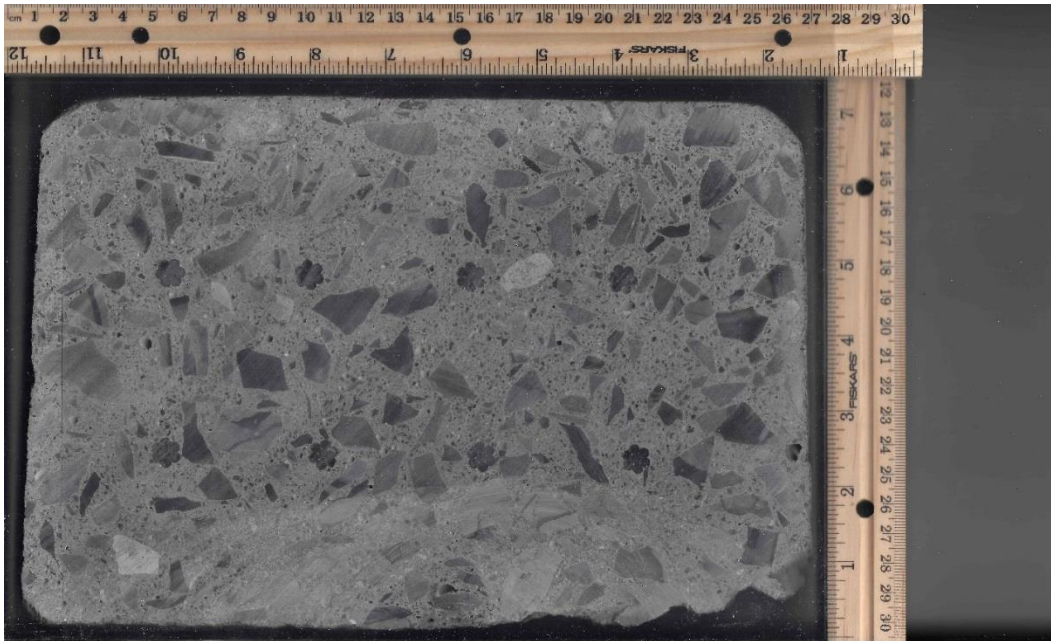


**Figure A.14 Typical mid-span cross-section of tie type G**



**Figure A.15 Typical side and top view of tie type H**

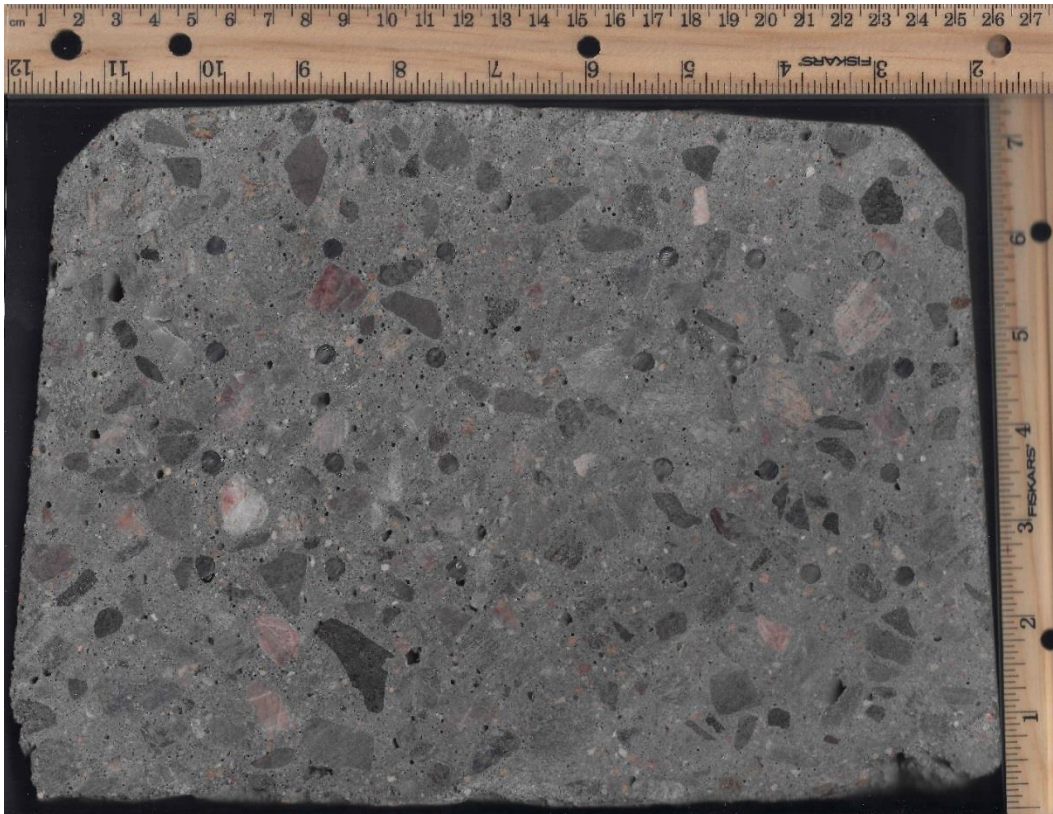


**Figure A.16 Typical mid-span cross-section of tie type H**

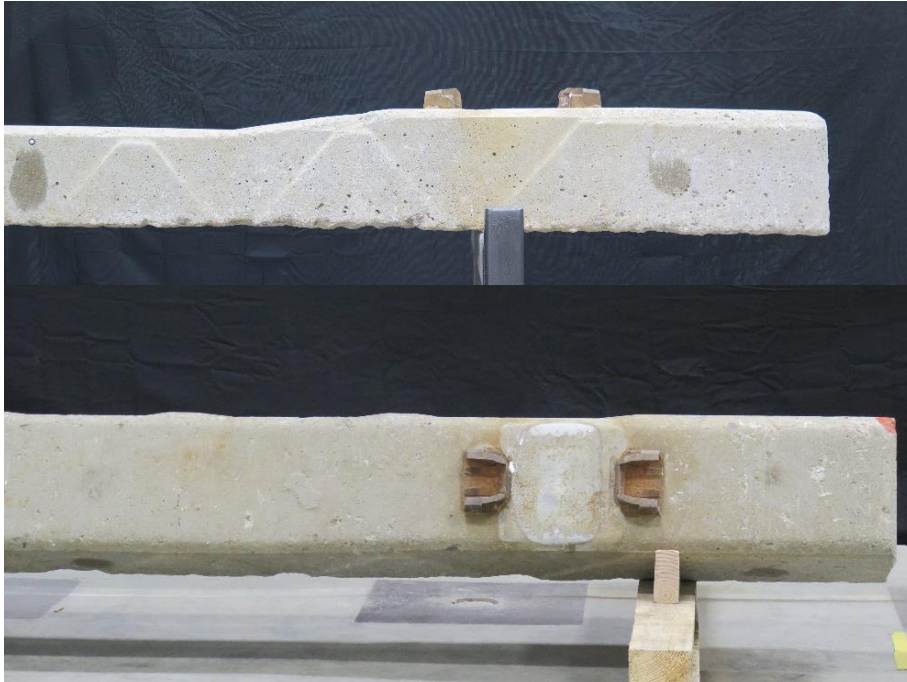


**Figure A.17 Typical side and top view of tie type J**

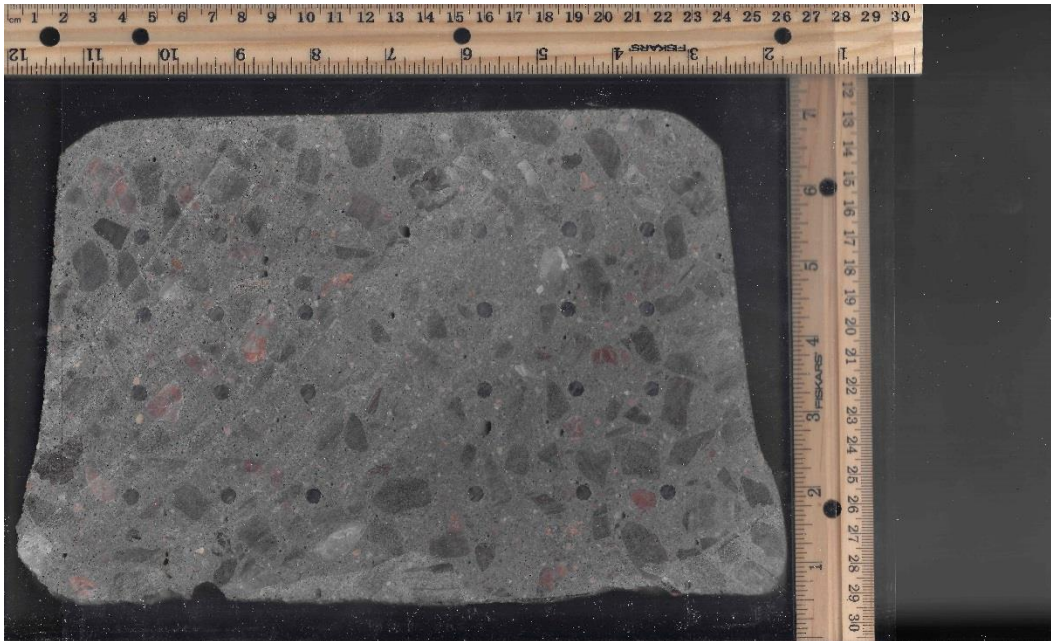


**Figure A.18 Typical mid-span cross-section of tie type J**



**Figure A.19 Typical side and top view of tie type K**



**Figure A.20 Typical mid-span cross-section of tie type K**



**Figure A.21 Typical side and top view of tie type L**

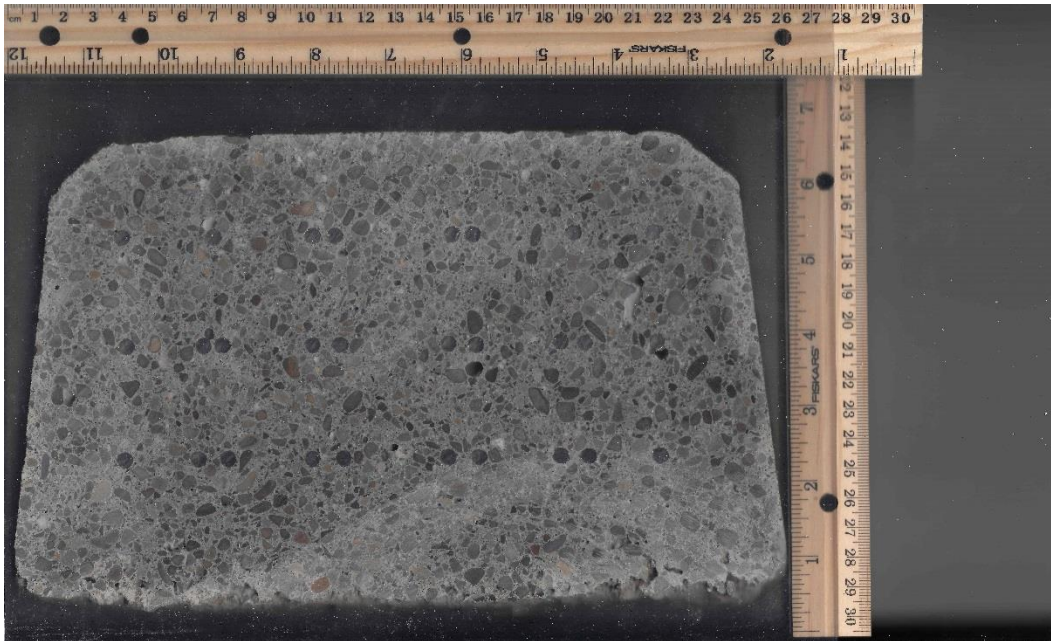


**Figure A.22 Typical mid-span cross-section of tie type L**



**Figure A.23 Typical side and top view of tie type M**



**Figure A.24 Typical mid-span cross-section of tie type M**

## Appendix B - Summary of Testing Conducted on Ties

**Table B.1 Summary of tests conducted on ties**

Tie	Source	Manufacturer/ Type	Flexural Crack Reopening	Direct Tension Test	Strain Gage Method	Wire Extraction
A-1	TTCI	ITISA	Yes	-	-	-
A-3	TTCI	ITISA	Yes	-	-	-
A-4	TTCI	ITISA	Yes	-	-	-
A-6	TTCI	ITISA	-	Yes	-	-
B-1	TTCI	Abetong	Yes	-	-	-
B-2	TTCI	Abetong	Yes	-	-	-
B-3	TTCI	Abetong	Yes	-	-	-
B-4	TTCI	Abetong	Yes	-	-	-
B-7	TTCI	Abetong	-	Yes	-	-
C-1	TTCI	F.E.C.	Yes	-	-	-
C-2	TTCI	F.E.C.	Yes	-	-	-
C-3	TTCI	F.E.C.	Yes	-	-	-
D-1	TTCI	Santa Fe/ San Vel	Yes	-	-	-
D-2	TTCI	Santa Fe/ San Vel	-	Yes	-	-
D-3	TTCI	Santa Fe/ San Vel	Yes	-	-	-
D-4	TTCI	Santa Fe/ San Vel	Yes	Yes	-	-
D-7	Amtrak	Santa Fe/ San Vel	-	Yes	-	-
D-8	Amtrak	Santa Fe/ San Vel	-	Yes	-	-
E-1	TTCI	CXT 497S	Yes	-	-	-
E-4	TTCI	CXT 497S	Yes	-	-	-
E-5	TTCI	CXT 497S	Yes	-	-	-
F-1	TTCI	Con-Force Costain	Yes	-	-	-
F-2	TTCI	Con-Force Costain	Yes	-	-	-
F-3	TTCI	Con-Force Costain	Yes	-	-	-
F-6	TTCI	Con-Force Costain	-	Yes	-	-
G-1	TTCI	Koppers	Yes	-	-	-
G-2	TTCI	Koppers	Yes	-	-	-

G-5	TTCI	Koppers	Yes	-	-	-
H-1	TTCI	Rocla	Yes	-	-	-
H-2	TTCI	Rocla	Yes	-	-	-
H-3	TTCI	Rocla	-	Yes	-	-
H-6	TTCI	Rocla	Yes	-	-	-
J-1	TTCI	Rocla	Yes	-	-	-
J-3	TTCI	Rocla	Yes	-	-	-
J-5	TTCI	Rocla	Yes	-	-	-
K-1	TTCI	Costain	Yes	-	-	-
K-2	TTCI	Costain	Yes	-	-	-
K-3	TTCI	Costain	Yes	-	-	-
K-5	TTCI	Costain	-	Yes	-	-
L-1	TTCI	CXT	Yes	-	-	-
L-2	TTCI	CXT	Yes	-	-	-
L-4	TTCI	CXT	Yes	-	-	-
L-6	TTCI	CXT	-	Yes	-	-
M-1	TTCI	Rocla	Yes	-	-	-
M-2	TTCI	Rocla	Yes	-	-	-
M-6	TTCI	Rocla	Yes	-	-	-
R-1	Rocla	Vossloh 101L	Yes	-	-	-
R-2	Rocla	Vossloh 101L	Yes	-	-	-
R-3	Rocla	Vossloh 101L	Yes	-	-	-
R-4	Rocla	Vossloh 101L	-	Yes	-	-
R-5	Rocla	Vossloh 101L	-	-	Yes	Yes
NT-1	Nortrak	Nortrak	-	Yes	Yes	-
NT-2	Nortrak	Nortrak	-	-	-	-
CXT-1	CXT	CXT 505S	-	Yes	Yes	-
CXT-2	CXT	CXT 505S	-	-	-	Yes

## Appendix C - Net Effect of Elastic Shortening and the Weight of the Top Block on tie D-4

The following calculations are for the net effect of both the elastic shortening, and the weight of the block above the crack, on the estimated remaining prestress force in tie D-4. Table A1 lists the values for the parameters used in the calculations, where the Modulus of Elasticity of Concrete was calculated assuming 10,000 psi concrete in the tie.

**Table C.1 Values of parameters used in calculations**

Parameter	Value
Prestress Force - P (lb)	94,000
MOE, Steel - $E_s$ (psi)	28,500,000
MOE, Concrete - $E_c$ (psi)	5,700,000
Initial Area - $A_0$ (in <sup>2</sup> )	73
Final Area - $A_F$ (in <sup>2</sup> )	34
Area of Steel - $A_s$ (in <sup>2</sup> )	0.688
Concrete Block Density (lb/ft <sup>3</sup> )	150

Loss of prestress force due to elastic shortening:

Initial stress,  $\sigma_0$

$$\sigma_0 = \frac{P}{A_0} = \frac{94,000 \text{ lbs}}{73 \text{ in}^2} = 1,290 \text{ psi}$$

Final stress,  $\sigma_F$

$$\sigma_F = \frac{P}{A_F} = \frac{94,000 \text{ lbs}}{34 \text{ in}^2} = 2,760 \text{ psi}$$

Change in stress,  $\Delta\sigma$

$$\Delta\sigma = \sigma_F - \sigma_0 = 1470 \text{ psi}$$

Elastic shortening strain,  $\epsilon$

$$\epsilon = \frac{\Delta\sigma}{E_c} = \frac{1,470 \text{ psi}}{5,700,000 \text{ psi}} = 0.000258$$

Stress reduction in steel due to shortening,  $\sigma_s$

$$\sigma_s = E_s \epsilon = 28,500,000 \text{ psi} \times 0.000258 = 7,350 \text{ psi}$$

Loss of prestress force,  $P_L$

$$P_L = \sigma_s A_s = 7,350 \text{ psi} \times 0.688 \text{ in}^2 = 5,060 \text{ lbs}$$

Weight of the block above the crack,  $W_B$ :

$$W_B = \frac{36 \text{ in} \times 18.5 \text{ in} \times 43.25 \text{ in}}{12^3 \text{ in}^3/\text{ft}^3} \times 150 \frac{\text{lb}}{\text{ft}^3} = 2,500 \text{ lbs}$$

Net force difference,  $F$ :

$$F = |W_B - P_L| = |5,060 \text{ lbs} - 2,500 \text{ lbs}| = 2,560 \text{ lbs}$$

Net error,  $E$ :

$$E = \frac{F}{P} \times 100 = \frac{2,560 \text{ lbs}}{94,000 \text{ lbs}} \times 100 = 2.7\%$$